University of Alberta

PLGA-BASED NANOPARTICLES FOR TARGETING OF DENDRITIC CELLS IN CANCER IMMUNOTHERAPY AND IMMUNOMONITORING

by

ZAHRA GHOTBI

A thesis submitted to the Faculty of Graduate Studies and Research
in partial fulfillment of the requirements for the degree of

MASTER OF SCIENCE

in

PHARMACEUTICAL SCIENCES

Faculty of Pharmacy and Pharmaceutical Sciences

Spring 2010
Edmonton, Alberta

Examining Committee

Dr. Afsaneh Lavasanifar, Faculty of Pharmacy and Pharmaceutical Sciences

Dr. Mavanur Suresh, Faculty of Pharmacy and Pharmaceutical Sciences

Dr. Kamaljit Kaur, Faculty of Pharmacy and Pharmaceutical Sciences

Dr. Hasan Uludağ, Department of Chemical and Materials Engineering, Faculty of Engineering

Dedication

This thesis is dedicated to:

My wonderful husband, Mohammad, for years of unconditioned love, understanding and invaluable support throughout the hardest times of this study and our life.

My lovely son, Sepand for his love, support and unique patience during peaks and valleys of this journey.

The loving memory of my dad, to my mom and my parents-in-laws, who supported me from the beginning and offered me love, support and encouragement.

The memory of my great mentor and late supervisor, Dr. John Samuel, who was an exemplar of an enthusiastic, modest and peaceful scientist with an ocean-like knowledge and a heart to love.

Abstract

Cancer vaccines have shown little success in clinic. Dendritic cells (DCs) are of particular interest in cancer vaccination due to their role in cell-mediated immunity. Active targeting of DCs, through PLGA nanoparticles (PLGA-NPs) decorated with ligands for DC-expressed mannose receptor (MR) can enhance internalization, processing and presentation of antigens and subsequent immnuostimulation. In this study we have shown PLGA-NPs decorated with mannan and the synthetic hydrophobized mannan, especially those with covalent attachment, can target DCs leading to increased uptake of nanoparticles and DC maturation. This approach may be used for improved delivery of antigens and adjuvants to DCs and development of more efficient cancer vaccines.

Moreover, significant progress in cancer vaccination requires immunomonitoring. Live imaging using a Positron Emission Tomography (PET) probe encapsulated in PLGA-NPs can elucidate dynamics of recruitment and fate of DCs to develop successful vaccines. The PET-nanoprobe prepared by radio-iodinated 5-IDFPdR demonstrated uncontrolled high burst release implying low quality images.

Acknowledgements

- I would like to express my gratitude and appreciation to my supervisor, the late Dr. John Samuel for his guidance and continuous support. His creativity and enthusiasm towards science was always a source of inspiration and encouragement. I would have never been able to convey my appreciation fully. I am deeply indebted to him and I dedicate all my accomplishments I had or will have in the future to him.
- This thesis would not have been possible unless with the guiding advices and invaluable support of my supervisor Dr. Afsaneh Lavasanifar, who assisted me to overcome the barriers I encountered in all stages of this study. The essence of her responsible and willing supervision of our group after the sad loss of Dr. John Samuel is gratefully appreciated.

It is also my pleasure to extend my sincere thanks to the following people:

- My supervisory committee members, Dr. Mavanur Suresh and Dr. Kamaljit Kaur and my examination committee for their advice and constructive feedback.
- Dr. Steve McQuarrie from Division of Oncologic Imaging for his advice and guidance in PET studies, and Dr. Leonard Wiebe for his co-operation and providing the cold PET probe used in this study.
- Dr. Edward Knaus for his generous support and using his lab for the synthesis of OPM.
- My friend and lab colleague Dr. Samar Hamdy with her kind endless support, generous help and constructive critics throughout the whole program.
- My friend and lab colleague Dr. Azita Haddadi who trained me in bench work and provided me indebted help and support throughout the course of study.
- Dr. Ryan W. Hung from Department of Radiology and Diagnostic Imaging, whose fresh look and enthusiasm to knowledge represents the essence of scientific research. His precise advices with the confocal laser scanning microscopy are greatly appreciated.
- Faculty staff, particularly Joyce Johnson for her assistance, cooperation and consideration as a graduate coordinator. Don White and Drew Price for their endless technical assistance. Jeff Turchinsky, for his excellent hard work and responsibility in providing needed supplies.
- Ann Berg from Cross Cancer Institute, for her technical assistance and advice with the flow cytometry.
- My friends and lab colleagues Aws Alshamsan and Leila Molavi for their positive discussions and help.
- My family for their love and incredible encouragement.
- The last but not the least, my husband Mohammad Hajizaman , whose love, patience, thoughtfulness and never-ending support provided me a peaceful environment in this journey; and my lovely son, Sepand who helped me during the whole process with his patience and positive attitude.

Finally, I would like to thank the Natural Sciences and Engineering Research Council of Canada (NSERC) for their financial support.

Table of contents

CHAPTER ONE: Introduction

List of Tables

List of Figures

LIST OF ABBREVIATIONS

µCi	microcurie
µg	microgram
µL	microlitre
^{1}H-NMR	proton nuclear magnetic resonance
Ab	antibody
Ag	antigen
ANOVA	analysis of variance
APCs	antigen presenting cells
BLI	bioluminescence imaging
BM	bone marrow
BM-DCs	bone-marrow-derived dendritic cells
C	Celsius
CD	cluster of differentiation
CLRs	c-type lectin receptors
CPM	counts per minute
CRDs	carbohydrate recognition domains
CT	computed tomography
CTL	cytotoxic T lymphocyte
Da	dalton
DAPI	4,6-diamidino-2-phenylindole
DCC	N**,**N'-dicyclohexyl-carbodiimide
DCM	dichloromethane
DCs	dendritic cells
DC-SIGN	dendritic cell-specific intercellular adhesion molecule-3-grabbing non-integrin
DLS	dynamic-light scattering
DMF	N,N-Dimethylformamide
DMSO	dimethyl sulfoxide

ELISA	enzyme-linked immunosorbent assay
FACS	fluorescent-activated cell sorting
FBS	foetal bovine serum
FDA	food and drug administration
FITC	fluorescein isothiocyanate
FMT	fluorescence-mediated tomography
g	gravitation force
GM-CSF	granulocyte-monocyte colony stimulating factor
h	hour
IDFPdR	iodo-2, 4-difluro-1-{2-deoxy-b-D-ribofuranosyl} benzene
LPS	lipopolysaccharide
LSCM	laser scanning confocal microscopy
M	molar
mAb	monoclonal antibody
mCi	millicurie
mg	milligram
MHC	major histocompatibility complex
MHz	megahertz
min	minutes
mL	millilitre
MLR	mixed lymphocyte reaction
MLR	mixed lymphocyte reaction
mM	millimolar
MMR	macrophage mannose receptor
MN	mannan
MN-Ads-NPs	mannan-adsorbed nanoparticles
MN-cov-NPs	mannan covalent nanoparticles
MN-W1-NPs	mannan in primary aqueous phase nanoparticles
MN-w2-NPs	mannan in secondary aqueous phase nanoparticles
MRI	magnetic resonance imaging
MRs	mannose receptors

mV	milivolt
MW	molecular weight
N	normal
Ng	nanogram
NK cells	natural killer cells
NKT cells	natural killer T cells
nm	nanometre
NMR	nuclear magnetic resonance
NPs	nanoparticles
OPM	*o*-palmitoyl mannan
OPM-Ads-PLGA	OPM-adsorbed nanoparticles
OPM-W1-PLGA	OPM in primary aqueous phase nanoparticles
OPM-W2-PLGA	OPM in secondary aqueous phase nanoparticles
PAMPs	pathogen-associated molecular patterns
PBS	phosphate buffer saline
PE	phycoerythrin
PET	positron-emission tomography
PGA	poly glycolic acid
PI	polydispersity index
PLA	poly lactic acid
PLGA	poly (D, L-lactide-*co*-glycolide)
PVA	polyvinyl chloride
rad	radiation absorbed dose
RP-HPLC	reverse phase high performance liquid chromatography
RT	retention time
RT	room temperature
saPET	small-animal positron emission tomography
SD	standard deviation
SDS	sodium dodecyl sulphate
sec	seconds
SR	scavenger receptor

Sulfo-NHS	sulfo-N-hydroxysuccinimide
T cells	T- lymphocytes
$T_{1/2}$	half-life
THF	tetrahydrofuran
TLC	thin-layer chromatography
TLRs	toll-like receptors
TMRD	tetramethyl rhodamine dextran
T_{reg} cell	T-regulatory cell
TNF-α	tumour necrosis factor- α
UV	ultraviolet
V	volume
v/v	volume-to-volume ratio
W	weight
w/o	water-in-oil
w/o/w	water-in-oil-in-water
w/v	weight-to-volume ratio
w/w	weight-to-weight ratio
WHO	world health organization
β^+	positron
δ	chemical shift
ξ	zeta potential

Chapter one:

Introduction

1.1. Cancer immunotherapy

Cancer malignancies are among the most life-threatening diseases according to World Health Organization (WHO). The cancer incidence has been increasing annually with approximately 78000 new cases in 2008 and a high mortality rate (12% of total deaths) worldwide [1]. Although the primary tumour can be treated by a combination of conventional therapies (surgical resection, radiotherapy and chemotherapy) preventing the metastatic spread through tumour cells is usually ineffective. To win the battle against cancer, it is a primary objective to develop strategies to eradicate the circulated cancer stem cells as well as stimulating an immune response so that the immune system can keep remaining tumour cells in check.

Cancer is widely considered to be a disease that results from alterations in oncogenes, tumour-suppressor genes and genome-stability genes. The tumour-cell microenvironment, the stroma and immunity play a crucial role in cancer, while cancer cells are considered as poorly immunogenic. The fact that tumour cells can progress and kill the host only when they overcome immune control is evidenced by several observations. First, spontaneous tumour regression have been observed in immunocompetent, but increased cancer incidence in immunosuppressed individuals. Second, tumour immunity was demonstrated experimentally in several animal models. Third, the immune system often recognizes the presence of tumours, as reflected by an accumulation of immune cells at tumour sites. Fourth, the tumour-specific cytotoxic T cells (CTLs) or antibodies have a positive impact on tumour regression [2, 3].

1.1.1. "Immunosurveillance" and "immunoediting" theory

Cancer immunotherapy is referred to cancer therapeutic approaches that exploit specific molecules and cells of the immune system to disrupt the growth of cancer cells. The rational for cancer immunotherapy is based on the "cancer immunosurveillance" theory, proposed in 1967 [4], describing lymphocytes as sentinels capable of recognizing nascent transformed cells, and thus preventing tumour growth [5]. In 1980s, it was evidenced that the immune system

encompasses mechanisms that confront and destroy transforming cells continuously produced in our body, as a result of the spontaneous mutations during one's life. It is exactly these mechanisms that immunotherapy attempts to enhance to achieve tumour destruction [6]. However, despite the ability of the immune system to react against cancer cells, the presence of a tumour indicates that the developing cancer can avoid detection or to escape the immune response.

The "immunoediting" concept, postulated very recently by Robert Schreiber [7] attempted to shed light on the mechanism of evasion by describing tumour progression as a process following three phases: elimination; equilibrium and escape **(Figure 1.1)**. In the first phase of "elimination", cells and molecules of innate and adaptive immunity, which comprise the cancer immunosurveillance network, may eradicate the developing tumour and protect the host from tumour formation. However, if this process is not successful, the tumour cells may enter the "equilibrium phase" where they may be either maintained chronically or immunologically sculpted by immune "editors" to produce new populations of tumour variants. These variants may eventually evade the immune system by a variety of strategies to avoid their immune-mediated elimination and become clinically detectable in the "escape phase" [8]. Mechanisms used to evade recognition include tumour-induced impairment of antigen presentation, activation of negative co-stimulatory signals, and production of immunosuppressive factors [9]. In addition, cancer cells may promote the expansion and/or recruitment of regulatory cells including regulatory T cells (Treg), myeloid suppressor cells, natural killer T cells (NKT) [10] and distinct subsets of regulatory dendritic cells (DCs) [11]. The complex contribution of these molecules and cells should be considered in designing a successful cancer immunotherapeutic agent.

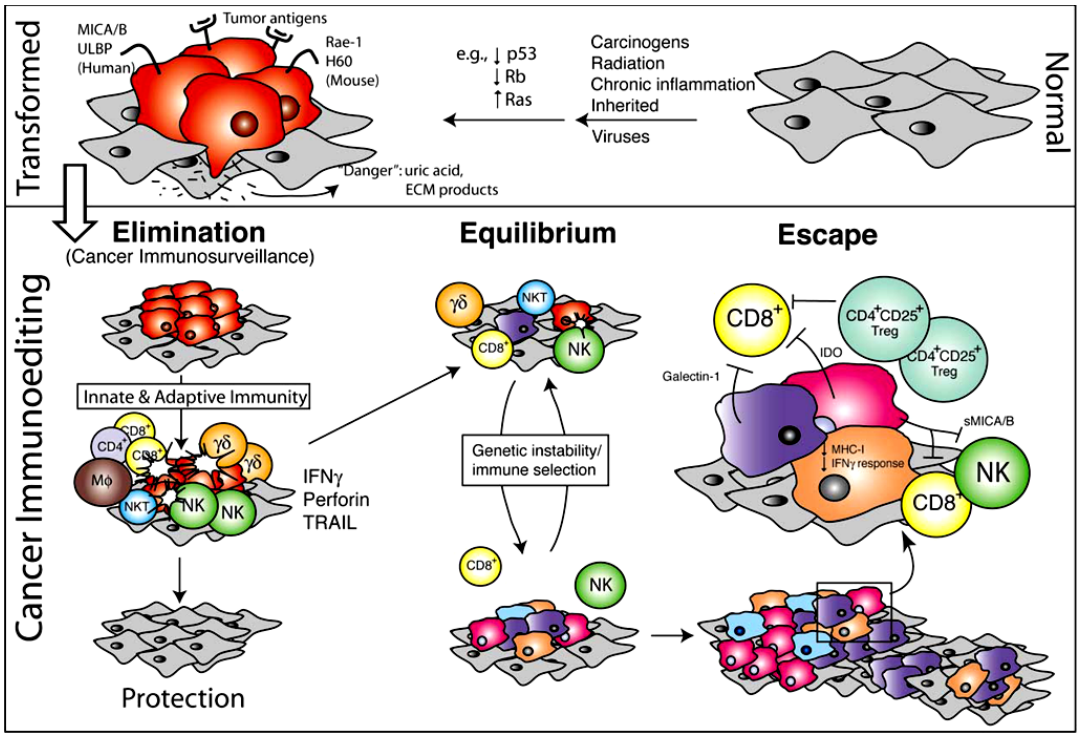

Figure 1.1: The three phases of the cancer immunoediting process: elimination, equilibrium and escape. Normal cells (*gray*) subject to common oncogenic stimuli ultimately undergo transformation and become tumour cells (*red*) (*top*). Even at early stages of tumourigenesis, these cells may express distinct tumour-specific markers and generate pro-inflammatory "danger" signals that initiate the cancer immunoediting process (*bottom*). (Adapted from [8]).

1.1.2. Passive versus active immunotherapy

Immunotherapy is categorized as either passive or active (**Figure 1.2,** adapted from [12]). "Passive" immunotherapy includes any immunologically active agent that is made outside the body and does not rely on host machinery to function. The most widely applied passive immunotherapy is administration of *ex-vivo* generated tumour-targeting monoclonal antibodies (mAbs) that disrupt tumourigenic cascades [13]. Adoptive transfer is another example that typically involves *ex vivo* amplification and infusion of autologous tumour-infiltrating T cells or lymphokine-activated killer cells [14]. Despite the unique specificity of passive immunotherapy, it is short-lived, and dependent on repeated applications [12]. Furthermore, passively applied antibodies cause the threat of inducing an antibody response against the applied antibody [15].

By contrast, “active” cancer immunotherapy uses the host’s immune cells and/or molecules and requires an intact immune system to function actively to target and eliminate cancer cells. This approach aims at the induction of an endogenous, long-lasting tumour antigen-specific immune response. Active immunotherapy is derived from the knowledge that the immune system can discriminate cancer cells from normal cells based on tumour antigen recognition [16]. The processing and presentation of tumour-associated antigens (TAAs) via the antigen presenting cells (APCs) to the T cells seems to be essential for the recognition of tumour antigens, rather than a direct activation of T cells [17]. Approaches that directly incorporate tumour antigen are conventionally referred to as vaccines. Cancer vaccines can be divided into protein- or polypeptide-containing vaccines, whole cell vaccines or viral vector vaccines. They can result in various polyclonal immune responses such as simultaneous activation of APCs, $CD4^+$ and $CD8^+$ T-lymphocytes and cells of innate immune systems (e.g. natural killer (NK) cells and NKT cells) [12]. The immune response can be further enhanced by unspecific stimulation of the immune system using adjuvants or so-called biological response modifiers (e.g., cytokines). An alternative to the induction of an immune response *in vivo* (administration of a tumour antigen as a vaccine to the host’s APCs) is *ex vivo* stimulation of autologous DCs with re-application of the DCs to the patient, as a method to break the patient’s immune tolerance for TAAs [12]. Cancer vaccines with the advantages of specificity, long-lasting effect via the immunological memory, reduced quantity of required antigen, and low toxicity comparing to conventional cancer therapies and/or passive immunotherapy represent a candidate for cancer therapy [2, 12].

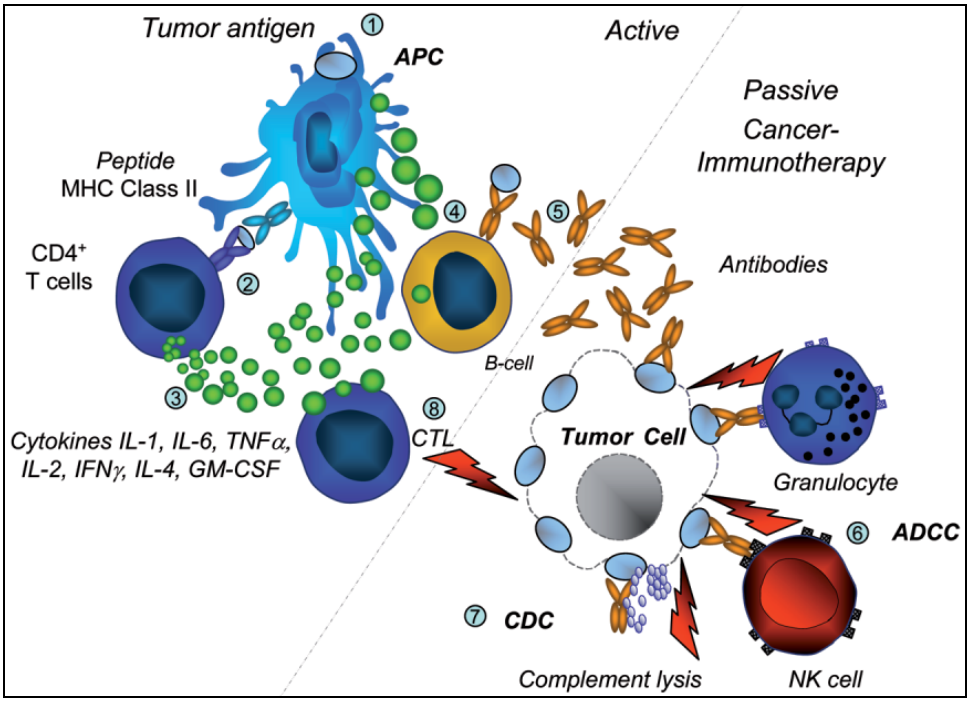

Figure 1.2: Immunological aspects of passive and active cancer immunotherapy. Active immunotherapy includes tumour antigen uptake by APCs (***1***), epitope (peptide) presentation to $CD4^+$ T cells (***2***), cytokine release (***3***), B cell activation (***4***), and Ab production (***5***), leading to the lysis of tumour cells by multiple processes. Passive immunotherapy comprises mechanisms such as ADCC (***6***), complement-dependent cytotoxicity (CDC) (***7***) or unspecific attack by CTLs (***8***).

Cancer vaccines are classified in five categories. The first are cell-based cancer vaccines exploiting various cell types including tumour cells or DCs [18]. The second category are peptide-based cancer vaccines employing molecules with antigenic epitopes such as purified antigens, synthetic peptides, tumour cell lysates and conjugated antigens [19]. The third category is plasmid and viral vectors encoding tumour antigens [20] . The complex of heat shock protein (HSP)/tumour peptide belongs to the forth category. The peptides are a cargo transported intracellular by HSP. The fifth category is particle-based cancer vaccines. The nano/micro-sized particulate systems are utilized as an integrated vehicle for the vaccine components to the specialized immune cells [21] . The rationale for the choice of DCs as a target for delivering vaccine components will describe in the next sections.

1.2. Antigen presenting cells (APCs)

APCs are the cells to be able to process antigens upon internalization, display antigenic peptides in association with major histocompatibility complex class II (MHC-II) molecules and deliver co-stimulatory signals required for T-cell activation. Different cell types can process and present antigens at different efficiencies, but the term “APC” is limited to particular cells called “professional” APCs: a group that typically includes macrophages, B cells and DCs.

In general, endogenous antigens (tumour or viral antigens and normal intracellular proteins) are processed in the cytosol and fed to the proteasome to initiate fragmentation for major histocompatibility complex class I (MHC-I) presentation and further recognition through T-cell receptor (TCR) of $CD8^+$ T cells (“Cytosolic pathway”) [22]. Upon the T cell interaction with APCs, an additional co-stimulatory signal is produced by the APC, stimulates activation of T cells to become "cytotoxic" $CD8^+$ T cells (CTLs).

Alternatively, APCs are also capable of internalizing exogenous “extracellular” antigens by clathrin-mediated endocytosis, macropinocytosis, phagocytosis or a combination of these pathways. Those antigens are processed in specialized acidic endocytic vesicle compartments called endosomes and lysosomes; consequently presented in the context of MHC-II molecules to be recognized by $CD4^+$ T cells (“Endocytic pathway”).

Until recently, MHC-I and MHC-II were thought to focus on the presentation of peptides derived from distinct sources. MHC-I ligands were derived from endogenous cytosolic proteins, whereas MHC-II ligands were exogenous. Although this paradigm remains largely correct, it is now known that boundary can be crossed: MHC-I can present peptides derived from exogenous antigens leading to the activation of antigen specific $CD8^+$ T cells (Cross-presentation). Efficiency of antigen uptake, processing and presentation differs according to the primary function of each APC. The main purpose for antigen presentation by B cells is to get the help needed for antibody secretion. B cells have moderate capacity for endocytosis, as they are restricted to a single antigenic specificity [23] . The primary function of macrophages is to clear tissues from any

invading pathogen and they have extraordinary ability of endocytosis. However, macrophages are not efficient in antigen presentation, as endocytosed antigens are often subjected to complete degradation by proteases in lysosomes [23]. Moreover, macrophages have lower expression of MHC-II and co-stimulatory molecules, compared to B cells and DCs [24].

1.3. DCs as the key APCs

Unlike B cells or macrophages, the primary function of DCs seems to be antigen presentation [23]. DCs are a heterogeneous population of cells serving as 'sentries' in most peripheral tissues where antigens typically first encounter the immune system [25]. Before antigen encounter, DCs are in the immature state. As they encounter antigens, they engulf them [26] and this leads to their activation, maturation and migration to lymph nodes, where they initiate antigen specific T cell immunity. DCs are unique in immune system in many critical ways.

1.3.1. Intrinsic migratory and screening capability of DCs

The intrinsic migratory capability of DCs is mediated by the change of their responsiveness to different chemokines during their development. Immature DCs express a variety of chemokine receptors (CCR). These receptors participate in the localization of DCs in the peripheral tissues and also help in their recruitment to the site of inflammation. Upon maturation, DCs down regulate these receptors (so they can leave the inflamed tissue) and up-regulate the expression of CCR7, which directs them into the T cell area of lymph nodes.

CCR7 ligands direct antigen-loaded DCs into the T cell area of draining lymph node, where continuously moving naïve T cells come to search for their cognate peptide/MHC complexes. Antigen bearing DCs are very efficient in seeking out rare antigen specific T cells (1 in 10^5-10^6) [27]. The presence of many extensions "dendrites" increases the surface area of DCs and enables them to make contact with multiple T cells simultaneously [28]. Such a competent scanning of the T cell repertoire by DCs helps to guarantee that, even a small number of DCs can initiate an antigen-specific T cell response [29].

1.3.2. Unique ability of DCs to activate naïve T cells

Upon activation/maturation, DCs are capable of providing the three signals required for efficient priming of naïve T cells. Mature DCs down regulate their endocytic activity and express high levels of surface MHC-I and MHC-II molecules that present the processed peptides to the naïve $CD8^+$ and $CD4^+$ T cells, respectively (signal 1). Mature DCs also express high levels of accessory molecules, which interact with other receptors in T cells to augment adhesion and co-stimulation (signal 2). Secretion of large amounts of IL-12 by mature DCs provides the third signal required for the induction of efficient T cell activation [30]. In contrast to B cells and macrophages that require activation to express co-stimulatory molecules; DCs have a unique ability to activate immunologically naïve T cells. This is because DCs are the only APCs that have constitutive expression of MHC-I and MHC-II as well as co-stimulatory molecules.

1.3.3. Exclusive ability of DCs to cross-present exogenous antigens

Cross-presentation ensures that DCs can develop CTL immunity against tumour cells and viral infected cells (by taking up tumour or virus-derived antigen/cellular debris and cross-present them to $CD8^+$ T cells) [28, 31]. Cross-presentation is highly relevant for anti-tumour vaccines.

Because of their wide distribution, location at critical sentinel sites (e.g skin and mucosal surfaces), intrinsic migratory capability and ability to activate naïve T cells, DCs are considered the most professional APCs. Targeting vaccine antigens to DCs would be a valuable strategy to exploit the unique abilities of these cells for antigen acquisition and display, leading to the initiation of robust antigen specific T cell responses.

Development of cancer vaccine formulations capable of delivering tumour antigens intracellularly into the MHC-I processing pathway would facilitate cross-presentation and the subsequent induction of anti-tumour CTL responses.

1.4. Targeting of DCs by vaccine delivery systems

The recognition of DC role in initiating T cell immune response, along with the development of protocols for the isolation and culture of large number of DCs *in vitro*, have sparked studies on the use of DC-based cancer vaccines.

1.4.1. Ex-vivo loading of DC-based cancer vaccines

In these strategies, monocytes are isolated from peripheral blood and cultured in the presence of granulocyte-macrophage colony stimulating factor (GM-CSF) and IL-4 to generate immature DCs [32]. Immature DCs are then loaded with tumour antigens through the addition of proteins [33], peptides [34-36] or tumour lysates [37] to culture medium or transfection of complementary DNA (cDNA) encoding tumour antigens [38]. The generation of DC-tumour cell hybrid is also reported [39]. To ensure the co-stimulatory capacity and the ability to induce potent antigen-specific cellular immune responses, loaded DCs are treated with various maturation stimuli such as: CD40L or pro-inflammatory cytokines [40]. The final step is the injection of fully loaded and mature DCs back into the patient through intravenous (i.v.), subcutaneous (s.c.), intradermal (i.d.), intratumoural (i.t.) or intralymphatic (i.l.) route of administration [41].

Ex-vivo loaded DC-based cancer vaccines have been extensively studied in a variety of experimental models and clinical trials (Reviewed in [42]). Over 60 different clinical studies have been carried out between 1996 and 2004, applying these vaccines[43].These studies have shown that this strategy is safe, well tolerated and capable of inducing cellular immune responses. However, the overall rate of objective clinical response in patients is only 7% [44]. One major concern is that, the migration of *ex-vivo* generated DCs to the lymph nodes is inefficient. Only 3-5% of the injected DCs could actually migrate to the lymph node for presenting the loaded antigen to T cells [45]. This can be improved by pre-conditioning of the vaccine injection site with pro-inflammatory cytokines such as Tumour Necrosis Factor- α (TNF-α) and/or IL-6. However, administration of these cytokines often leads to non-specific immune stimulation and undesirable side effects. There are numerous limitations of the *ex vivo* loaded DCs that truly

hinder their development for human use (reviewed in [42]). *Ex vivo* loaded DCs have to be tailor-made for each individual. Therefore, the process of vaccine development is time consuming, requires extensive lab work and is costly. The strategy is restricted to DC subsets that can be isolated in sufficient quantity or cultured *in vitro*. Besides, the excessive physical handling of DCs/precursors may increases the risk of endotoxin contamination. The half life of peptide/MHC complexes on the DC surface is relatively short. Furthermore, in addition to added proteins/peptide or tumour lysates, cultured DCs take up all sorts of proteins in the culture medium, decreasing the number of effective peptide/MHC complexes. Finally, the lack of standard culture/activation protocols for the generation of clinical grade DCs and existence of several variable parameters in the process (e.g. dose of DCs, route and frequency of administration) makes the process irreproducible with variable vaccine quality.

1.4.2. In vivo targeting of DCs using particulate-based cancer vaccines

The alternative improved strategy is to target DCs with tumour antigens along with appropriate adjuvants *in vivo* using particulate vaccine delivery systems. Such vaccines deliver antigens and maturation stimuli to the same cell enabling the usage of the intricate migratory capacity of DCs in their natural environment. Delivering both antigen and adjuvant coincidently to DCs will maximize the immune activation and limits the undesired toxicities that often result from systemic administration of adjuvants. Furthermore, the particulate delivery of antigens to DCs provides continuous supply of peptide to be presented by the newly formed MHC molecules on DC surface [46]. Particulate vaccine delivery systems can circumvent the extensive laboratory work that is needed to generate tailor-made DC vaccines for individual patients. With application of particulate cancer vaccines, clinical intervention is only limited to vaccine administration and there is no need for several cycles of blood withdrawal, cytapheresis, *in vitro* culture and DC administration [42]. Additionally this approach will provide on-shelf products, feasible large scale production with lower costs, equal product quality and accessibility to a large number of patients.

Particulate delivery systems include micro/nanoparticles, liposomes, archaeal lipid liposomes (archaeosomes), immune-stimulating complexes (ISOCOMs) and virus like particles (VLPs) [47]. Unlike other cancer vaccination strategies, most of particulate cancer vaccine delivery systems are still under development [21] and have not been extensively studied in clinic yet. A list of particulate cancer vaccines that passed the pre-clinical stage and are currently tested in human is given in **Table 1.1** [48-51]. Detailed description of various nano-sized particulate delivery systems has been extensively reviewed in [21, 47].

Table 1.1: Particulate cancer vaccines that passed the pre-clinical stage and are currently tested as therapeutic vaccines in human

DELIVERY SYSTEM	VACCINE	OBSERVED RESULTS
immune-stimulating complexes (ISOCOMs)	NY-ESO-1 ISCOMATRIX	NY-ESO1 positive melanoma patients receiving the vaccine had developed high antibody titre, strong $CD4^+/CD8^+$ T cell responses and less relapse compared to control groups [49] .
	HPV-16 E6E7 fusion protein/ ISCOMATRIX	Patients with cervical neoplasia receiving the vaccine have shown higher Ab titre, higher IFN-γ secretion and stronger activation of antigen specific $CD8^+$ responses [50].
Liposomes	L-BLP25: Liposomal formulation of BLP-25/MLPA	Patients with stage IIIB non-small-cell lung cancer that were immunized with L-BLP25 showed better survival trend than patients in the control group [51].
Gold particles	Gold particle coated with DNA for melanoma antigen and GM-CSF	The vaccine was well tolerated in melanoma patients (phase I clinical trial) with no risk of autoimmunity [48].

1.5. PLGA nanoparticles as vehicles for immunotherapy and immunomonitoring

The main focus of this section will be on the use of polymeric nanoparticles made of poly(D,L-lactic-co-glycolic acid) (PLGA). Those nanoparticles can be both as a competent vaccine delivery system capable of targeting DCs with cancer antigens along with adjuvants and also as a vehicle for carrying the immunomonitoring imaging probes.

1.5.1. PLGA composition and applications: an overview

PLGA is a FDA approved biodegradable and biocompatible polymer that had been widely used in the manufacturing of surgical sutures and in several

controlled release drug products for human use [52, 53]. PLGA co-polymers are aliphatic polyesters composed of varying proportions of lactic and glycolic acids. Upon encountering aqueous media, PLGA is hydrolyzed (degraded) into lactic and glycolic acid monomers (**Figure 1.3**), which are normal metabolites and well tolerated in the human body [54].

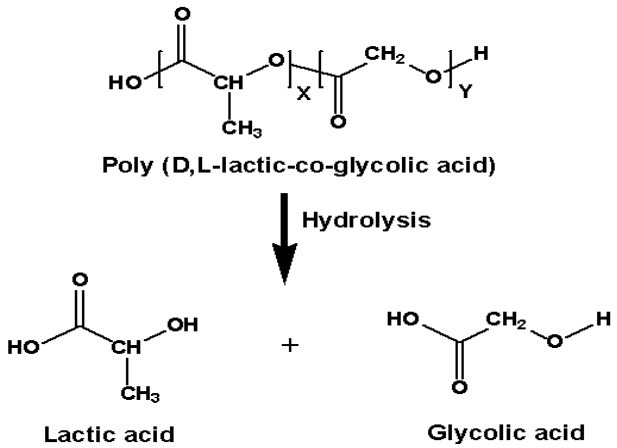

Figure 1.3: Chemical structure and biodegradation products of PLGA. X and Y represent number of units of lactic and glycolic acid, respectively. Degradation of the polymer occurs by non-enzymatic hydrolysis of the backbone ester linkages.

Several studies have employed PLGA co-polymer to fabricate micro/nanoparticles. These nanoparticles can entrap a wide range of biologically active compounds varying in their therapeutic indications (e.g. hormones, antibiotics, anti-cancer drugs). Many of these products are either marketed or in clinical trials (reviewed in [53]).

PLGA nano/micro particles are well suited for vaccine delivery. Numerous antigens (proteins, peptides, lipopeptides, viruses or plasmid DNA) have been successfully formulated in PLGA particles [46, 55-62]. Formulating antigens in PLGA nanoparticles offers distinct advantages over soluble formulations [63]. PLGA nanoparticles can protect the antigen from proteolytic degradation and deliver it to the phagocytic cells (mainly DCs) in a targeted and prolonged manner while restricting the entry of encapsulated antigen to the systemic circulation. Besides, particulate antigens are more efficiently cross-

presented than the soluble antigens. Furthermore, PLGA nanoparticles facilitate co-delivery of various immunomodulators to DCs. Tumour-induced impairment in DC functions is one of the leading causes of compromised anti-tumour immune responses [64]. Vaccine strategies that co-deliver cancer antigens along with TLR ligands to the same DC population, can not only target antigen to DCs, but also provide immune activation and rescue impaired DCs from immuosupression [65].

L-BLP25 is a cancer vaccine formulation originally developed by our research group in 1998 [66] and is currently in a phase III clinical trial. L-BLP25 consists of synthetic human MUC I 25-mer peptide and the immunoadjuvant MPLA both enclosed in a liposomal vehicle. Despite these promising results, there are drawbacks related to its liposomal formulation; such as tedious and expensive process of preparation, scale-up problems and difficulty in production of sterile products. In contrast to liposomes, the process of PLGA nanoparticle formulation and scaling-up are much easier and cost-effective [56]. In addition, the use of PLGA co-polymer provides additional advantage over liposomes, in terms of the ability to manipulate various physico-chemical properties of the carrier and tailor its rate of degradation and release profile.

1.5.2. Manipulating the physico-chemical properties of PLGA

PLGA is a polymer that goes through bulk erosion during its degradation. Bulk erosion refers to a biodegradation mechanism where the diffusion of water within the polymer mass is faster than the rate of covalent bond cleavage within the polymer chain. In this case, degradation takes place throughout the whole polymer matrix and continues until a critical molecular weight (MWt) is reached, at which the degradation products become small enough to be solubilized. At this stage, the structure start to become extensively porous and hydrated, and it is possible for encapsulated molecules of large MWt to be released from the polymer matrix. Therefore, for the release of high MWt materials from PLGA, usually lag phase is observed. The length of this lag phase corresponds to the time required to reach the porous PLGA particles [67, 68]. The degradation bulk erosion model of release is an advantage for vaccine delivery since it will hinder

the early release of large antigens or adjuvants before the nanoparticle is taken up by DCs and reduces the systemic distribution of encapsulated molecules. Once inside the acidic endosomal compartment of DCs, the PLGA degradation will be accelerated [69] and antigen/adjuvant will be released.

A major advantage of PLGA co-polymer is the ability to manipulate its physico-chemical properties in order to tailor its rate of degradation and the release profile of the encapsulated molecules. The rate of PLGA degradation depends mainly on the MWt, hydrophilicity and crystalinity of the polymer [70-72]. The smaller MWt and the more hydrophilic PLGA polymers, tend to increase the rate of polymer degradation. The hydrophilicity of the polymer is mainly influenced by the monomers' ratio used in its production and also the polymer type (carboxylic acid or ester chain end). Glycolic acid is more hydrophilic than lactic acid. Employing higher proportions of glycolic acid results in increased hydrophilicity and hence increased degradation rate of the nanoparticle formulation. One exception is the co-polymer with 50:50 glycolic:lactic acid ratio which has the fastest degradation rate (half-life ($t_{1/2}$) about 2 weeks) among PLGA polymers of different glycolic:lactic acid ratios even those with higher glycolic acid content [71]. This is due to the amorphous nature of PLGA 50:50.

PLGA end groups also have an influence on the hydrophilicity of polymer and release behaviour from the nanoparticle formulation. Two types of PLGA polymers were usually used for the preparation of nanoparticles: the more hydrophilic uncapped -or so called COOH-terminated PLGA- with a carboxylic acid end group and capped (ester-terminated) PLGA with a methyl ester end group. The presence of COOH end group may enhance the polymer and protein/drug interaction leading to more efficient encapsulation in nanoparticle formulations. Moreover, in contrast to more inert capped PLGA, uncapped polymer provides the possibility of a stable attachment of polymer to incorporated molecules through a covalent bond. However, variable release has been reported from uncapped polymer [73, 74]. In both PLGA types, the large surface area of nanoparticles allows for increased protein load by adsorption [46, 60].

The rate of polymer degradation can also be manipulated by changing the ratio of crystalline:amorphous regions, which in turn depends on polymer stereochemistry. Because L-lactic acid is crystalline, nanoparticle formulations employing L-lactic acid have slower rate of degradation. However, the D, L lactic acid is preferred as it forms an amorphous polymer where in the encapsulated molecules are homogeneously dispersed within the polymeric matrix [56].

At 50:50 glycolic:lactic acid ratio, PLGA polymer has the least crystalinity in its structure and is more prone to hydrolysis and degradation than other PLGA polymers with lower or higher glycolic:lactic acid ratios.

1.6. Targeting DCs using PLGA nano/ micro particles in cancer immunotherapy

1.6.1. Passive targeting of DCs

Plain PLGA nano/ micro particles are taken up by human and mouse DCs [75-79]. Without specific recognition, PLGA nanoparticles are targeted to DCs and are subject to uptake as their size is comparable to that of pathogens (passive targeting). Uptake of plain PLGA nanoparticles by *in vitro*-generated immature DCs had been investigated using human peripheral blood-monocytes-derived DCs [77], human cord-blood $CD34^+$ stem cells-derived DCs [75] and mouse bone marrow-derived DCs [78]. The results have shown that more than 90% of DCs are able to internalize plain PLGA nanoparticles within 24h incubation. This observation was supported by electron microscopy studies, where membrane ruffling around the internalized particle was visualized [75]. The uptake of plain PLGA nanoparticles by DCs was abolished by inhibiting actin polymerization [78]; pointing to the involvement of actin polymerization in uptake. Intracellular localization had been confirmed by confocal microscopy [78].

The site of administration was shown to significantly affect the type of cells internalizing the particles in mice. Administration of PLGA nanoparticles either i.d. [80] or s.c. [81] results in their uptake by DCs. In contrast, following i.p. administration, PLGA particles were found in CD14 (macrophage marker)

positive cells and macrophages were found to be the predominant cells internalizing PLGA nanoparticles in the peritoneal cavity [54].

DCs and macrophages are highly phagocytic cells, capable of taking up any particles with similar dimensions to the pathogens (up to 10 μm). However, for targeting vaccine antigens to DCs, nanoparticles are more preferred than microparticles. Earlier studies had shown that DCs preferentially take up smaller particles in the viral size range, whereas macrophages ingest more of the bigger, bacterial size particles [82]. PLGA nanoparticles (<500 nm) were more effective than microparticles (> 2um) in stimulating CTL responses *in* vivo [83]. The large surface area of the nanoparticles allows faster degradation and rapid release of the encapsulated antigens inside the phagosome. The uptake of PLGA nano/microparticles is also affected by surface charge. Cationic particles are more effective for uptake by DCs and macrophages. The ionic attraction between the positively charged particles and the negatively charged cell surface initiates efficient binding and facilitate particle internalization [84]. However, the uptake of positively charged particles is less specific than the negatively charged ones.

1.6.2. Active targeting of DC-expressed pattern-recognition receptors

The innate immune system functions to protect the host in the first hours of infection and this is primarily achieved by professional APCs particularly DCs engulfing the invading organisms and degrading them within the phagolysosome/lysosome. This process requires that DCs express receptors termed “pattern recognition receptors” (PRRs) on their cell surface which can recognise a wide range of conserved motifs in pathogens and/or ligands termed “pathogen-associated molecular patterns” (PAMPs). Reis e Sousa and colleagues show that DCs activated by pro-inflammatory cytokines are not equivalent to those activated by PRRs. The authors speculate that DCs activated by cytokines induce tolerance rather than protective immunity [85].

Logically the DC surface molecule to be targeted should be as DC-specific as possible, to reduce the dose of antigen required. Binding to other cells could "mop up" the injected vaccine, as well as cause unwanted side effects. Ideally the

surface molecule targeted should be an endocytic receptor, and there is evidence that different receptors can shuttle antigens into different processing pathways [86]. The well-identified PRPs found in DCs are Toll-like receptors, Scavenger receptors and C-type lectin receptors, described below.

1.6.2.1. Toll-like receptors (TLRs)

TLRs are a family of non-endocytic PRRs which directly or in collaboration with other molecules play an essential role in innate recognition of PAMPS, and in the triggering of adaptive immunity in higher organisms alike. In 1996, insect Toll has been shown to be essential for anti-fungal immunity. This finding led to identification of TLRs in mammals. Ten mammalian TLRs (TLR1–10) have been identified to date **(Figure 1.4)** [87].

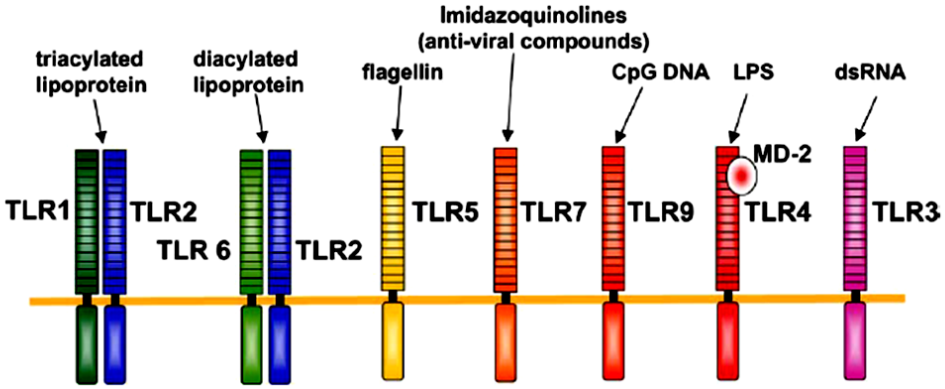

Figure 1.4: TLRs and their ligands. TLR2 is essential for recognition of microbial lipopeptides. TLR1 and TLR6 associate with TLR2, and discriminate differences between triacyl- and diacyl lipopeptides. TLR4 recognizes LPS. TLR9 is the CpG DNA receptor and TLR3 is implicated in the recognition of viral dsRNA. TLR5 is a receptor for flagellin.

The significance of TLRs in activating adaptive immunity is well established; TLR-mediated activation of DCs is a crucial step in this process [88, 89]. The control exerted by TLRs in linking innate and adaptive immunity is instrumental in the efficacy of vaccines containing TLR ligands. TLR ligands enhance vaccine efficacy through multiple mechanisms: TLR stimulation of DCs results in an increase in surface peptide/MHC complexes, co-stimulatory molecules, and cytokine secretion; the three signals required for T cell activation

and proliferation [85]. Moreover, enhanced cross-presentation of exogenous vaccine antigens has been demonstrated. Remarkably, TLR activated DCs are also capable of reversing the Treg suppressive effects [90]. Particulate delivery of TLR ligands offers several advantages over their administration in a soluble form. When antigens co-delivered with TLR ligands to the same population of DCs, antigenic peptide presentation on MHC is augmented. Up-regulation of co-stimulatory and MHC molecules, expression of chemokine receptors, secretion of cytokines and chemokines are further accelerated in TLR-activated DCs. Vaccine strategies utilizing nanoscale particulate delivery systems to aim at co-delivery of both antigen and TLR ligands coincidently to DCs could provide immune system activation and also rescue impaired DCs from tumour-induced immuosupression. These strategies also facilitate simultaneous delivery of more than one PRP ligand in the same formulation and could facilitate a sustained TLR signalling in DCs to overcome tumour-induced immuosupression mediated by Treg cells [44] and avoid the need of repeated administration or high dosages of TLR ligands. To date, various TLR ligands have been successfully incorporated into PLGA nanoparticles along with antigens in cancer vaccines (**Table 1.2)**.

Table 1.2: A list of studies that have shown superior DC and/or T cells activation when antigens are co-delivered in PLGA nanoparticles with TLR ligands.

TYPE OF CANCER ANTIGEN	TLR LIGANDS	REFERENCE
Melanoma lysate	TLR9 ligand: CpG	[91]
TRP2	TLR4 ligand: 7-acyl lipid A	[91]
MUC1 lipopeptide	TLR4 ligand: MPLA	[75, 78, 92]

1.6.2.2. Scavenger receptors (SRs)

Scavenger receptors are transmembrane PRPs present on the surface of phagocytes facilitating phagocytosis by recognition of negatively charged ligands and/or ligands with lipid moieties such as lipoproteins and lipopolysaccharides. SRs are shown to be involved in adhesion, phagocytosis of apoptotic cells and

protection from endotoxic shock in mice [93]. SRs do not induce production of pro-inflammatory cytokines by themselves [94].

1.6.2.3. C-type lectin receptors (CLRs)

CLRs are one of the PRRs that are expressed in high levels by APCs and have been known as receptors involved in initial recognition and subsequent uptake of antigens by DCs. This function is absolutely crucial for establishing a balanced immune response in favour of immunity rather than tolerance. To date, more than 60 CLRs are identified in human [95].

The term “C-type lectin” was originally introduced to distinguish a family of Ca^{2+}-dependent (C-type) carbohydrate-binding (lectins) proteins from the Ca^{2+}-independent types [96, 97]. C-type lectins were among the first animal lectins discovered. Bovine conglutinin (a collectin) has been identified since 1906, and activity of the snake venom lectins was described in 1860 [97].

When the structures of C-type lectins were established biochemically and functions of different domains were defined, it was revealed that carbohydrate-binding activity was attributed to a compact structural module that contains conserved residue motifs and determines the carbohydrate specificity of the CLR [5]. Classification of lectins and recognition of endogenous and exogenous carbohydrate residues by CLRs was through this domain called carbohydrate recognition domain (CRD) [97, 98]. Although the hallmark of classical CLRs is the dependence on Ca^{2+} ions for carbohydrate recognition through CRD [99-101], for some of the members of this super-family evident Ca^{2+} binding or carbohydrate specificity has not yet been demonstrated [102].To resolve the contradiction, a more general term of C-type lectin (-like) domain(s) (CTLD) was introduced. What all the members of this large and heterogeneous family of proteins have in common is the presence of one or more CTLD domains [103]. CTLDs selectively bind to a wide variety of ligands.

Table 1.3: Characteristics of DC-expressed C-type lectin receptors [96, 98]

CLR	Expression	Glycan ligands (PAMPs)	Main pathogenic (exogenous) ligands	Main immunological outcome
Group I CLRs (mannose receptor family)				
Mannose receptor (CD206)	Myeloid DCs and macrophages	High mannose (e.g. mannan in yeast cell wall), fucose& sulfated sugars (sLeX)	M. tuberculosis, C. Albicans; K. pneumonia; S. Pneumonia; HIV-1 & dengue virus; P. carinii	Endocytosis, phagocytosis and antigen presentation
DEC205 (LY75, CD205	Myeloid DCs	ND	ND	Endocytosis and antigen presentation
Group II CLRs (asialoglycoprotein receptor family)				
DC-SIGN (CD209)	Myeloid DCs,	High mannose (e.g. mannan) and fucose (LeX, LeY, LeA, LeB),	M. tuberculosis, M. leprae, H. pylori, HIV-1, measles virus, dengue virus, C. albicans, BCG, leishmania spp, S. mansoni	Upregulation of TLR-induced IL-10 production, induction of TH_1,TH_2,TH_{17} ,T_{reg} and inhibition of TH_1 cell differentiation, Ag presentation
Langerin (CLEC4K, CD207)	Langerhans cells and dermal DC subset	High mannose, fucose and GlcNAc	M. leprae, HIV-1	M. Leprae endocytosis and Ag presentation; HIV-1 uptake and degradation
MGL (CLEC10A, CD301)	Myeloid DCs and macrophages	Terminal GalNAc (Tn Ag, LDN)	Filoviruses and S. mansoni	ND
Group II CLRs (asialoglycoprotein receptor family; Dectin-1 subfamily)				
Dectin-1 (CLEC7A)	Myeloid DCs, monocytes, B cells and macrophages	β-1,3-glucan	M. tuberculosis, C. albicans, A. fumigates, P. mameffei, P. carinii,	induction of TH_1 &TH_{17} cell differentiation; phagocytosis; induction of TNF & CXCL2 production;
MICL (CLEC12A, DCAL2)	Myeloid DCs, monocytes, macrophages & neutrophiles	ND	ND	Inhibition of TLR4-induced IL-12 production
DNGR1 (CLEC9A	DCs, monocytes and B cells	ND	ND	Induction of TNF production; Antigen cross presentation
Group II CLRs (asialoglycoprotein receptor family; DCIR subfamily)				
Dectin-2 (CLEC6A)	Myeloid DCs, pDCs. monocytes, B cells, macrophages and neutrophiles	High mannose	M. tuberculosis; C. albicans; A.fumigatus; M. audouinii	Induction of TNF and IL-6 production; cysteinyl leukotriene synthesis
BDCA2 (CLEC4C, CD303)	pDCs, monocytes, macrophages and and neutrophiles	ND	ND	Inhibition of TLR-9-induced type I IFN, TNF and IL-6 production; Upregulation of TLR-9-induced IL-10 production
Mincle (CLEC4E)	Myeloid DCs, monocytes and macrophages	α-mannose	Malassezia spp	Induction of TNF, IL-10; CXCL2 production
DCIR (CLEC4A)	Myeloid DCs, pDCs; monocytes; macrophages; B cells; nutrophiles	ND	HIV-1	Inhibition of TLR8-induced TNF & IL_12 production; inhibition of TNF & IFNα production
DCAR	BM-DCs	ND	ND	Cell activating receptor through association with Fcγ receptor [105]

Abbreviations: *Mycobacterium tuberculosis (M. tuberculosis), Candida albicans (C. albicans), Helicobacter pylori (H. pylori), Schistosoma mansoni (S. mansoni), Aspergillus fumigates (A. fumigates), Pneumocystis carinii (P. Carinii), Penicillium marneffei (P. marneffei), Microsporum audouinii (M. audouinii), Mycobacterium lepeae (M. leprae), Klebssiela pneumonia (K. pneumonia), Streptococcus pneumonia (S. pneumonia), human immunodeficiency virus-1 (HIV-1).*

The CLR super family is divided into 17 groups based on their phylogeny and domain organisation. Despite the presence of a highly conserved domain, CLRs are functionally diverse and have been implicated in various processes such as endocytosis, phagocytosis, pathogen recognition, complement activation, cell adhesion, tissue integration and platelet activation [102] **(Table 1.3).**

C-type lectins form oligomers within the cell membrane to strengthen and limit binding to a specific structure with a certain carbohydrate density and spacing of ligand. This indicates that CLRs, which have similar basic carbohydrate specificities, can interact with a very diverse set of ligands. By binding to carbohydrate moieties, CLRs mediate biological events [104].

Two types of CLRS present on DCs designated as type I and type II [98]. The type I (also noted as mannose receptor family) involve type I transmembrane proteins with an N-terminal cysteine-rich (CR) domain, a fibronectin type II (FNII) domain, multiple CTLDs (eight or 10) in the extracellular domain, and a short cytoplasmic domain. Representatives of this type are mannose receptor (MR) and lymphocyte antigen 75 (DEC-205) [106] (**Figure 1.5**).

The type II is characterized by a short cytoplasmic tail, a transmembrane domain, an extracellular stalk region, and a Ca^{2+}⁄ carbohydrate binding CTLD. The length of the stalk region varies among the different members and is involved in oligomerization. The classical members of type II of CLRs include DC-specific ICAM-3 grabbing non-integrin (DC-SIGN) (**Figure 1.5**), MF galactose N-acetyl-galactosamine specific lectin 1 (MGL), Langerhans cell specific C-type lectin (Langerin), MF-inducible C-type lectin (Mincle), DC-associated C-type lectin-2 (Dectin-2), blood DC antigen-2 (BDCA-2), DC- immunoreceptor (DCIR), and DC immunoactivating receptor (DCAR). The non-classical members including DC-NK lectin group receptor-1 (DNGR-1), DC-associated lectin-1 (DCL-1), DCL-2, and Dectin-1 (**Figure 1.5**) are similar in structure to classical ones, although their CTLD does not bind Ca^{2+} [9].

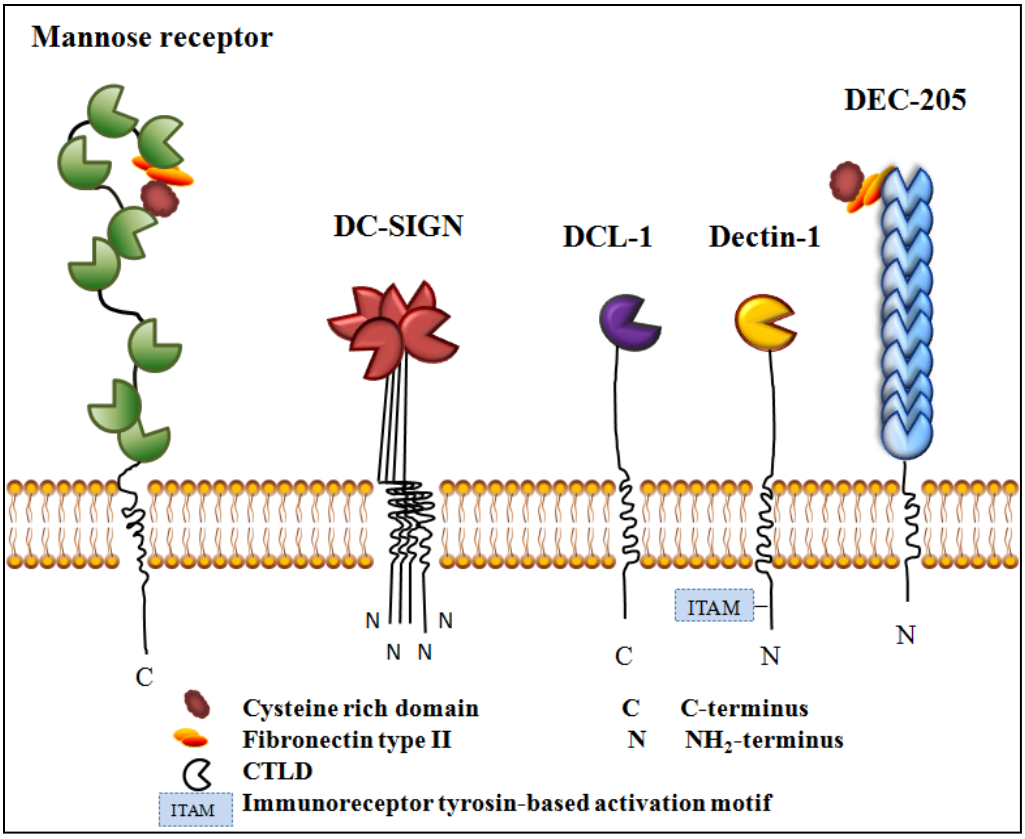

Figure 1.5: Cartoon representation of typical CLRs expressed by DCs: MR (bent confirmation with 8 CRDs); DC-SIGN (multimerization); DCL-1 (only one CRD); Dectin-1 (Ca^{2+} independent); DEC-205 (large type with 10 CRDs).

1.6.2.4. CLRs and DC internalization

CLRs were initially emerged as a powerful tool for DC internalization and called endocytic receptors or antigen-uptake receptors [97]. Immature DCs express a large variety of CLRs, which are often down-regulated upon maturation. Recognition of exogenous ligands by CLRs is important for their internalization and degradation for innate immune protection.

The term “endocytosis” includes several mechanisms by which cells internalize micromolecules into transport vesicles derived from the plasma membrane. It controls entry into the cell and has a crucial role in development of immune responses, cell-cell interaction and signalling [107]. DCs can internalize antigens via macropinocytosis, phagocytosis and clathrin-mediated endocytosis (previously referred to as receptor-mediated endocytosis) [107-110] **(Figure 1.6)**.

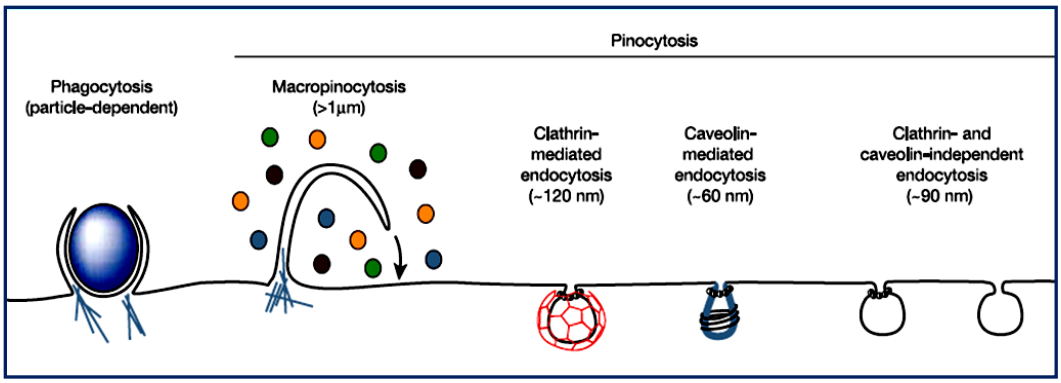

Figure 1.6: Various endocytic pathways in mammalian cells. These pathways differ with regard to the size of the endocytic vesicle, the nature of the cargo (ligands, receptors and lipids) and the mechanism of vesicle formation. Immature DCs in the periphery are specialized in a variety of mechanisms including phagocytosis, macropinocytosis and clathrin-mediated endocytosis.

Macropinocytosis is a form of high-volume; non-specific internalization that involves extension of membrane ruffles **(Figure 1.6**). Immature DCs are the only cells that constitutively carry out macropinocytosis [108], which contributes to antigen (1-5 μm in diameter) uptake and targeting into the MHC-I and MHC-II-restricted antigen presentation pathways [110].

Clathrin-mediated endocytosis is the mechanism by which eukaryotic cells internalise molecules such as antigens and enzymes through clathrin coated pits in the membrane **(Figure 1.6).** Small particles (<150 nm in diameter) [108] which bind to their cognate endocytic receptors are prone to uptake by this pathway. The size of the vesicles is restrained by the proportions of the clathrin coat [109].

Clathrin-mediated endocytosis in DCs includes the endocytosis of receptors such as transferrin receptor and CLRs. Receptors such as MR, DEC-205, DC-SIGN, MGL, Langerin, Dectin-1 and Mincle are all capable of internalizing glycosylated antigens [104]. Several CLRs have been demonstrated to target these endocytosed antigens for loading on MHC-I and MHC-II molecules, to induce antigen-specific CD4 and CD8 T-cell responses [111, 112].

It has been estimated that constitutively endocytosed receptors such as MR family members, mediate 10 or more rounds of recycling each hour. Clathrin-mediated internalisation requires a ‘‘signal’’ within the cytoplasmic domain that

allows association of the transmembrane proteins with adaptor complexes [113]. The adaptor proteins not only link the receptors to the clathrin molecules but also recruit the transmembrane receptors to the clathrin-coated pits [113]. Once recruited into those pits, the receptor is automatically internalised into early endosomes (**Figure 1.7)**. At this stage, receptors must be separated and either targeted for budding off into recycling vesicles (which will fuse with the plasma membrane), or into vesicles for transport to the late endosomes. Late endosomes are characterised by abundant intravesicular membranes and the presence of lysosomal hydrolases. The relationship between the late endosomes and the lysosomes is dynamic with the lysosomes representing the final degradative compartment of internalised cargo **(Figure 1.7)** [113]. Whether recycling from the early endosome is a signal-dependent mechanism in not answered yet [114].

By contrast, the other major mechanism for receptor-mediated internalisation of extracellular components into DCs, phagocytosis, refers to the uptake of large particles (>0.5 μm in diameter) [108]. It is an active and highly regulated process involving specific cell-surface receptors and signalling cascades and plays a critical role in innate immunity and tissue remodelling. In addition to the size of the material internalised, clathrin-mediated endocytosis and phagocytosis are mechanistically and functionally distinct **(Figure 1.7**) [110]. The best characterised phagocytic receptors are the Fcγ receptor (FcγR) and complement-3 (CR3) receptors [102]. Engagement of these receptors initiates a phagocytic stimulus in the cells resulting in localised polymerisation of actin and extension of the membrane to engulf the particle into an intracellular phagosome [110]. During FcγR-mediated phagocytosis, actin-rich pseudopodia extend circumferentially around the particle and draw it into the cell forming a tight-fitting ‘‘zippered’’ phagosome [102]. These phagosomes rapidly fuse with the endosomes and/or lysosomes in the cells to expose their contents to the hydrolytic enzymes (**Figure 1.7**) [109]. In addition to these receptors, there is strong evidence that other receptors such as MR, DEC-205, DC-SIGN, MGL, DCL-1, Langerin, Dectin-1 and Mincle can mediate phagocytosis of glycosylated antigens in an actin-dependent manner (**Figure 1.8**) [102, 104]. The mechanisms of

phagocytosis by CLRs are not very well characterised but are clearly complex and appear to be unique to each receptor [102]. Most studies have focused on particular receptors in isolation, but mechanism of uptake in phagocytes will be a result of the collective contribution of the several receptors involved.

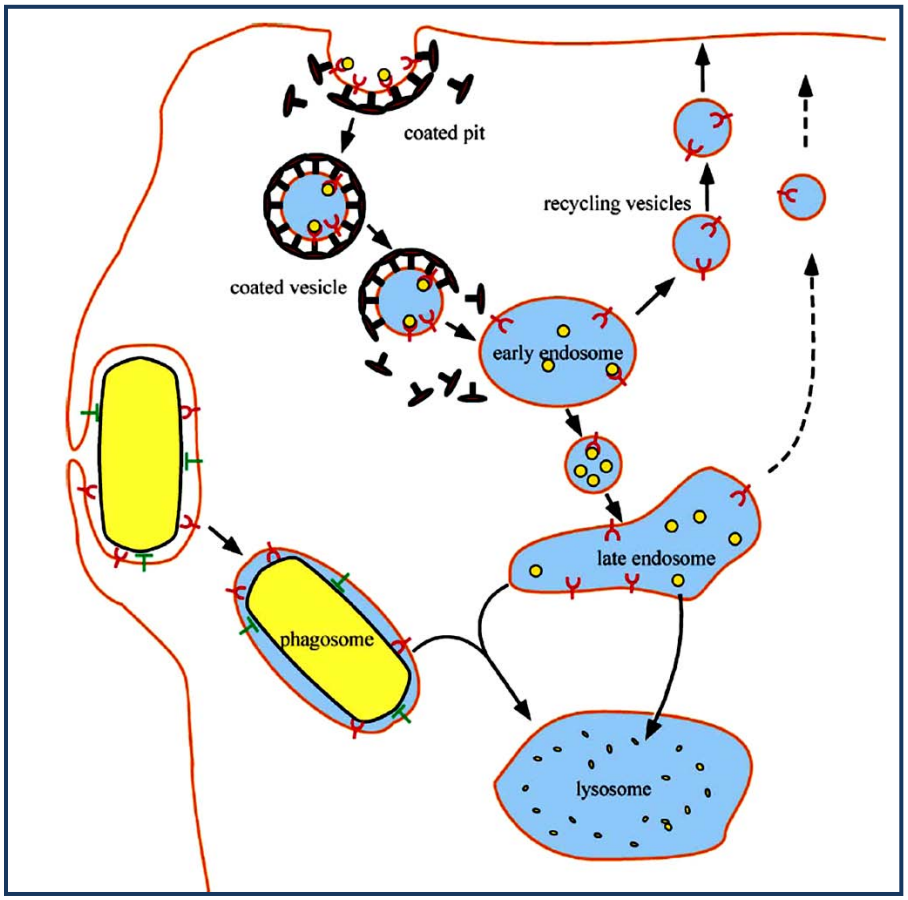

Figure 1.7: Endocytic and phagocytic pathways. The receptor is recruited into coated pits via motifs in cytoplasmic domains. These internalise to give coated vesicles which rapidly uncoat and generate the early endosomes. The early endosome is a sorting site where recycling receptors are targeted back to cell surface. The low pH of these compartments will result in ligand/receptor dissociation. Phagocytosis involves recognition following by actin-dependent membrane movement to engulf the phagocytic particle. The resulting phagosome matures by a series of events to form a phagolysosome.

1.6.2.5. CLRs and signalling

The expression of CLRs on immature DCs is linked to the function of DCs: capture antigen for further processing and presentation onto MHC-I and MHC-II molecules and subsequent T-cell activation. Antigen presentation by DCs

is not itself sufficient to induce effective T cell responses against pathogens: $CD4^+$ T cells need to differentiate into distinct TH cell subsets depending on the type of infection. In fact, pathogen recognition is central to the induction of T cell differentiation and DCs need to translate information about the invading pathogen into a cytokine gene expression profile that directs the correct TH cell pathway. DCs can receive direct maturation signals through several pathways including TLRs and CLRs **(Figure 1.8**). Although CLRs have primarily known as endocytic PRRs, some CLRs possess intrinsic signalling properties and are capable of modulating immune reactions (**Table 1.3 and Figure 1.8**).

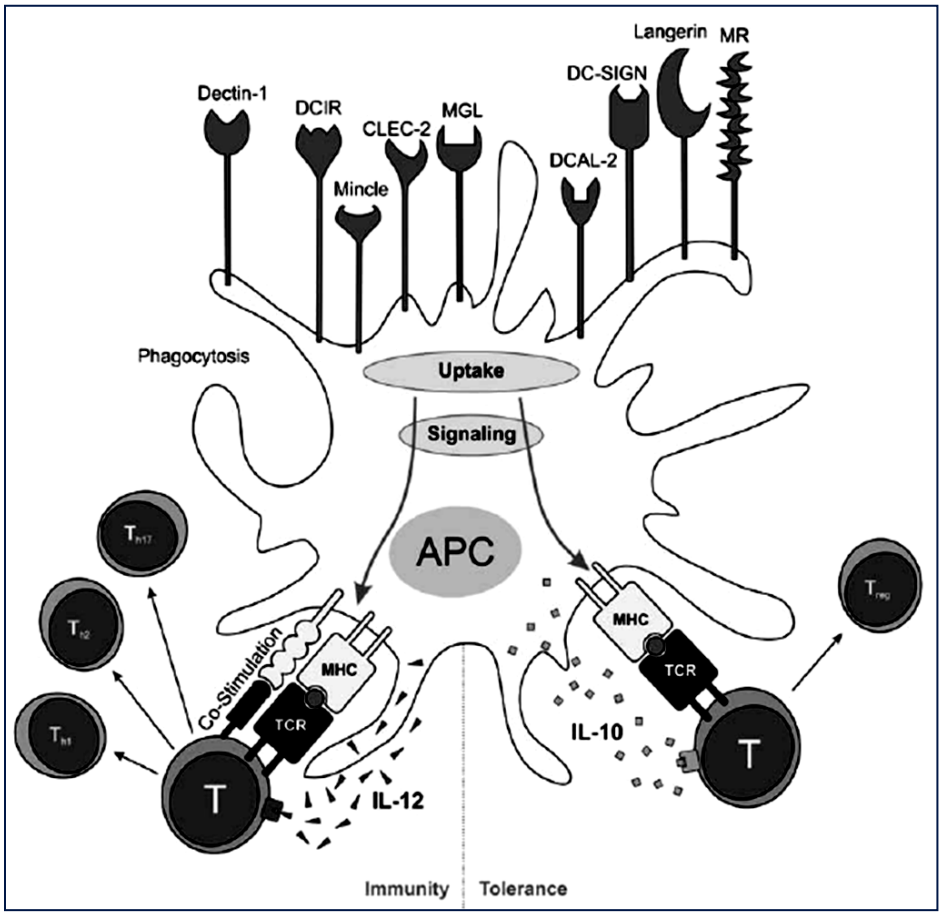

Figure 1.8: Innate function of CLRs in antigen uptake and signalling processes in APCs. CLRs can function as signalling molecules that trigger specific cytokines. In the presence of TLR signalling, co-stimulatory molecules are upregulated, and antigen uptake and presentation through CLRs can initiate immunity through T cell stimulation (TH_1, TH_2 or TH_{17}). In the absence of any danger signals and co-stimulation, uptake of antigen through CLRs leads to presentation to T cells and development of tolerance through Treg cells.

Recent studies have identified CLRs as important PRRs involved in the induction of specific gene expression profiles to specific pathogens, either by modulating TLR signalling or by directly inducing gene expression [96]. CLR triggering by different pathogens can induce diverse immune responses **(Table1.3**). The signalling processes are complex and depend on cross-talk with other PRRs (particularly TLRs), the ligand and the DC subset [96]. TLR activation in turn leads to upregulation of maturation markers and production of pro-inflammatory cytokines. Combined triggering of certain CLRs and TLR4 results in enhanced IL-10 secretion that can modulate the TH_1/TH_2 balance. The close link between certain CLRs and TLR2 tends to enhanced production of TNF-α and IL-12 **(Figure 1.9**) [115].

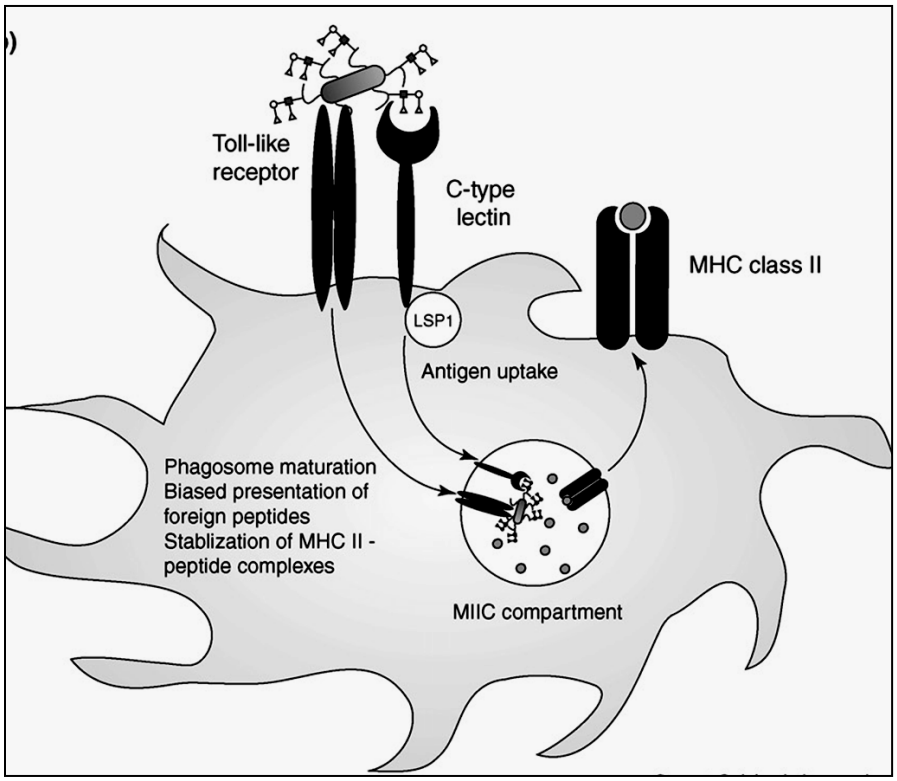

Figure 1.9: Cross-talk between TLRs and CLRs in DCs. TLR-mediated signalling augments presentation of antigens endocytosed by CLRs. CLRs participate in the uptake and subsequent degradation of antigens for presentation in MHC molecules. If TLRs and CLRs are transported to identical compartments after antigen uptake, TLR activation can induce phagosome maturation. Accompanied TLR triggering promotes presentation of foreign antigenic peptides and stabilizes MHC-peptide complexes at the cell surface [115].

To shape immune responses, it may be very important that TLRs and CLRs communicate to direct the antigen for antigen processing and efficient loading on MHC if the antigen is pathogenic and not a self-antigen [115].

Recent studies suggest that there are two general ways by which CLRs induce signalling pathways. CLRs such as Mincle, Dectin-2 and BDCA2 are associated with and induce signalling pathways through immunoreceptor tyrosine‑based activation motif (ITAM), containing adaptor molecules such as FcγRs [96, 115]. Some other CLRs, such as Dectin-1, DC-SIGN, DCIR and MICL induce signalling pathways through the activation of protein kinases or phosphatases interacting with their cytoplasmic domains [96, 116].

CLRs vary based on their capability to induce signalling independently or linked to other PRRs. Several CLRs, such as DC-SIGN, BDCA2, DCIR and MICL, induce signalling pathways that modulate TLR‑induced gene expression at the transcriptional level. By contrast, other CLRs, such as Dectin-1, Dectin-2 and Mincle, induce gene expression following carbohydrate recognition independently of other PRRs. The transcription factor nuclear factor-κB (NF-κB) is a key mediator of inducible gene expression in the immune system, although many other transcription factors have an equally essential role.

1.6.2.6. CLRs and cancer immunotherapy

The activation and antigen presentation by DCs, in particular, plays a key role in the initiation of anti-tumour responses. However, tumour cells use several strategies to dampen both antigen presentation and T-cell responses initiated by DCs. TAAs interacting with DCs may modify DC function (such as production of immunosuppressive cytokines) or inhibit DC migration to tumour sites. TAAs are often auto-antigens that become deregulated, and changes in glycosylation often accompany on co-transformation. These changes include increased expression of the Lewis family of antigens (serum tumour markers in diagnosis of cancer). Good examples of aberrant glycosylated tumour antigens are epithelial Mucin 1 (MUC1) and carcinoembryonic antigen (CEA), which can be secreted or expressed by cancer cells. The alteration of carbohydrates on the cell surface

during carcinogenesis might also influence the interaction with CLRs on resident APCs. Indeed, some of the tumour glycans are ligands for CLRs [117]. Previous findings have demonstrated that DCs recognize these modified glycosylations on CEA or MUC1 through CLRs such as DC-SIGN and MGL, respectively, while these CLRs do not interact with 'normal' CEA or MUC1[118, 119]. At first sight, this may be an adequate system for immune surveillance with the aim of early detection and removal of cells with aberrant glycosylation, similar to the recognition of microbial glycans. However, tumour carbohydrates might manipulate DCs through CLRs to escape from immune surveillance. Therefore, tumours that contain CLR-targeting glycan structures within their tumour antigens might create an immunosuppressive microenvironment that contains DCs of immature phenotype (**Figure 1.10a**) [117]. The altered glycosylation of tumours has been a target for therapy development for a long time. This is not surprising, as a vaccine that triggers an immune response against a tumour-specific carbohydrate structure would be widely applicable. Tumour glycans are not very immunogenic, however, and so far are not as effective as vaccines in eliminating tumours [120].

Today, immunotherapy against cancer mainly focuses on the induction of CTLs against tumour specific peptides. DC vaccine strategies are of particular interest due to the critical role of DCs for induction of CTL responses. In fact a more direct strategy is needed to target antigens to cell-specific receptors DCs, *in vivo*. Some CLRs are interesting candidates for targeted immunotherapy because of their cell-restricted expression pattern and their function to facilitate antigen uptake in DCs. In fact, delivery of TLRs and CLRs together in a vaccine, would suppress a tolerogenic response (**Figure 1.10b**).

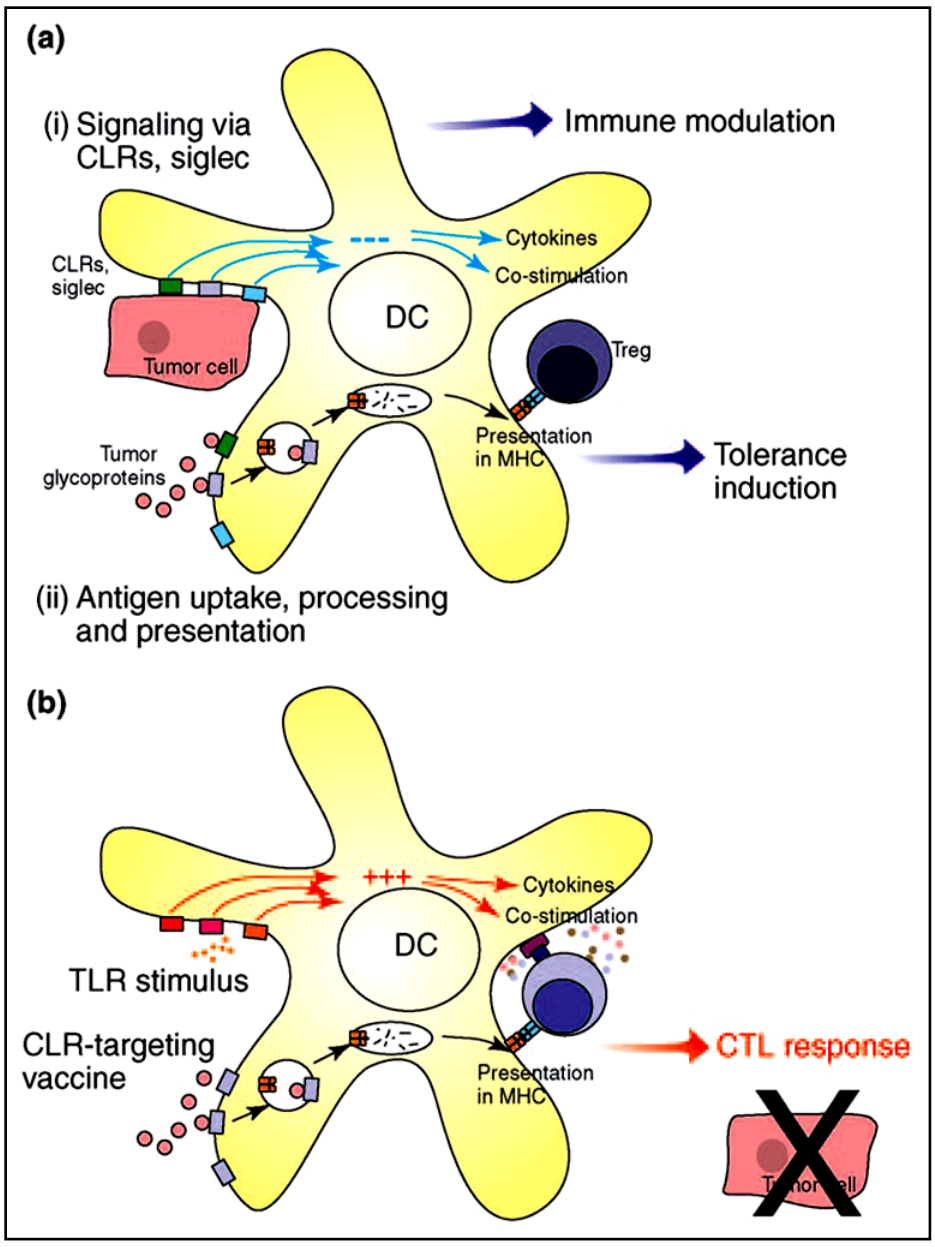

Figure 1.10: A model for the interaction of tumour glycans with CLRs on DCs. (a) Tumour environment: absence of TLR signals. Possible consequences are (i) down-modulation of immune response via CLR signalling and (ii) tumour glycoproteins that bind to CLR are internalized, processed and presented, but in the absence of inflammatory signals via TLRs, tolerogenic T cells will be induced. (b) Vaccination: CLR targeting and TLR stimulus. The tissue-specific distribution of CLRs and their function in antigen uptake make them good candidates for *in vivo* targeting of DCs for immunotherapy. The inclusion of TLR stimuli in the vaccine will tip the balance towards anti-cancer immunity[117].

Targeting CLRs on DCs are a fertile area of research for immunomodulation and several studies demonstrated that immunoresponses were induced or modified by coupling CLR ligands to particles or proteins. To actively target DCs and enhance internalization, ligands of CLRs can be used to decorate the surface of PLGA nanoparticles (e.g. mannose grafted-nanoparticles). PLGA nanoparticles can also be conjugated with DC-specific antibodies (e.g. anti DEC-205 and anti DNGR1). Interaction between PLGA nanoparticles attached ligand and/or antibody with CLRs could improve the specificity of nanoparticles for DCs [121, 122]. The attachment of targeting moieties on PLGA surface can not only facilitate the uptake of nanoparticles by DCs, but can also enhance DC maturation and ultimately lead to improving the effectiveness of vaccine formulation (the induction of immune responses will discuss in the next section). In fact, the engineered PLGA nanoparticles that are attached to several DC-specific antibodies (e.g. anti-CD40, Fcγ, α(v)β3 and α(v)β5 integrin receptors) either by physical adsorption or chemical conjugation have demonstrated a superior ability to induce DC maturation as evidenced by the increase in IL-2 secretion and the up-regulation of DC maturation markers (CD83 and CD86) compared to the plain PLGA nanoparticles [123].

It has become clear that targeting of CLRs is a powerful method to enhance antigen presentation and, depending on the CLR that is targeted, can determine whether the antigen is presented in the context of MHC-I or MHC-II molecules or both. MHC-I presentation is crucial for inducing strong $CD8^+$ T cell responses, which are necessary for immunity to cancer. Several studies have demonstrated that targeting antigens to CLRs can result in strong anti-tumour responses. An elegant study demonstrated that *in vivo* and *ex-vivo* targeting of MRs with oxidized mannan conjugated to MUC1 induces potent MHC-restricted CTL and tumour protection in mouse [124]. Moreover, Pilot phase III immunotherapy study in early-stage breast cancer patients using oxidized mannan-MUC1 supported the effectiveness of this strategy [125]. In addition, it is evidenced that *in vivo* targeting of antigen to human MR can lead to enhanced humoral and cellular responses sufficient to induce tumour immunity [126].

Another study demonstrated *in vivo* targeting of CLRs in the mouse can induce antigen-specific auto-immunity, when the antigen was coupled to an anti-DEC-205 antibody [127]. In contrast, when antigen coupled to DEC-205 was simultaneously combined with a strong DC activator such as a TLR stimulus, a strong antigen-specific immune activation was induced that resulted in an anti-tumour response and clearance of the tumour [95].

Furthermore, a very recent study showed antigen epitopes covalently coupled to an antibody specific for a mouse CLR (DNGR-1) were selectively cross-presented by CD8+ DCs *in vivo* and, when given with adjuvants, induced potent CTL responses that could mediate eradication or prevent development of cancer cells [128].

Still, other CLRs have also been used for targeting purposes, resulting in strong induction of immunity. However, differences can be observed between CLRs that are targeted with antigens, as some are more prone to induce $CD4^+$ T-cell responses, whereas others process antigens in such a way that strong $CD8^+$ T-cell responses are induced. Clearly, this indicates that the interplay and balance between CLR and TLR signalling is crucial for the outcome of any immune response and may lead to the induction of either tolerance or immunity.

The most-identified CLRs that are candidates for DC targeting include MR [115,116], DC-SIGN [129], DEC-205 [72], Dectin-1 and DNGR1 [103].

A) DC-SIGN

DC-SIGN is a type II transmembrane receptor originally cloned from a placental library capable of binding to the HIV-1 envelope [130]. It was 'rediscovered' later as a cell-adhesion receptor with a DC-restricted expression that supports primary immune responses and enhanced HIV infection of $CD4^+$ T cells [131]. DC-SIGN is expressed by immature DCs in peripheral tissue as well as mature DCs in lymphoid tissues (such as lymph nodes, tonsils, and spleen), but not by follicular DCs or Langerhans cells [132]. DC-SIGN contains a Ca^{2+}-dependent mannose-binding CTLD with a dual specificity for high-mannose and fucose as well as Lewis-type structures. There seems to be dissociation in the type

of carbohydrates recognized by DC-SIGN on endogenous ligands and on pathogens. Though there is no preference in the type of carbohydrates used to recognize pathogens, the preferred carbohydrates on endogenous ligands are the Lewis-type structures [133]. It has been proposed that aberrantly expressed mannose-containing glycans could act as a trigger for an innate immune response mediated by mannose specific CLR, programmed to recognize high-mannose glycans as a PAMP [134]. Carbohydrate recognition plays a central role in the DC-SIGN binding of pathogens. Mannan is one of the potent physiological ligands known for DC-SIGN [98, 135]. Butyrophilin was recently identified as a novel ligand [136], although binding could only be demonstrated to butyrophilin from different tumour cell lines and not from primary material. However, no effects on DCs upon binding to butyrophilin were reported so far [136]. Lewis-type antigen- carrying molecules support DC-SIGN binding on both colon cancer cell lines and primary tumour material [137]. Recently, it has been found that DCs grown in co-culture with colon cancer cell lines, cluster in a DC-SIGN-dependent manner and this eventually leads to modulate the cytokine response of these DCs to the TLR4 ligand (LPS). Supernatants from these cell lines inhibited the maturation of DCs and attenuated the development of TH_1 responses [138].

Recently, it has been shown neutrophiles have an interaction with DC-SIGN [139] (**Table 1.3**). The functionality of this interaction seems to be cell adhesive, to support a contact between neutrophiles and DCs and facilitate exposure of DCs to cytokines produced by the activated neutrophil. However, upon exposure to the cytokines, DCs get mature and promote a strong immune response characterized by a TH_1 shift [140].

Binding of DC-SIGN to its endogenous ligands determines its multiple functions in maintenance of immune homeostasis, both as a cell adhesion and signalling receptor (**Figure 1.5**).

DC-SIGN has eight different homologues in the mouse clustered in the same genomic region. The most like human DC-SIGN is mouse DC-SIGN-related 3 (SIGNR3) with the ability to bind both high mannose and fucose-terminated

glycans, and can mediate endocytosis of glycoprotein ligands [141]. However, it is not expressed on DCs.

B) DEC-205 (CD 205)

DEC-205 is an antigen uptake and processing receptor, first identified in the mouse and its human isoform was cloned in 1998 [142]. It belongs to a family of type I transmembrane multi-lectin receptors (MR family) consisting of 10 multiple CTLDs **(Fig 1.5).** The cytosolic domain of DEC-205 has a tyrosine-based coated pit localization sequence that is responsible for targeting to coated vesicles and endosomes [142]. However, despite the presence of 10 CTLDs, lack of conservation of key residues predicts that DEC-205 does not have C-type lectin activity and also it has been shown that the CR domain does not bind sulfated sugars [109]. It was primarily named DEC-205 (also known as Ly75), due to its DC expression and the MWt [143]. However, it has shown a wider distribution than on DCs alone, with expression on thymic and pulmonary epithelial cells, B cells and Langerhans cells. This wider distribution reflects a number of proposed functions in addition to antigen processing [109].

During the process of antigen capture and processing by DCs, expression of DEC-205 increases dramatically. DEC-205 is internalised from the cell surface by clathrin-mediated endocytosis but unlike the other receptors, it is localised intracellularly to late endosome/lysosomes containing MHC-II molecules. This suggests that DEC-205 functions to internalise ligand which can be processed intracellularly and loaded onto MHC-II molecules for presentation to T cells [109].

To date, no physiological ligands have been identified for DEC-205 and the basis of its ligand specificity remains to be determined. The endocytic properties of DEC-205 has been shown using mAb against DEC-205 and multiple studies show the potential of mAbs to modulate the immune system. However, DEC-205$^{-/-}$ mice have no obvious immunological abnormalities [144].

When antigens are targeted *in vivo* to murine DEC-205 by conjugation to anti-DEC-205 mAb it resulted in lymph nodes filled with antigen-loaded DC,

efficient antigen presentation and development of Treg cells [127]. The administration of TLR9 ligand (CpG) together with the antibody-coupled antigen results in the induction of efficient immunity [145], demonstrating a TLR–CLR cross-talk that controls tolerance and immunity.

Loss of DEC-205 is associated with tumour malignancy in some, but not all, tumours [109] suggesting that in some tissues, DEC-205 may have a tumour suppressor role.

C) Dectin-1

Another member of the CLR family is Dectin-1, a non-classic CLR expressed on the surface of several DC subsets, such as sub-epithelial and some myeloid DCs. This receptor is a type II transmembrane protein (**Figure 1.5)** with homology to the NK cell receptor family. Dectin-1 plays a major role in immune responses against fungal infections. The specificity of Dectin-1 has shown β-glucans as its most important ligands up to now. Dectin-1 induces gene expression profile independently through the recognition of β‑glucan expressed by a broad range of fungal pathogens (**Table 1.3**), which ultimately leads to the activation of NF-κB. Although the binding of β-glucans to Dectin-1 generates an activating signal in DCs, the microenvironment has a major impact on the outcome of the immune reaction (tolerance or eradication) **(Figure 1.8)**. The identification of an intracellular signalling motif may lead to better understanding of the interactions between PRRs and induction of tolerance or immunity.

D) DNGR1 (CLEC9A)

The novel DC-restricted DNGR1 is the most recently characterized CLR from the Dectin-1 cluster and is expressed in many tissues [146]. It was identified by gene expression profiling of murine DC subtypes in 2008 [147] . DNGR1 is selectively expressed at high levels by mouse $CD8^+$ DCs and also at low levels by plasmocytoid DCs (pDCs). Human DNGR1 is also expressed on small human DC subsets of blood [148]. Human DNGR1 and selected murine isoforms are expressed at the cell surface as glycosylated dimmers [146]. However, this receptor is also detected on small subsets of monocytes and B cells [146].

The cytoplasmic tail of DNGR-1 contains a single tyrosine residue within a sequence showing similarity to that of Dectin-1 (**Figure 1.5**), suggesting that DNGR-1 may function as an activation receptor. Indeed, DNGR-1 was shown to be capable of inducing inflammatory cytokine production and signalling [147]. Although this receptor did not mediate particle uptake via phagocytosis, DNGR-1 was capable of internalizing bound antigens via endocytosis and directing them to the endosomal/lysosomal pathway [128, 147].

The selective expression pattern and observed endocytic activity of DNGR-1 suggested that it could be used for antigen targeting to DCs. In fact, in a murine model, the cross-presentation of tumour antigens targeted to DNGR-1 was found to elicit potent anti-tumour responses [128, 149]. DNGR-1–targeted antigen is efficiently cross-presented to $CD8^+$ T cells indicating that like the MR and DEC-205, DNGR-1 can deliver cargo to selected endosomal compartments that intersect with the MHC-I processing and presentation pathway [128]. Interestingly, antigens targeted to DNGR-1 could induce humoral, $CD4^+$ and $CD8^+$ T-cell responses, even in the absence of adjuvant, suggesting that this receptor could be exploited as a novel target on DCs to drive CTL cross-priming and tumour therapy [128]. However, the ligand(s) and physiological function of this receptor are still unknown.

E) MR (CD206)

MR was originally termed the “macrophage mannose receptor”, but as expression is not restricted to macrophages it is now commonly referred to as the MR. It was first recognized in rabbits in the late 1970s as a 175 kDa transmembrane receptor involved in clearance of endogenous glycoproteins [150]. Based on peptide sequences, human MR cDNA was isolated in 1990 [109].

Structure and biochemical characteristics- The MR was the first discovered member of a family of four mammalian endocytic receptors (MR family) sharing the same overall structure (**Figure 1.11**) [151].

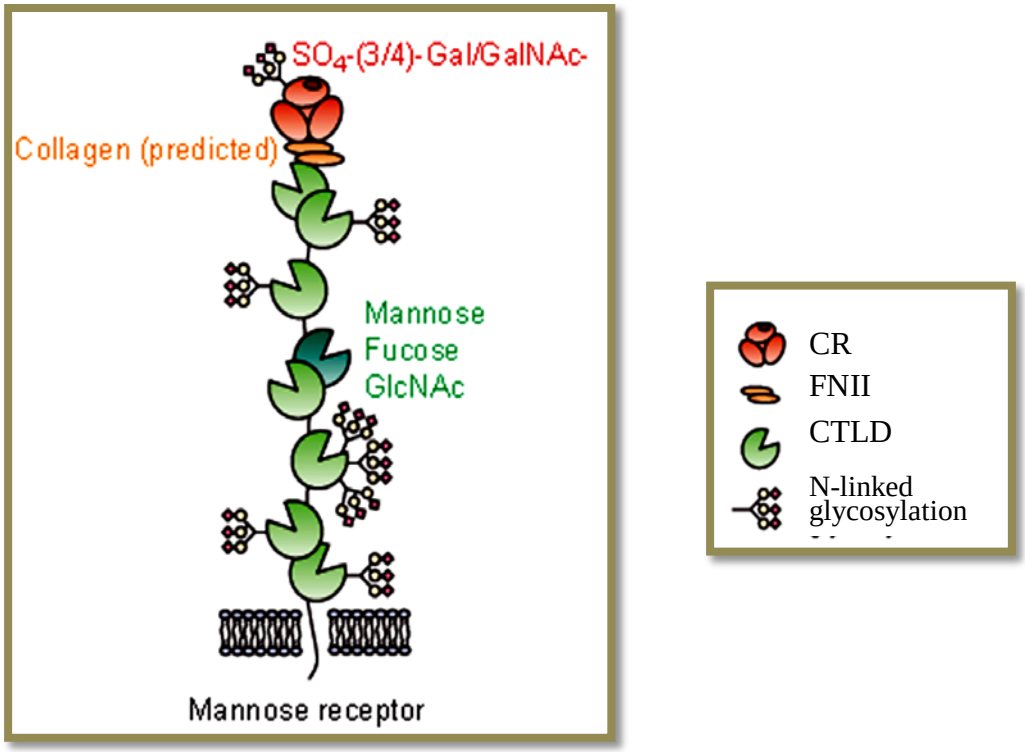

Figure 1.11: A schematic structure of the MR. MR is a monomeric, elongated and asymmetric molecule. Domain structure of the MR showing a proposed extended conformation and predicted N-linked glycosylation (proposed sialylation indicated by red diamonds). The CR domain (red), FNII repeat (brown) and eight CTLDs (green) are shown. CTLD4, the CTLD mostly responsible for carbohydrate binding, is shown in dark green.

The CTLDs mediate binding of MR to carbohydrates and each CTLD contains approximately 120 amino acids forming a common fold held in place by covalent and non-covalent interactions. Sequence analysis and sugar binding studies shows that MR contains only two CTLDs that could act as carbohydrate recognition domains: CTLD4 and 5 [152]. In functional CTLDs, interaction with carbohydrates occurs in a hydrophobic fold which brings into contact the residues required for the coordination of Ca^{2+} ions and sugar [152]. In fact, it has been shown that all eight CTLDs contain residues necessary for the formation of the hydrophobic fold but only CTLD4 and CTLD5 contain the residues required for Ca^{2+}-dependent carbohydrate ligation [109]. The CTLD4 requires two Ca^{2+} ions for sugar binding. One Ca^{2+} interacts directly with sugars, whereas binding to the second Ca^{2+} involves residues located at an extended loop unique to the CTLD4

[152]. This loop might act as a pH sensor and mediate pH-dependent Ca^{2+} release in the endosome. This could lead to the release of the carbohydrate ligands in the endosomal compartment upon acidification [151].

MR ligands- MR obtained its name because of its lectin activity for carbohydrates terminated in mannose (such as mannan), fucose or N-acetylglucosamine (mannose=fucose>N-acetylglucosamine) [153]. Although CTLD4 binds monosaccharides in isolation, multiple CTLDs in the CTLD4–8 segment are required for binding to multivalent ligands with the same affinity as the whole receptor [154]. Truncated receptors expressing CTLDs 5–8 retained weak sugar binding and were able to internalise, although inefficiently, mannose conjugated to bovine serum albumin (BSA). The geometry of the ligand is also critical for high affinity binding [153].

The CR region in the MR is able to bind to glycoproteins terminating in sulfated N-acetylgalactosamine and high mannose oligosaccharides via the CTLDs (**Figure 1.11**) [109]. This activity will not be shared by CR domains of the other members of MR family, because the involved amino acids are absent [155]. MR has a role in regulating serum levels of bioactive glycoproteins. It also plays a role in the regulation and maintenance of tissue homeostasis.

The FNII domain is predicted to bind to collagen and gelatine (**Figure 1.11**). Other MR ligands are chondroitin sulfates, sulfated Lewis-type antigens and endogenous glycoproteins, such as lysosomal hydrolases. [156]. MR can appear in at least two conformations, extended and bent, as a structural mechanism to regulate accessibility to ligand binding and/or oligomerization. In the bent conformation, some ligands could bind to specific domains of the receptor, whereas others would not interact if the access to the binding site has been blocked [157].

Mannan: a well-identified ligand for MR- Mannan is a complex branched mannose polymer, derived from the cell wall of saprophytic yeast *Saccharomyces cerevisiae*. It is a major virulence and protective factor of *S. cerevisiae* naturally found in the form of a glycoprotein containing D-mannose in a variety of α and β linkage arrangements [158]. Chemical analysis has shown that mannan from *S.*

cerevisiae is structurally similar to that of *C. albicans* [158]. It consists of long, linear chains of D-mannose units joined through α-(1→6) linkages, which provide a "backbone" for attachment of either single mannose residues or oligomers side branches containing a variable number of mannose residues joined through α-(1→2) and occasional terminal α-(1→3) linkages [159] (**Figure 1.12**). To some of these side branches, additional β-(1→2) oligomannosoides are attached through a phosphodiester (the acid-labile link). However, mannose units are bound by 1→4 linkages in mannan from plant sources. Indeed, it is evidenced that mannan composition influenced on its immunomodulatory effects [183]. It has been demonstrated that MR recognises the highly branched mannan chains. Kanbe and Cutler [160] showed that the mannan chain length is more important than a specific side branch conformation for binding.

Mannan is a molecule with established roles in immune system. Immunization of DCs using oxidized mannan-MUC1 to target MR has shown generation of high frequency of CTLs through MHC-I antigen presentation pathway [124, 161]. Recent studies demonstrated that N-linked mannan was specifically recognized by both MR and DC-SIGN on human DCs (despite the differences in the receptors) and directly influences the production and release of the pro-inflammatory cytokine IL-6; a process crucial for the activation and modulation of the adaptive immune responses [135]. Earlier studies have suggested cooperative recognition of mannan by MR (or DC-SIGN) and TLR4 is required for immune sensing of pathogens [162]. TNF-α production was induced in a dose-dependent manner upon stimulation with purified mannan. However, in contribution with the TLR4 ligand (LPS) the response was highly triggered [162, 163]. Netea and Kullberg [162] have shown the recognition of mannan was mediated by MR binding to N-linked mannosyl residues and by TLR4 binding to O-linked mannosyl residues.

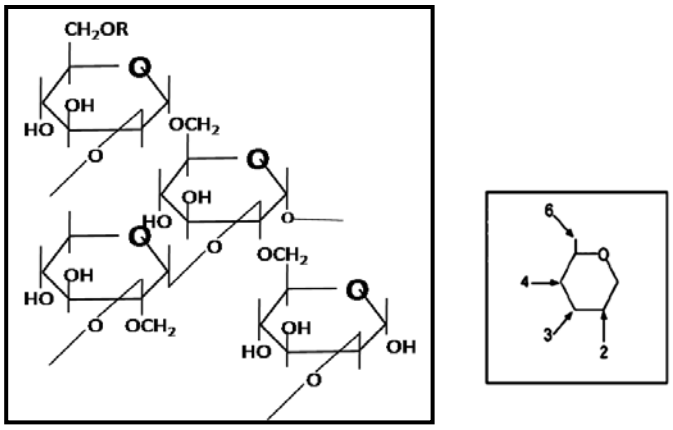

Figure 1.12: Chemical structure of mannan from *S. cerevisiae*

It has been also suggested that phospholipomannan is recognized by TLR2 and induces production of pro-inflammatory cytokines [164]. However, the relative contribution of these PRPs to cytokine stimulation by mannan is not known. Mannan also plays a role in adhesion of pathogenic cells to the endothelium which is related to the O-linked mannan (β-1,2- Oligomannosoides, which are acid-stable side branches) [165].

Expression of MR and regulation of the expression level- MR was primarily detected in most murine tissue macrophages in lymphoid organs [166]. High levels of MR expression have been detected in human monocyte-derived DCs [167, 168] and murine BM-derived DCs [28]. It is expressed by myeloid DCs, a DC subset that constitutively have dendritic form with antigen uptake and presentation functions and are subdivided to migratory and lymphoid-resident DCs [96]. In addition, dermal, mucosal lamina, tracheal smooth muscle cells, lymphatic and hepatic epithelium and the T-cell areas of tonsil DC subsets express the MR in human [14, 10]. As would be expected for a receptor involved in a diverse range of physiological functions, the MR is subject to complex regulation. MR levels are increased in response to cytokines such as IL-4, IL-10 and IL-13[169], whereas IFN-γ has a negative effect [151]. However, IL-4-mediated signalling is not required for MR expression in tissues, *in vivo.* Dexamethasone, prostaglandin-E and dihydroxyvitamin D3 have a positive effect on MR expression [150, 170, 171]. Expression of MR by DCs in mice is strain-

depended. DCs from C3H/HeN inbred mice displayed significantly increased expression of MR, compared to BALB/c or C57BL/6 strains [172].

MR: a well-identified endocytic receptor-A characteristic feature of MR is the ability of rapidly internalisation of soluble and particulate ligands from plasma membrane via clathrin-coated vesicles for delivery into the endosomal system. The short cytoplasmic tail of MR confers an ability to rapidly recycle between the cell surface and intracellular compartments[173]. The pH–dependency of MR-recognition would explain how, once acidification takes place in the endosomal compartment, MR dissociate from their ligands and the empty receptors recycle back to plasma membrane [151]. In fact, at steady state the majority of cellular MR (70-90%) is found within the endocytic pathway with only 10-30% on the cell surface [150]. The majority of the MR inside the cell is located in early endosomes [174], not in the late endosomes/early lysosomes (**Figure 1.7**). Intracellular targeting of MR is mediated by a tyrosine-based motif in cytoplasmic tail [175]. Although there is substantial evidence that MR has a role to play in phagocytosis and that this is important for the innate immune system, the mechanisms of this event have yet to be elucidated. It has been reported that mutation of the conserved cytoplasmic tyrosine reduces the phagocytosis in a similar manner to the reduction in clathrin-mediated endocytosis [109]. It remains a possibility that the MR alone is not responsible for phagocytosis: it may function to bind particles with terminal mannose residues and then engage a classical phagocytosis receptor to drive the phagocytic machinery [176].

MR role in innate and adaptive immune system- Much of the initial interest in the MR was focussed on its role in the innate immune system. MR can recognize most classes of human pathogens through its CTLDs: mannose specificity allows the recognition of viruses, fungi and mycobacteria; fucose structures are expressed by certain bacteria and helminths; and glucan structures are present on mycobacteria (**Table 1.3**) [109]. The MR distinguishes between self and non-self through the patterns that it recognises via its CTLDs and cross-talking with TLRs. Mannose and N-acetylglucosamine are not commonly found as terminal residues

in mammalian glycoproteins, but in the glycoproteins on surface of many microorganisms.

MR has also been demonstrated to play a role in antigen presentation following uptake, as mannosylated antigens are better internalized and presented to T cells [124]. MR can interact with the adaptive immune system by two mechanisms. *First*, it has been demonstrated in DCs that the MR can take up antigens and deliver them to the MHC compartments. In contrast to the phagocytic uptake of microorganisms, this would involve clathrin-mediated endocytosis of ligands [168, 177, 178]. *Second*, following binding to antigens through its CTLDs, MR would be proteolytically released from the cell surface and move to the germinal centres as a soluble form (sMR). Subsequently, it binds to specialised sialoadhesin positive macrophages and DCs via its CR domain for the generation of immune responses. The sMR has been detected in supernatants of MR^+ cells as well as mice and human serum [109]. In higher organisms, there is increasing evidence for MR that may play a role in antigen processing [109]. MR expression would also enable DCs and macrophages to increase uptake of antigen for presentation to T cells, moving from chronic inflammation to more adaptive immune responses [151].

Specifically, the MR supplied an early endosomal compartment distinct from lysosomes, which was committed to cross-presentation. These findings imply that antigen does not require intracellular diversion to access the cross-presentation pathway, because it can enter the pathway already during endocytosis [179, 180]. In human, it has been shown both humoral and CD4 and CD8 cellular responses can be induced by MR targeting indicating antigens acquired through MR targeting can be presented *in vivo* to both B and T cells and accesses both the exogenous and cross-presentation pathways [180]. Remarkably, the cross-presentation emphasizes on the possible effectiveness of MR in targeting of DCs in cancer vaccines.

IL-4 has also been shown to promote the cleavage of MR from the cell surface while IFN-γ and LPS inhibit this process, supporting the idea that the MR is upregulated to increase antigen presentation. This findings along with recent

studies show a cross-talk between MR and TLRs, particularly TLR4 and TLR2 (**Figure 1.13**) inducing a cell-mediate immune response [115]. Together, this led to the suggestion that MR functioned on DCs as an antigen uptake receptor targeting its cargo to intracellular compartments where it is processed for presentation to T cells.

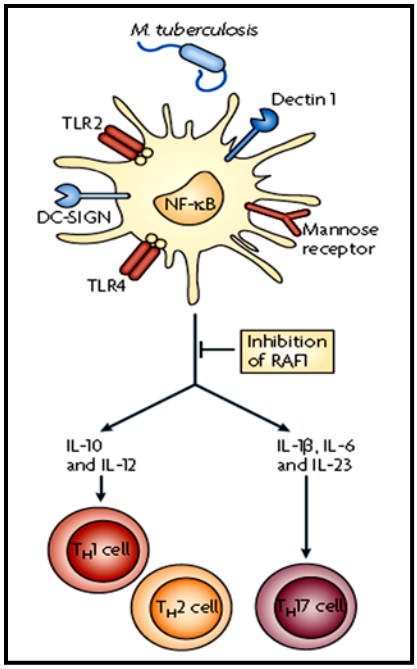

Figure 1.13: Cross-talk between MR and TLRs triggers adaptive immune responses. M. tuberculosis interacts with TLRs, MR, DC-SIGN and Dectin-1 and induces a TH1 and TH17 cell response. [115].

1.7. PLGA nanoparticles as vehicles for DC immunomonitoring

1.7.1. Immunomonitoring of DCs in cancer vaccines

The tumour microenvironment has emerged as an important component contributing to DC malfunction. Several lines of evidence indicated that tumours affecting DC maturation, differentiation and migration may induce the generalized failure of the host to mount an effective anti-tumour response. Significant progress in cancer immunotherapy is only to be expected by careful immunomonitoring studies in order to measure an “effective” tumour specific immune response and obtain detailed insight of the underlying processes. Different compartments and modalities are considered to monitor induced

immune responses such as accuracy of delivery, immune responses in peripheral blood, tumour and delayed-type hypersensitivity test biopsies, differentiation pathway of the anti-vaccine $CD8^+$ T cells and clinical trials [181, 182].

So far, monitoring of immune responses in cancer vaccine has provided very little information on the recruitment of immune cells to the tumours, their functional characteristics, and their anticancer effects [183]. DCs are of particular interest in cancer vaccination, either utilized for ex-vivo loading or in vivo targeting [42], and are predominantly aimed for immunomonitoring among other immune cells.

In general, the development of novel anticancer strategies requires more sensitive and less invasive methods to detect and monitor a minimal number of immune cells *in vivo*. Imaging modalities that reveal the combat in tumour microenvironment would provide vital information on infiltrating immune cells, their functional status, and their interaction with tumour cells *in vivo.* This would assist the development of immunotherapeutic strategies that can shift the balance in favour of the immune system in its battle against cancer. It is expected that advances in live imaging will provide opportunities to elucidate the phenotypic and activation status as well as dynamics of recruitment, differentiation, mobilization, and fate of DCs. The pioneer imaging method introduced into immunological research providing new insights into the dynamics of cellular interactions and migration patterns of immune cells in lymphoid organs *in vivo* were microscopic techniques [184, 185]. However, due to the limited tissue penetration depth (<500 μm), two-photon intravital microscopy is limited to the use in animal models [186].

Imaging systems can be classified by the energy used to derive visual information (X-rays, positrons, photons or sound waves), the spatial resolution that is attained or the type of information that is obtained (anatomical, physiological, cellular or molecular) [187]. Absolute quantification is possible in techniques where signals are independent of position in the sample [187]. The imaging techniques recently used in molecular oncology, including Positron-emission tomography (PET) [188-191], Magnetic resonance imaging (MRI) [192,

193], Computed tomography (CT) [186], Fluorescence-mediated tomography (FMT) [194-196], and Bioluminescence imaging (BLI) [197] are summarized and compared in **Table 1.4**.

Table 1.4: Features of the most common imaging systems [187, 189, 198-200]

Technique	Sensitivity	Resolution	Depth	Acquisition time	Imaging agent	Targeting capability
MRI	Medium	25-100 µm	No limit	Minutes to hours	paramagnetic chelates or particles	Anatomical, physiological
CT	Medium	50 µm	No limit	Minutes	Iodinated molecules	Anatomical, physiological
PET	High	1-2 mm	No limit	Minutes	positron-emitter labelled compounds	Physiological, molecular
FMT	High	1 mm	10 cm	Seconds to Minutes	Near-infrared fluorochromes	Physiological, molecular
BLI	High	Several mm	cm	Minutes	Luciferins	molecular
Intravital microscopy	Low	1 µm	400-800 µm	Seconds to Hours	Photoproteins, fluorochromes	Anatomical, Physiological, molecular

The strengths of these imaging modalities should be considered to achieve a picture of the challenging task of immune cells-tumour interactions at cellular/molecular levels [201]. Recent advances and adaptations of these modalities with much higher spatial resolutions made them available for use in experimental living small animal models allowing the development of new imaging probes [187].

1.7.2. PET imaging as a tool for immunomonitoring of DCs

Among these modalities PET and MRI are the most of interest. MRI provided high spatial resolution and PET potentially offers an unrivalled detection sensitivity and specificity with the ability to monitor in the picomolar range [197]. However, the potential features of PET allows to lower the dose substantially and accomplish cellular-molecular investigation without any adverse effects from the labelled probe [202]. Moreover, direct linear correlation between the count densities measured by PET with the concentration of an established labelled biomarker allows to readily quantify the PET signal [188] in molecular scale.

PET technique assesses the three-dimensional spatial distribution of special tracers incorporating positron (anti-particles of electrons) emitting radioactive isotopes based on the individual decay of these radionuclides [203]. Physical properties of some positron emitting radionuclides are summarized at **Table 1.5.**

Table 1.5: Physical characteristics of selected radionuclides used in PET [204, 205].

Positron (β+) emitting radionuclide	**Half-life ($T_{1/2}$)**	**Maximum positron energy (Mev)**
^{11}C	20 minutes	0.96
^{18}F	110 minutes	0.64
^{64}Cu	12.7 hours	0.87
^{124}I	4.18 days	2.1

To date, most PET studies have used ^{18}F as the radiotracer. However, the rapid radioactive decay of ^{18}F ($T_{1/2}$ 109 min) has limited the histological and molecular studies necessary for *in vivo* imaging of immune cells including DCs. Recent studies have used ^{64}Cu as another option for targeting macrophages [188]. Considering the time required for DC tracking, ^{124}I with a relatively long half-life ($T_{1/2}$ 4.18 days) is an alternative for *in vivo* transporting labelled compounds even to destinations very far away.

Recently, PLGA nanoparticles have been widely used as a vehicle to enhance the accuracy and efficiency of carrying the imaging probe(s) to the specific target *in vivo* [69, 206-212].

In PET imaging, polymer-based nanoparticles, in general, have emerged as important platforms for molecular imaging in the last few years [187-189, 213]. Use of PLGA-based systems to carry diagnostic radionuclides with high target specificity can provide an excellent vehicle for DC immunomonitoring by *in vivo* imaging with the key advantages of low toxicity and biocompatibility. A PET nanoprobe labelled with radionuclides with a relatively long $t_{1/2}$ such as ^{124}I (**Table 1.5**) can provide sufficient time for DC monitoring. This includes the time required for labelling and preparation process, DC uptake and vesicular transport, DC migration to lymph nodes, DC-T cell interaction and finally *in vivo* imaging.

1.8. Thesis proposal

1.8.1. Rational

The development of cancer vaccines capable of generating an active tumor-specific immune response serves as a promising tool for cancer therapy. However, despite demonstrated efficacy in murine models, cancer vaccines have found little success in the clinic. To date, monitoring of immune responses in cancer vaccines has provided very little information on the recruitment of immune cells to the tumours, their functional characteristics, and their anticancer effects. This highlights the need for developing novel immunotherapy strategies that can induce effective, prolonged immune responses against cancer. Due to the exclusive role of DCs in initiation and maintenance of cell-mediated immune responses, they are of particular interest in cancer vaccination, either as cells manipulated *ex-vivo* for vaccination or cells targeted by *in vivo* vaccination strategies.

Enhancing the immunogenicity of the vaccines requires more efficient targeting of cancer antigens and immunostimulatory adjuvants to DCs. One strategy is active targeting of DCs with ligands for DC-expressed receptors such as MR (a well-identified CLR) incorporated in a nanoparticulate PLGA-based vehicle which mimics the viruses in size and can specifically deliver its cargo to DCs. This less-explored strategy can enhance DC internalization, processing and presentation (in cooperation with TLRs) and eventually can shift the balance in favour of the immune system in its battle against cancer.

On the other hand, significant progress in cancer vaccines is only to be expected by careful immunomonitoring studies in order to measure an “effective” tumour specific response and obtain detailed insight of the underlying processes. This can be achieved by using sensitive and non- invasive imaging techniques to detect and monitor a minimal number of DCs *in vivo*. Imaging modalities that reveal the combat in tumour microenvironment would provide vital information on infiltrating immune cells, their functional status, and their interaction with tumour cells. It is expected that live imaging using a PET probe encapsulated in

PLGA nanoparticles can provide opportunities to elucidate the phenotypic and activation status as well as dynamics of recruitment, differentiation, mobilization, and fate of DCs to assist the development of successful immunotherapeutic strategies.

1.8.2. Hypothesis

The central hypotheses of this study were that PLGA nanoparticle formulations can be utilized to target DCs for both active immunotherapy and immunomonitoring purposes. Decoration of PLGA nanoparticles with the MR ligand (mannan and hydrophobized mannan) will accomplish two goals:

First, to enhance recognition and DC uptake of nanoparticles by the sake of targeted MR.

Second, to improve the immunological responses expected from the cross-talk between MR and TLRs as well as the known effect of mannan as an adjuvant.

Encapsulation of a PET-probe radiolabeled with ^{124}I (a PET radionuclide with an adequate $t_{1/2}$ for DC monitoring) in PLGA nanoparticles will provide a PET-nanoprobe that will be retained in DCs upon uptake for subsequent monitoring of DC recruitment, differentiation, mobilization, and fate by *in vivo* imaging.

1.8.3. Objectives

1. To develop mannan decorated PLGA nanoparticle formulations through: a) physical incorporation of mannan or palmitoyl mannan to ester-terminated and COOH-terminated PLGA nanoparticles; b) chemical conjugation of mannan to COOH-terminated PLGA nanoparticles.

2. To characterize the mannan (or palmitoyl mannan)-decorated nanoparticles for their size, Zeta potential, level of manna incorporation and DC uptake, to make comparisons with plain PLGA nanoparticles.

3. To assess the effect of mannan decoration on the immunological stimulatory activity of PLGA formulations on DCs.

4. To develop PET-nanoprobe in PLGA nanoparticles and characterise the formulations.

References

1. http://www.wpro.who.int/home.htm
2. Zitvogel, L., et al., *Immunological aspects of cancer chemotherapy.* Nat Rev Immunol, 2008. **8**(1): p. 59-73.
3. Matar, P., et al., *Immunotherapy for liver tumors: present status and future prospects.* J Biomed Sci, 2009. **16**: p. 30.
4. Burnet, F.M., *Immunological aspects of malignant disease.* Lancet, 1967. **1**(7501): p. 1171-4.
5. Smyth, M.J., D.I. Godfrey, and J.A. Trapani, *A fresh look at tumor immunosurveillance and immunotherapy.* Nat Immunol, 2001. **2**(4): p. 293-9.
6. Germenis, A.E. and V. Karanikas, *Immunoepigenetics: the unseen side of cancer immunoediting.* Immunol Cell Biol, 2007. **85**(1): p. 55-9.
7. Dunn, G.P., L.J. Old, and R.D. Schreiber, *The three Es of cancer immunoediting.* Annu Rev Immunol, 2004. **22**: p. 329-60.
8. Dunn, G.P., L.J. Old, and R.D. Schreiber, *The immunobiology of cancer immunosurveillance and immunoediting.* Immunity, 2004. **21**(2): p. 137-48.
9. Rivoltini, L., et al., *Immunity to cancer: attack and escape in T lymphocyte-tumor cell interaction.* Immunol Rev, 2002. **188**: p. 97-113.
10. Franco, A., *Glycoconjugates as vaccines for cancer immunotherapy: clinical trials and future directions.* Anticancer Agents Med Chem, 2008. **8**(1): p. 86-91.
11. Zou, W., *Regulatory T cells, tumour immunity and immunotherapy.* Nat Rev Immunol, 2006. **6**(4): p. 295-307.
12. Schuster, M., A. Nechansky, and R. Kircheis, *Cancer immunotherapy.* Biotechnol J, 2006. **1**(2): p. 138-47.
13. Hirschowitz, E.A. and J.R. Yannelli, *Immunotherapy for lung cancer.* Proc Am Thorac Soc, 2009. **6**(2): p. 224-32.
14. Dudley, M.E. and S.A. Rosenberg, *Adoptive cell transfer therapy.* Semin Oncol, 2007. **34**(6): p. 524-31.
15. Frodin, J.E., A.K. Lefvert, and H. Mellstedt, *The clinical significance of HAMA in patients treated with mouse monoclonal antibodies.* Cell Biophys, 1992. **21**(1-3): p. 153-65.
16. Pardoll, D., *Does the immune system see tumors as foreign or self?* Annu Rev Immunol, 2003. **21**: p. 807-39.
17. Huang, A.Y., et al., *Role of bone marrow-derived cells in presenting MHC class I-restricted tumor antigens.* Science, 1994. **264**(5161): p. 961-5.
18. Wischke, C., et al., *Poly(I:C) coated PLGA microparticles induce dendritic cell maturation.* Int J Pharm, 2009. **365**(1-2): p. 61-8.
19. Nestle, F.O., et al., *Vaccination of melanoma patients with peptide- or tumor lysate-pulsed dendritic cells.* Nat Med, 1998. **4**(3): p. 328-32.
20. Lathe, R., et al., *Tumour prevention and rejection with recombinant vaccinia.* Nature, 1987. **326**(6116): p. 878-80.
21. Xiang, S.D., et al., *Promising particle-based vaccines in cancer therapy.* Expert Rev Vaccines, 2008. **7**(7): p. 1103-19.

22. T.J.K.B.A.O.R.A. Goldsby, Kuby Immunology, W.H Freeman, New York, 2006.
23. Trombetta, E.S. and I. Mellman, *Cell biology of antigen processing in vitro and in vivo.* Annu Rev Immunol, 2005. **23**: p. 975-1028.
24. Demento, S.L., et al., *Inflammasome-activating nanoparticles as modular systems for optimizing vaccine efficacy.* Vaccine, 2009. **27**(23): p. 3013-21.
25. Shortman, K., M.H. Lahoud, and I. Caminschi, *Improving vaccines by targeting antigens to dendritic cells.* Exp Mol Med, 2009. **41**(2): p. 61-6.
26. Underhill, D.M. and A. Ozinsky, *Phagocytosis of microbes: complexity in action.* Annu Rev Immunol, 2002. **20**: p. 825-52.
27. Garg, S., et al., *Genetic tagging shows increased frequency and longevity of antigen-presenting, skin-derived dendritic cells in vivo.* Nat Immunol, 2003. **4**(9): p. 907-12.
28. Rescigno, M., et al., *Dendritic cell maturation is required for initiation of the immune response.* J Leukoc Biol, 1997. **61**(4): p. 415-21.
29. Bousso, P. and E. Robey, *Dynamics of CD8+ T cell priming by dendritic cells in intact lymph nodes.* Nat Immunol, 2003. **4**(6): p. 579-85.
30. Kalinski, P., et al., *T-cell priming by type-1 and type-2 polarized dendritic cells: the concept of a third signal.* Immunol Today, 1999. **20**(12): p. 561-7.
31. Kurts, C., *Cross-presentation: inducing CD8 T cell immunity and tolerance.* J Mol Med, 2000. **78**(6): p. 326-32.
32. Romani, N., et al., *Proliferating dendritic cell progenitors in human blood.* J Exp Med, 1994. **180**(1): p. 83-93.
33. Nash, J. and A. Pini, *Making the connections in nerve regeneration.* Nat Med, 1996. **2**(1): p. 25-6.
34. Morse, M.A., et al., *A Phase I study of active immunotherapy with carcinoembryonic antigen peptide (CAP-1)-pulsed, autologous human cultured dendritic cells in patients with metastatic malignancies expressing carcinoembryonic antigen.* Clin Cancer Res, 1999. **5**(6): p. 1331-8.
35. Osman, Y., et al., *Generation of bcr-abl specific cytotoxic T-lymphocytes by using dendritic cells pulsed with bcr-abl (b3a2) peptide: its applicability for donor leukocyte transfusions in marrow grafted CML patients.* Leukemia, 1999. **13**(2): p. 166-74.
36. Pinilla-Ibarz, J., et al., *Vaccination of patients with chronic myelogenous leukemia with bcr-abl oncogene breakpoint fusion peptides generates specific immune responses.* Blood, 2000. **95**(5): p. 1781-7.
37. Fields, R.C., K. Shimizu, and J.J. Mule, *Murine dendritic cells pulsed with whole tumor lysates mediate potent antitumor immune responses in vitro and in vivo.* Proc Natl Acad Sci U S A, 1998. **95**(16): p. 9482-7.
38. Smith, S.G., et al., *Human dendritic cells genetically engineered to express a melanoma polyepitope DNA vaccine induce multiple cytotoxic T-cell responses.* Clin Cancer Res, 2001. **7**(12): p. 4253-61.
39. Kugler, A., et al., *Regression of human metastatic renal cell carcinoma after vaccination with tumor cell-dendritic cell hybrids.* Nat Med, 2000. **6**(3): p. 332-6.

40. Ogihara, T., H. Iinuma, and K. Okinaga, *Usefulness of immunomodulators for maturation of dendritic cells.* Int J Oncol, 2004. **25**(2): p. 453-9.
41. Onaitis, M., et al., *Dendritic cell gene therapy.* Surg Oncol Clin N Am, 2002. **11**(3): p. 645-60.
42. Tacken, P.J., et al., *Dendritic-cell immunotherapy: from ex vivo loading to in vivo targeting.* Nat Rev Immunol, 2007. **7**(10): p. 790-802.
43. Steinman, R.M. and J. Banchereau, *Taking dendritic cells into medicine.* Nature, 2007. **449**(7161): p. 419-26.
44. Rosenberg, S.A., J.C. Yang, and N.P. Restifo, *Cancer immunotherapy: moving beyond current vaccines.* Nat Med, 2004. **10**(9): p. 909-15.
45. De Vries, I.J., et al., *Effective migration of antigen-pulsed dendritic cells to lymph nodes in melanoma patients is determined by their maturation state.* Cancer Res, 2003. **63**(1): p. 12-7.
46. O'Hagan, D.T. and R. Rappuoli, *Novel approaches to vaccine delivery.* Pharm Res, 2004. **21**(9): p. 1519-30.
47. Saupe, A., et al., *Immunostimulatory colloidal delivery systems for cancer vaccines.* Expert Opin Drug Deliv, 2006. **3**(3): p. 345-54.
48. Cassaday, R.D., et al., *A phase I study of immunization using particle-mediated epidermal delivery of genes for gp100 and GM-CSF into uninvolved skin of melanoma patients.* Clin Cancer Res, 2007. **13**(2 Pt 1): p. 540-9.
49. Davis, I.D., et al., *Recombinant NY-ESO-1 protein with ISCOMATRIX adjuvant induces broad integrated antibody and CD4(+) and CD8(+) T cell responses in humans.* Proc Natl Acad Sci U S A, 2004. **101**(29): p. 10697-702.
50. Frazer, I.H., et al., *Phase 1 study of HPV16-specific immunotherapy with E6E7 fusion protein and ISCOMATRIX adjuvant in women with cervical intraepithelial neoplasia.* Vaccine, 2004. **23**(2): p. 172-81.
51. Sangha, R. and C. Butts, *L-BLP25: a peptide vaccine strategy in non small cell lung cancer.* Clin Cancer Res, 2007. **13**(15 Pt 2): p. s4652-4.
52. Jain, R.A., et al., *Controlled release of drugs from injectable in situ formed biodegradable PLGA microspheres: effect of various formulation variables.* Eur J Pharm Biopharm, 2000. **50**(2): p. 257-62.
53. Bala, I., S. Hariharan, and M.N. Kumar, *PLGA nanoparticles in drug delivery: the state of the art.* Crit Rev Ther Drug Carrier Syst, 2004. **21**(5): p. 387-422.
54. Chong, C.S., et al., *Enhancement of T helper type 1 immune responses against hepatitis B virus core antigen by PLGA nanoparticle vaccine delivery.* J Control Release, 2005. **102**(1): p. 85-99.
55. Hunter, S.K., M.E. Andracki, and A.M. Krieg, *Biodegradable microspheres containing group B Streptococcus vaccine: immune response in mice.* Am J Obstet Gynecol, 2001. **185**(5): p. 1174-9.
56. Cohen, S., M.J. Alonso, and R. Langer, *Novel approaches to controlled-release antigen delivery.* Int J Technol Assess Health Care, 1994. **10**(1): p. 121-30.
57. Newman, K.D., J. Samuel, and G. Kwon, *Ovalbumin peptide encapsulated in poly(d,l lactic-co-glycolic acid) microspheres is capable of inducing a T helper type 1 immune response.* J Control Release, 1998. **54**(1): p. 49-59.

58. Diwan, M., M. Tafaghodi, and J. Samuel, *Enhancement of immune responses by co-delivery of a CpG oligodeoxynucleotide and tetanus toxoid in biodegradable nanospheres.* J Control Release, 2002. **85**(1-3): p. 247-62.
59. Wang, D., et al., *Encapsulation of plasmid DNA in biodegradable poly(D, L-lactic-co-glycolic acid) microspheres as a novel approach for immunogene delivery.* J Control Release, 1999. **57**(1): p. 9-18.
60. O'Hagan, D.T. and M. Singh, *Microparticles as vaccine adjuvants and delivery systems.* Expert Rev Vaccines, 2003. **2**(2): p. 269-83.
61. Putney, S.D. and P.A. Burke, *Improving protein therapeutics with sustained-release formulations.* Nat Biotechnol, 1998. **16**(2): p. 153-7.
62. Uchida, T. and S. Goto, *Oral delivery of poly(lactide-co-glycolide) microspheres containing ovalbumin as vaccine formulation: particle size study.* Biol Pharm Bull, 1994. **17**(9): p. 1272-6.
63. Audran, R., et al., *Encapsulation of peptides in biodegradable microspheres prolongs their MHC class-I presentation by dendritic cells and macrophages in vitro.* Vaccine, 2003. **21**(11-12): p. 1250-5.
64. Pinzon-Charry, A., et al., *Numerical and functional defects of blood dendritic cells in early- and late-stage breast cancer.* Br J Cancer, 2007. **97**(9): p. 1251-9.
65. Mesa, H., et al., *Diagnosis of nonprimary pancreatic neoplasms by endoscopic ultrasound-guided fine-needle aspiration.* Diagn Cytopathol, 2004. **31**(5): p. 313-8.
66. Samuel, J., et al., *Immunogenicity and antitumor activity of a liposomal MUC1 peptide-based vaccine.* Int J Cancer, 1998. **75**(2): p. 295-302.
67. Hutchinson, F.G. and B.J. Furr, *Biodegradable polymers for the sustained release of peptides.* Biochem Soc Trans, 1985. **13**(2): p. 520-3.
68. Gombotz, W.R. and D.K. Pettit, *Biodegradable polymers for protein and peptide drug delivery.* Bioconjug Chem, 1995. **6**(4): p. 332-51.
69. van Apeldoorn, A.A., et al., *Raman imaging of PLGA microsphere degradation inside macrophages.* J Am Chem Soc, 2004. **126**(41): p. 13226-7.
70. Eldridge, J.H., et al., *Biodegradable microspheres as a vaccine delivery system.* Mol Immunol, 1991. **28**(3): p. 287-94.
71. Miller, R.A., J.M. Brady, and D.E. Cutright, *Degradation rates of oral resorbable implants (polylactates and polyglycolates): rate modification with changes in PLA/PGA copolymer ratios.* J Biomed Mater Res, 1977. **11**(5): p. 711-9.
72. Cutright, D.E., et al., *Degradation rates of polymers and copolymers of polylactic and polyglycolic acids.* Oral Surg Oral Med Oral Pathol, 1974. **37**(1): p. 142-52.
73. Cai, C., et al., *Influence of morphology and drug distribution on the release process of FITC-dextran-loaded microspheres prepared with different types of PLGA.* J Microencapsul, 2008: p. 1-12.
74. Jaklenec, A., et al., *Sequential release of bioactive IGF-I and TGF-beta 1 from PLGA microsphere-based scaffolds.* Biomaterials, 2008. **29**(10): p. 1518-25.

75. Diwan, M., et al., *Biodegradable nanoparticle mediated antigen delivery to human cord blood derived dendritic cells for induction of primary T cell responses.* J Drug Target, 2003. **11**(8-10): p. 495-507.
76. Heath, W.R. and F.R. Carbone, *Cross-presentation, dendritic cells, tolerance and immunity.* Annu Rev Immunol, 2001. **19**: p. 47-64.
77. Lutsiak, M.E., et al., *Analysis of poly(D,L-lactic-co-glycolic acid) nanosphere uptake by human dendritic cells and macrophages in vitro.* Pharm Res, 2002. **19**(10): p. 1480-7.
78. Diwan, M., et al., *Dose sparing of CpG oligodeoxynucleotide vaccine adjuvants by nanoparticle delivery.* Curr Drug Deliv, 2004. **1**(4): p. 405-12.
79. Waeckerle-Men, Y. and M. Groettrup, *PLGA microspheres for improved antigen delivery to dendritic cells as cellular vaccines.* Adv Drug Deliv Rev, 2005. **57**(3): p. 475-82.
80. Newman, K.D., et al., *Uptake of poly(D,L-lactic-co-glycolic acid) microspheres by antigen-presenting cells in vivo.* J Biomed Mater Res, 2002. **60**(3): p. 480-6.
81. Alpar, H.O., *Strategies for vaccine delivery.* J Drug Target, 2003. **11**(8-10): p. 459-61.
82. Gamvrellis, A., et al., *Vaccines that facilitate antigen entry into dendritic cells.* Immunol Cell Biol, 2004. **82**(5): p. 506-16.
83. Nixon, A.J., et al., *Relationship of tumor grade to other pathologic features and to treatment outcome of patients with early stage breast carcinoma treated with breast-conserving therapy.* Cancer, 1996. **78**(7): p. 1426-31.
84. Josephson, L., et al., *High-efficiency intracellular magnetic labeling with novel superparamagnetic-Tat peptide conjugates.* Bioconjug Chem, 1999. **10**(2): p. 186-91.
85. Joffre, O., et al., *Inflammatory signals in dendritic cell activation and the induction of adaptive immunity.* Immunol Rev, 2009. **227**(1): p. 234-47.
86. Burgdorf, S., et al., *Distinct pathways of antigen uptake and intracellular routing in CD4 and CD8 T cell activation.* Science, 2007. **316**(5824): p. 612-6.
87. Akira, S., *Toll receptor families: structure and function.* Semin Immunol, 2004. **16**(1): p. 1-2.
88. Pasare, C. and R. Medzhitov, *Toll-like receptors: linking innate and adaptive immunity.* Microbes Infect, 2004. **6**(15): p. 1382-7.
89. Takeda, K. and S. Akira, *TLR signaling pathways.* Semin Immunol, 2004. **16**(1): p. 3-9.
90. Pasare, C. and R. Medzhitov, *Toll-like receptors: balancing host resistance with immune tolerance.* Curr Opin Immunol, 2003. **15**(6): p. 677-82.
91. Goforth, R., et al., *Immune stimulatory antigen loaded particles combined with depletion of regulatory T-cells induce potent tumor specific immunity in a mouse model of melanoma.* Cancer Immunol Immunother, 2009. **58**(4): p. 517-30.
92. Elamanchili, P., et al., *"Pathogen-mimicking" nanoparticles for vaccine delivery to dendritic cells.* J Immunother, 2007. **30**(4): p. 378-95.
93. Linehan, S.A., L. Martinez-Pomares, and S. Gordon, *Mannose receptor and scavenger receptor: two macrophage pattern recognition receptors with*

diverse functions in tissue homeostasis and host defense. Adv Exp Med Biol, 2000. **479**: p. 1-14.
94. Akira, S., *Innate immunity to pathogens: diversity in receptors for microbial recognition.* Immunol Rev, 2009. **227**(1): p. 5-8.
95. van Kooyk, Y., *C-type lectins on dendritic cells: key modulators for the induction of immune responses.* Biochem Soc Trans, 2008. **36**(Pt 6): p. 1478-81.
96. Geijtenbeek, T.B. and S.I. Gringhuis, *Signalling through C-type lectin receptors: shaping immune responses.* Nat Rev Immunol, 2009. **9**(7): p. 465-79.
97. Zelensky, A.N. and J.E. Gready, *The C-type lectin-like domain superfamily.* Febs J, 2005. **272**(24): p. 6179-217.
98. Figdor, C.G., Y. van Kooyk, and G.J. Adema, *C-type lectin receptors on dendritic cells and Langerhans cells.* Nat Rev Immunol, 2002. **2**(2): p. 77-84.
99. Drickamer, K., *Two distinct classes of carbohydrate-recognition domains in animal lectins.* J Biol Chem, 1988. **263**(20): p. 9557-60.
100. Weis, W.I., M.E. Taylor, and K. Drickamer, *The C-type lectin superfamily in the immune system.* Immunol Rev, 1998. **163**: p. 19-34.
101. Drickamer, K., *Demonstration of carbohydrate-recognition activity in diverse proteins which share a common primary structure motif.* Biochem Soc Trans, 1989. **17**(1): p. 13-5.
102. Kerrigan, A.M. and G.D. Brown, *C-type lectins and phagocytosis.* Immunobiology, 2009.
103. Garcia-Vallejo, J.J. and van Kooyk, Y. Endogenous ligands for C-type lectin receptors: the true regulators of immune homeostasis, Immunol Rev, 2009.230:p.22-37
104. van Vliet, S.J., J.J. Garcia-Vallejo, and Y. van Kooyk, *Dendritic cells and C-type lectin receptors: coupling innate to adaptive immune responses.* Immunol Cell Biol, 2008. **86**(7): p. 580-7.
105. Kanazawa, N., et al., *Dendritic cell immunoactivating receptor, a novel C-type lectin immunoreceptor, acts as an activating receptor through association with Fc receptor gamma chain.* J Biol Chem, 2003. **278**(35): p. 32645-52.
106. McGreal, E.P., J.L. Miller, and S. Gordon, *Ligand recognition by antigen-presenting cell C-type lectin receptors.* Curr Opin Immunol, 2005. **17**(1): p. 18-24.
107. Conner, S.D. and S.L. Schmid, *Regulated portals of entry into the cell.* Nature, 2003. **422**(6927): p. 37-44.
108. Xiang, S.D., et al., *Pathogen recognition and development of particulate vaccines: does size matter?* Methods, 2006. **40**(1): p. 1-9.
109. East, L. and C.M. Isacke, *The mannose receptor family.* Biochim Biophys Acta, 2002. **1572**(2-3): p. 364-86.
110. Johannes, L. and C. Lamaze, *Clathrin-dependent or not: is it still the question?* Traffic, 2002. **3**(7): p. 443-51.
111. Bonifaz, L.C., et al., *In vivo targeting of antigens to maturing dendritic cells via the DEC-205 receptor improves T cell vaccination.* J Exp Med, 2004. **199**(6): p. 815-24.

112. Smith, A.L., et al., *Leukocyte-specific protein 1 interacts with DC-SIGN and mediates transport of HIV to the proteasome in dendritic cells.* J Exp Med, 2007. **204**(2): p. 421-30.
113. Mellman, I., *Endocytosis and molecular sorting.* Annu Rev Cell Dev Biol, 1996. **12**: p. 575-625.
114. Gruenberg, J., *The endocytic pathway: a mosaic of domains.* Nat Rev Mol Cell Biol, 2001. **2**(10): p. 721-30.
115. van Vliet, S.J., et al., *Innate signaling and regulation of Dendritic cell immunity.* Curr Opin Immunol, 2007. **19**(4): p. 435-40.
116. Gringhuis, S.I., et al., *C-type lectin DC-SIGN modulates Toll-like receptor signaling via Raf-1 kinase-dependent acetylation of transcription factor NF-kappaB.* Immunity, 2007. **26**(5): p. 605-16.
117. Aarnoudse, C.A., et al., *Recognition of tumor glycans by antigen-presenting cells.* Curr Opin Immunol, 2006. **18**(1): p. 105-11.
118. van Gisbergen, K.P., et al., *Dendritic cells recognize tumor-specific glycosylation of carcinoembryonic antigen on colorectal cancer cells through dendritic cell-specific intercellular adhesion molecule-3-grabbing nonintegrin.* Cancer Res, 2005. **65**(13): p. 5935-44.
119. van Vliet, S.J., et al., *Carbohydrate profiling reveals a distinctive role for the C-type lectin MGL in the recognition of helminth parasites and tumor antigens by dendritic cells.* Int Immunol, 2005. **17**(5): p. 661-9.
120. Dube, D.H. and C.R. Bertozzi, *Glycans in cancer and inflammation--potential for therapeutics and diagnostics.* Nat Rev Drug Discov, 2005. **4**(6): p. 477-88.
121. Foged, C., A. Sundblad, and L. Hovgaard, *Targeting vaccines to dendritic cells.* Pharm Res, 2002. **19**(3): p. 229-38.
122. Reddy, S.T., M.A. Swartz, and J.A. Hubbell, *Targeting dendritic cells with biomaterials: developing the next generation of vaccines.* Trends Immunol, 2006. **27**(12): p. 573-9.
123. Kempf, M., et al., *Improved stimulation of human dendritic cells by receptor engagement with surface-modified microparticles.* J Drug Target, 2003. **11**(1): p. 11-8.
124. Apostolopoulos, V., et al., *Ex vivo targeting of the macrophage mannose receptor generates anti-tumor CTL responses.* Vaccine, 2000. **18**(27): p. 3174-84.
125. Apostolopoulos, V., et al., *Pilot phase III immunotherapy study in early-stage breast cancer patients using oxidized mannan-MUC1 [ISRCTN71711835].* Breast Cancer Res, 2006. **8**(3): p. R27.
126. Anderson, R.J. and J. Schneider, *Plasmid DNA and viral vector-based vaccines for the treatment of cancer.* Vaccine, 2007. **25 Suppl 2**: p. B24-34.
127. Bonifaz, L., et al., *Efficient targeting of protein antigen to the dendritic cell receptor DEC-205 in the steady state leads to antigen presentation on major histocompatibility complex class I products and peripheral CD8+ T cell tolerance.* J Exp Med, 2002. **196**(12): p. 1627-38.
128. Sancho, D., et al., *Tumor therapy in mice via antigen targeting to a novel, DC-restricted C-type lectin.* J Clin Invest, 2008. **118**(6): p. 2098-110.

129. Adams, E.W., et al., *Carbohydrate-mediated targeting of antigen to dendritic cells leads to enhanced presentation of antigen to T cells.* Chembiochem, 2008. **9**(2): p. 294-303.
130. Curtis, B.M., S. Scharnowske, and A.J. Watson, *Sequence and expression of a membrane-associated C-type lectin that exhibits CD4-independent binding of human immunodeficiency virus envelope glycoprotein gp120.* Proc Natl Acad Sci U S A, 1992. **89**(17): p. 8356-60.
131. Geijtenbeek, T.B., et al., *Identification of DC-SIGN, a novel dendritic cell-specific ICAM-3 receptor that supports primary immune responses.* Cell, 2000. **100**(5): p. 575-85.
132. Garcia-Vallejo, J.J., et al., Endogenous ligands for C-type lectin receptors: the true regulators of immune homeostasis.Immunol Rev,2009, 230: p.22-37.
133. Garcia-Vallejo, J.J., et al., Endogenous ligands for C-type lectin receptors: the true regulators of immune homeostasis.Immunol Rev,2009, 230: p.22-37.
134. Green, R.S., et al., Ma*mmalian N-glycan branching protects against innate immune self-recognition and inflammation in autoimmune disease pathogenesis. I*mmunity, 2007. 27**(2**): p. 308-20.
135. Cambi, A., et al., De*ndritic cell interaction with Candida albicans critically depends on N-linked mannan. J* Biol Chem, 2008. 28**3(2**9): p. 20590-9.
136. Malcherek, G., et al., The *B7 homolog butyrophilin BTN2A1 is a novel ligand for DC-SIGN. J* Immunol, 2007. 17**9(6**): p. 3804-11.
137. Garcia-Vallejo, J.J., et al., Endogenous ligands for C-type lectin receptors: the true regulators of immune homeostasis.Immunol Rev,2009, 230: p.22-37.
138. Nonaka, M., et al., Gly*cosylation-dependent interactions of C-type lectin DC-SIGN with colorectal tumor-associated Lewis glycans impair the function and differentiation of monocyte-derived dendritic cells. J* Immunol, 2008. 180**(5)**: p. 3347-56.
139. Bogoevska, V., et al., DC-*SIGN binds ICAM-3 isolated from peripheral human leukocytes through Lewis x residues. Gl*ycobiology, 2007. 17(**3)**: p. 324-33.
140. Garcia-Vallejo, J.J., et al., Endogenous ligands for C-type lectin receptors: the true regulators of immune homeostasis.Immunol Rev,2009, 230: p.22-37.
141. Hovius, J.W., et al., Salp*15 binding to DC-SIGN inhibits cytokine expression by impairing both nucleosome remodeling and mRNA stabilization. PLo*S Pathog, 2008. 4(2)**:** p. e31.
142. Jiang, W., et al., The *receptor DEC-205 expressed by dendritic cells and thymic epithelial cells is involved in antigen processing. Nat*ure, 1995. 375(**652**7): p. 151-5.
143. Erbacher, A., et al., Dendr*itic cells: functional aspects of glycosylation and lectins. Hum* Immunol, 2009. 70(5**):** p. 308-12.
144. Kronin, V., et al., DEC-*205 as a marker of dendritic cells with regulatory effects on CD8 T cell responses. Int* Immunol, 2000. 12(5**):** p. 731-5.
145. Mahnke, K., et al., Targ*eting of antigens to activated dendritic cells in vivo cures metastatic melanoma in mice. Can*cer Res, 2005. 65(1**5)**: p. 7007-12.

146. Huysamen, C. and G.D. Brown, The *fungal pattern recognition receptor, Dectin-1, and the associated cluster of C-type lectin-like receptors. FEM*S Microbiol Lett, 2009. 290(**2):** p. 121-8.
147. Huysamen, C., et al., CLEC9*A is a novel activation C-type lectin-like receptor expressed on BDCA3+ dendritic cells and a subset of monocytes. J B*iol Chem, 2008. 283(**24)**: p. 16693-701.
148. Caminschi, I., et al., The *dendritic cell subtype-restricted C-type lectin Clec9A is a target for vaccine enhancement. Blo*od, 2008. 112(**8):** p. 3264-73.
149. Sancho, D., et al., Iden*tification of a dendritic cell receptor that couples sensing of necrosis to immunity. Nat*ure, 2009. 458(**724**0): p. 899-903.
150. Pontow, S.E., V. Kery, and P.D. Stahl, Mann*ose receptor. Int* Rev Cytol, 1992. 137B**: p.** 221-44.
151. Taylor, P.R., S. Gordon, and L. Martinez-Pomares, The *mannose receptor: linking homeostasis and immunity through sugar recognition. Tre*nds Immunol, 2005. 26(2**):** p. 104-10.
152. Mullin, N.P., P.G. Hitchen, and M.E. Taylor, Mech*anism of Ca2+ and monosaccharide binding to a C-type carbohydrate-recognition domain of the macrophage mannose receptor. J B*iol Chem, 1997. 272(**9):** p. 5668-81.
153. Fraser, I.P., H. Koziel, and R.A. Ezekowitz, The *serum mannose-binding protein and the macrophage mannose receptor are pattern recognition molecules that link innate and adaptive immunity. Sem*in Immunol, 1998. 10(5**):** p. 363-72.
154. Taylor, M.E., K. Bezouska, and K. Drickamer, Contr*ibution to ligand binding by multiple carbohydrate-recognition domains in the macrophage mannose receptor. J B*iol Chem, 1992. 267(**3):** p. 1719-26.
155. Feinberg, H., et al., Struc*ture of a C-type carbohydrate recognition domain from the macrophage mannose receptor. J B*iol Chem, 2000. 275(**28)**: p. 21539-48.
156. Lee, S.J., et al., Mann*ose receptor-mediated regulation of serum glycoprotein homeostasis. Sci*ence, 2002. 295(**556**1): p. 1898-901.
157. Llorca, O., Exte*nded and bent conformations of the mannose receptor family. Cel*l Mol Life Sci, 2008. 65(9**):** p. 1302-10.
158. Nelson, R.D., et al., Cand*ida mannan: chemistry, suppression of cell-mediated immunity, and possible mechanisms of action. Cl*in Microbiol Rev, 1991. 4(1)**:** p. 1-19.
159. Shibata, N., et al., Struc*tural analysis of phospho-D-mannan-protein complexes isolated from yeast and mold form cells of Candida albicans NIH A-207 serotype A strain. Car*bohydr Res, 1989. 187(**2):** p. 239-53.
160. Kanbe, T. and J.E. Cutler, Mini*mum chemical requirements for adhesin activity of the acid-stable part of Candida albicans cell wall phosphomannoprotein complex. Inf*ect Immun, 1998. 66(1**2)**: p. 5812-8.
161. Sheng, K.C., et al., Mann*an derivatives induce phenotypic and functional maturation of mouse dendritic cells. Imm*unology, 2006. 118(**3):** p. 372-83.
162. Netea, M.G., et al., Immu*ne sensing of Candida albicans requires cooperative recognition of mannans and glucans by lectin and Toll-like receptors. J C*lin Invest, 2006. 116(**6):** p. 1642-50.

163. Tada, H., et al., Sacc*haromyces cerevisiae- and Candida albicans-derived mannan induced production of tumor necrosis factor alpha by human monocytes in a CD14- and Toll-like receptor 4-dependent manner. Mic*robiol Immunol, 2002. 46(7**):** p. 503-12.
164. Jouault, T., et al., Cand*ida albicans phospholipomannan is sensed through toll-like receptors. J I*nfect Dis, 2003. 188(**1):** p. 165-72.
165. Masuoka, J., Surf*ace glycans of Candida albicans and other pathogenic fungi: physiological roles, clinical uses, and experimental challenges. Cli*n Microbiol Rev, 2004. 17(2**):** p. 281-310.
166. Linehan, S.A., et al., Mann*ose receptor and its putative ligands in normal murine lymphoid and nonlymphoid organs: In situ expression of mannose receptor by selected macrophages, endothelial cells, perivascular microglia, and mesangial cells, but not dendritic cells. J E*xp Med, 1999. 189(**12)**: p. 1961-72.
167. Avrameas, A., et al., Expr*ession of a mannose/fucose membrane lectin on human dendritic cells. Eur* J Immunol, 1996. 26(2**):** p. 394-400.
168. Engering, A.J., et al., The *mannose receptor functions as a high capacity and broad specificity antigen receptor in human dendritic cells. Eur* J Immunol, 1997. 27(9**):** p. 2417-25.
169. Martinez-Pomares, L., et al., Anal*ysis of mannose receptor regulation by IL-4, IL-10, and proteolytic processing using novel monoclonal antibodies. J L*eukoc Biol, 2003. 73(5**):** p. 604-13.
170. Piemonti, L., et al., Gluc*ocorticoids increase the endocytic activity of human dendritic cells. Int* Immunol, 1999. 11(9**):** p. 1519-26.
171. Piemonti, L., et al., Vita*min D3 affects differentiation, maturation, and function of human monocyte-derived dendritic cells. J I*mmunol, 2000. 164(**9):** p. 4443-51.
172. Autenrieth, S.E. and I.B. Autenrieth, Vari*able antigen uptake due to different expression of the macrophage mannose receptor by dendritic cells in various inbred mouse strains. Imm*unology, 2009. 127(**4):** p. 523-9.
173. McGreal, E.P., L. Martinez-Pomares, and S. Gordon, Diver*gent roles for C-type lectins expressed by cells of the innate immune system. Mol* Immunol, 2004. 41(1**1)**: p. 1109-21.
174. Mahnke, K., et al., The *dendritic cell receptor for endocytosis, DEC-205, can recycle and enhance antigen presentation via major histocompatibility complex class II-positive lysosomal compartments. J C*ell Biol, 2000. 151(**3):** p. 673-84.
175. Schweizer, A., P.D. Stahl, and J. Rohrer, A di-*aromatic motif in the cytosolic tail of the mannose receptor mediates endosomal sorting. J B*iol Chem, 2000. 275(**38)**: p. 29694-700.
176. Savill, J., Apop*tosis. Phagocytic docking without shocking. Nat*ure, 1998. 392(**667**5): p. 442-3.
177. Sallusto, F., et al., Dendr*itic cells use macropinocytosis and the mannose receptor to concentrate macromolecules in the major histocompatibility complex class II compartment: downregulation by cytokines and bacterial products. J E*xp Med, 1995. 182(**2):** p. 389-400.

178. Tan, M.C., et al., Mannose receptor-mediated uptake of antigens strongly enhances HLA class II-restricted antigen presentation by cultured dendritic cells. Eur J Immunol, 1997. 27(9): p. 2426-35.
179. Backer, R., et al., CD8- dendritic cells preferentially cross-present Saccharomyces cerevisiae antigens. Eur J Immunol, 2008. 38(2): p. 370-80.
180. He, L.Z., et al., Antigenic targeting of the human mannose receptor induces tumor immunity. J Immunol, 2007. 178(**10**): p. 6259-67.
181. Aarntzen, E.H., et al., Dendritic cell vaccination and immune monitoring. Cancer Immunol Immunother, 2008. 57(1**0**): p. 1559-68.
182. Connerotte, T., et al., Functions of Anti-MAGE T-cells induced in melanoma patients under different vaccination modalities. Cancer Res, 2008. 68(1**0**): p. 3931-40.
183. Acres, B., P. Beverley, and S. Scholl, Tumor immunology and the Battle of Waterloo. Mol Cancer Ther, 2002. 1(8): p. 651-5.
184. Halin, C., et al., In vivo imaging of lymphocyte trafficking. Annu Rev Cell Dev Biol, 2005. 21: **p.** 581-603.
185. Germain, R.N., et al., An extended vision for dynamic high-resolution intravital immune imaging. Semin Immunol, 2005. 17(6): p. 431-41.
186. Baumjohann, D. and M.B. Lutz, Non-invasive imaging of dendritic cell migration in vivo. Immunobiology, 2006. 211(**6-8**): p. 587-97.
187. Weissleder, R. and M.J. Pittet, Imaging in the era of molecular oncology. Nature, 2008. 452(**718**7): p. 580-9.
188. Nahrendorf, M., et al., Nanoparticle PET-CT imaging of macrophages in inflammatory atherosclerosis. Circulation, 2008. 117(**3):** p. 379-87.
189. Devaraj, N.K., et al., 18F labeled nanoparticles for in vivo PET-CT imaging. Bioconjug Chem, 2009. 20(2): p. 397-401.
190. Kenny, L.M., et al., Quantification of cellular proliferation in tumor and normal tissues of patients with breast cancer by [18F]fluorothymidine-positron emission tomography imaging: evaluation of analytical methods. Cancer Res, 2005. 65(2**1)**: p. 10104-12.
191. Aboagye, E.O., Positron emission tomography imaging of small animals in anticancer drug development. Mol Imaging Biol, 2005. 7(1): p. 53-8.
192. de Vries, I.J., et al., Magnetic resonance tracking of dendritic cells in melanoma patients for monitoring of cellular therapy. Nat Biotechnol, 2005. 23(1**1)**: p. 1407-13.
193. Verdijk, P., et al., Sensitivity of magnetic resonance imaging of dendritic cells for in vivo tracking of cellular cancer vaccines. Int J Cancer, 2007. 120(**5):** p. 978-84.
194. Ntziachristos, V., et al., Visualization of antitumor treatment by means of fluorescence molecular tomography with an annexin V-Cy5.5 conjugate. Proc Natl Acad Sci U S A, 2004. 101(**33)**: p. 12294-9.
195. Graves, E.E., R. Weissleder, and V. Ntziachristos, Fluorescence molecular imaging of small animal tumor models. Curr Mol Med, 2004. 4(4): p. 419-30.
196. Christian, N.A., et al., In vivo dendritic cell tracking using fluorescence lifetime imaging and near-infrared-emissive polymersomes. Mol Imaging Biol, 2009. 11(3): p. 167-77.

197. Maes, W., et al., In v*ivo bioluminescence imaging in an experimental mouse model for dendritic cell based immunotherapy against malignant glioma. J N*eurooncol, 2009. 91(2**):** p. 127-39.
198. Ntziachristos, V., et al., Fluo*rescence molecular tomography resolves protease activity in vivo. Nat* Med, 2002. 8(7)**:** p. 757-60.
199. Lyons, S.K., Adv*ances in imaging mouse tumour models in vivo. J P*athol, 2005. 205(**2):** p. 194-205.
200. Frangioni, J.V., New *technologies for human cancer imaging. J C*lin Oncol, 2008. 26(2**4)**: p. 4012-21.
201. Lewis, J.S., et al., Smal*l animal imaging. current technology and perspectives for oncological imaging. Eur* J Cancer, 2002. 38(1**6)**: p. 2173-88.
202. Gambhir, S.S., Mole*cular imaging of cancer with positron emission tomography. Nat* Rev Cancer, 2002. 2(9)**:** p. 683-93.
203. Paans, A.M., et al., Posi*tron emission tomography: the conceptual idea using a multidisciplinary approach. Met*hods, 2002. 27(3**):** p. 195-207.
204. Blokland, J.A., et al., Posi*tron emission tomography: a technical introduction for clinicians. Eur* J Radiol, 2002. 44(1**):** p. 70-5.
205. Pagani, M., S. Stone-Elander, and S.A. Larsson, Alte*rnative positron emission tomography with non-conventional positron emitters: effects of their physical properties on image quality and potential clinical applications. Eur* J Nucl Med, 1997. 24(1**0)**: p. 1301-27.
206. Sitharaman, B., et al., Magn*etic resonance imaging studies on gadonanotube-reinforced biodegradable polymer nanocomposites. J B*iomed Mater Res A, 2009.
207. Pouponneau, P., J.C. Leroux, and S. Martel, Magn*etic nanoparticles encapsulated into biodegradable microparticles steered with an upgraded magnetic resonance imaging system for tumor chemoembolization. Bio*materials, 2009. 30(3**1)**: p. 6327-32.
208. Xu, R.X., et al., Fabri*cation of indocyanine green encapsulated biodegradable microbubbles for structural and functional imaging of cancer. J B*iomed Opt, 2009. 14(3**):** p. 034020.
209. Kempe, S., et al., Non-*invasive in vivo evaluation of in situ forming PLGA implants by benchtop magnetic resonance imaging (BT-MRI) and EPR spectroscopy. Eur* J Pharm Biopharm, 2009.
210. Doiron, A.L., et al., Poly*(lactic-co-glycolic) acid as a carrier for imaging contrast agents. Pha*rm Res, 2009. 26(3**):** p. 674-82.
211. Park, Y.J., et al., Surf*ace-modified poly(lactide-co-glycolide) nanospheres for targeted bone imaging with enhanced labeling and delivery of radioisotope. J B*iomed Mater Res A, 2003. 67(3**):** p. 751-60.
212. Delgado, A., et al., Radio*labelled biodegradable microspheres for lung imaging. Eur* J Pharm Biopharm, 2000. 50(2**):** p. 227-36.
213. Swirski, F.K., et al., A ne*ar-infrared cell tracker reagent for multiscopic in vivo imaging and quantification of leukocyte immune responses. PLo*S One, 2007. 2(10**)**: p. e1075.

Chapter Two

Active targeting of dendritic cells with mannan-decorated PLGA nanoparticles

A version of this chapter has been submitted for publication in

Journal of Drug Targeting

Ghotbi, Z.[1], Haddadi, A.[1], Hamdy, S.[1], Hung, R.W.[1,2], Samuel, J.[1] and Lavasanifar, A.[1,3].

[1], Faculty of Pharmacy and Pharmaceutical Sciences, 3133 Dentistry/Pharmacy Centre, University of Alberta, 4119 Dent/Pharm Centre, Edmonton, Alberta T6G 2N8, Canada.

[2], Faculty of Medicine, Department of Radiology and Diagnostic Imaging, University of Alberta, [3], Faculty of Engineering, Department of Chemical and Material Engineering, University of Alberta

and

presented as a poster in American Association of Pharmaceutical Scientists (AAPS), Los Angeles, California, USA, November 8-12, 2009

2.1. Introduction

Cancer vaccines involve stimulation of the immune system using cancer antigens with the goal of immune-mediated eradication of cancer cells. Unlike conventional therapies (such as radiation, chemotherapy and surgery), cancer vaccines are safer, more specific and offer long-term effects via development of immunologic memory [1]. A major limitation of current cancer vaccines is that the immune responses elicited by cancer vaccines are weak or modest [2]. Enhancing the immunogenicity of the vaccines requires more efficient targeting of cancer antigens and immunostimulatory adjuvants to dendritic cells (DCs), the key cells responsible for the activation of T cell-mediated immunity.

The first attempts to exploit DCs in cancer immunotherapy were based on *ex-vivo* loading of autologous DCs with tumor-associated antigens to enhance T-cell responses. Although the initial results are promising, this strategy suffers from high cost and labour-intensive procedures, insufficient distribution of transplanted DCs, limited homing of DCs to the lymph nodes (0.5-2%) as well as poor immune responses in clinic [3-5]. Development of particle-based cancer vaccines that mimic pathogens in size and deliver cancer antigens along with immunostimulatory adjuvants to DCs *in vivo* could overcome these limitations, increase antigen internalization and presentation resulting in enhanced DC maturation and more efficient T-cell-mediated immune responses. Among several delivery systems, FDA approved, biodegradable and biocompatible poly(D, L-lactide-*co*-glycolide) (PLGA) nanoparticles (NPs) are shown to be efficient vehicles for vaccine delivery [6-9]. In fact, several reports have demonstrated remarkable induction of DC maturation, T cell activation and anti-tumor immune responses following by co-delivery of antigens along with immunostimulatory adjuvants in PLGA-NPs [9-12].

PLGA-NP size is comparable to pathogens; hence, they are naturally targeted to DCs and other phagocytic cells without specific recognition [13]. Attachment of targeting moieties on PLGA surface could further facilitate the

uptake of NPs by DCs and also enhance DC maturation which ultimately leads to improving the effectiveness of vaccine formulation. There are two main strategies for specific targeting of PLGA-NPs to DCs. ***First***, is to decorate the NP surface with monoclonal antibodies (mAbs) against DC-specific receptors. This strategy could be applied when the natural ligand of the receptor is not known (e.g. DEC-205) [14]. Antibodies can bind to the receptors improving the specificity of vaccine for DCs. Recent studies have demonstrated targeting antigens to CD11c, a receptor predominantly expressed on DCs, to induce robust activation of antigen-specific immune responses [15]. PLGA-NPs have been successfully linked to a variety of DC-specific antibodies, including anti-CD40, Fcγ, α(v)β3 and α(v)β5 integrin receptors [16]. These formulations demonstrated a superior ability to induce DC maturation evidenced by an increase in IL-2 secretion and the up-regulation of DC maturation markers (CD83 and CD86) compared to the plain PLGA-NPs [16]. Despite promising results, large scale synthesis of mAb-decorated PLGA-NPs for clinical setting may be very expensive and time consuming.

An alternative strategy for targeting PLGA-NPs to DCs, which is less explored, is to decorate NPs with the natural ligands for DC-endocytic receptors, such as C-type lectin receptors (CLRs). The CLRs are a family of Ca^{2+}-dependent lectins that recognize endogenous and exogenous carbohydrate residues through their conserved carbohydrate recognition domain (CDR) [17, 18]. So far, more than 60 CLRs are identified in humans [19]. Mannose receptor (MR) is a member of CLR family expressed on immature murine and human monocyte-derived DC subsets as well as macrophages. Recognition by MR facilitates internalization and further antigen processing and presentation by both MHC-I and MHC-II pathways [20-22]. Uptake of soluble antigens through MR has been associated with a substantial increase in both antigen presentation and T cell stimulation (up to 100-fold) [20]. Mannan (MN) is a polysaccharide isolated from the cell wall of *Saccharomyces cerevisiae* with strong binding to MR and has been used for enhanced targeting of vaccine formulations to DCs and

macrophages [23-25]. In this context, chemical attachment of MN to chitosan [26], dendrimer [27], peptides [28] or antigens [24] has been exploited. More importantly, MN conjugated cancer antigens (MUC1 peptides) have been used in clinical trials [29]. In the current study, development of MN-decorated PLGA-NPs has been pursued. Our working hypothesis was that the incorporation of MN as active targeting ligand of MRs in PLGA-NPs would enhance the antigen uptake by DCs. Other phagocytic cells (e.g., macrophages) are also expected to internalize the particles. However, this is not expected to have any negative impact on the immunogenicity of the vaccine. Unlike mAbs, MN is a commercially available and inexpensive product. Therefore, large scale preparation of MN-decorated PLGA-NPs could be achieved in a reasonable time and minimal cost, compared to mAbs-decorated PLGA-NPs.

PLGA co-polymers are aliphatic polyesters composed of varying proportions of lactic and glycolic acids. These polymers are commercially available in two forms depending on end-group functionality; either free carboxylic acid end groups (uncapped) or esterified end groups (capped) (**Figure 2.1**). Several reports have demonstrated that PLGA structure can influence the incorporation efficiency and release pattern of loaded drugs [30-32]. In the light of these finding, we pursued incorporation of MN to PLGA-NPs made from either capped or uncapped PLGA. Furthermore, we have utilized various methods for incorporating MN into PLGA-NPs. Finally, the effect of polymer type and the incorporation method on the extent of MN incorporation and NP uptake by DCs have been investigated to identify an optimum targeted particulate vaccine formulation based on PLGA-NPs.

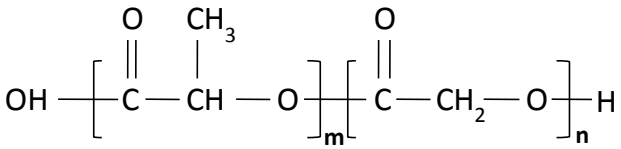

COOH-terminated (uncapped)

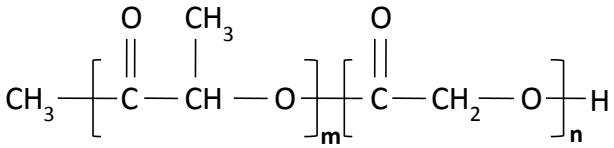

Ester-terminated (capped)

Figure 2.1-Chemical structure of carboxyl and ester-terminated PLGA.

2.2. Materials and Methods

2.2.1. Materials

Ester-terminated PLGA copolymer (average MW of 7KDa and lactide to glycolide ratio of 50:50) and COOH-terminated PLGA (inherent viscosity range of 0.15-0.25 dL/g and lactide/glycolide ratio of 50:50) were purchased from LACTEL®, Birmingham polymers (DURECT Corporation, USA). Polyvinyl alcohol (PVA) with MW 31-50KDa, MN derived from S. Cerevisiae, Sodium Dodecyl Sulphate (SDS), phenol and N**,**N'-Dicyclohexyl-Carbodiimide (DCC) were purchased from Sigma-Aldrich (St. Louis, MO, USA). Dichloromethane, chloroform, and sulfuric acid (98%) were purchased from Caledon Laboratories Ltd. (Toronto, ON, Canada). Sulfo-N-hydroxysuccinimide (sulfo-NHS) was purchased from ProteoChem, Inc. (Denver, CO USA). Gibco RPMI-1640 with L-glutamine, Gentamycin, Fetal Bovine Serum (FBS), Tetramethyl Rhodamine Dextran (TMRD) MW 40KDa, neutral , Gold Antifade reagent with DAPI were supplied by Invitrogen (Carlsbad, CA, USA). Recombinant murine granulocyte–macrophage colony-stimulating factor (GM-CSF) was purchased from Peprotech

(Rockville, IL). Anti-mouse Fluorescein isothiocyanate (FITC) anti-mouse CD11c and its respective Isotype control, purified anti mouse CD16/ CD32 (Fc_{γ}-III/II receptor) and Phycoerythrin-Cy5 (PE-Cy5) Streptavidin were purchased from BD Biosciences-Pharmingen (San Diego, CA, USA). Biotinylated anti-mouse CD206 (MMR Ab and its respective isotype control were purchased from BioLegend (San Diego, CA, USA).

2.2.2. Mice

C57Bl/6 mice were purchased from the Jackson Laboratory (Bar Harbor, ME, USA). All experiments were performed in accordance to University of Alberta guidelines for the care and use of laboratory animals. All experiments were performed using 6 to 12 week old female mice.

2.2.3. Preparation of MN-decorated NPs

2.2.3.1. Plain NPs - Ester-terminated PLGA-NPs were prepared using a double-emulsion solvent evaporation technique as previously reported in [33, 34]. In this method, a primary W/O emulsion is formed by emulsification of the first aqueous phase (100 µL PBS) with the organic phase (100 mg PLGA in 300 µL chloroform) using a microtip probe sonicator (Model XL2010, Heat Systems, Farmingdale, NY). The primary emulsion is further emulsified with a secondary aqueous phase (2 mL of 9% PVA in PBS) to form a secondary W/O/W emulsion. The resulting emulsion is transferred drop-wise to stirring 8 mL of 9% PVA in PBS to allow the removal of chloroform by evaporation. After 3 hours, the NP suspension is washed three times at 4 °C (35000 × g, 15 min) and freeze-dried **(Figure 2.2)**.

COOH-terminated PLGA-NPs were also prepared by double-emulsion solvent evaporation technique with some modifications from the previously reported method for ester-terminated PLGA. In brief, a primary W/O emulsion is formed by emulsification of the first aqueous phase (100 µL PBS) with the organic phase (100 mg PLGA in 1 mL DCM). The primary emulsion is further

emulsified with a secondary aqueous phase (4 mL of 5% PVA in PBS) to form a secondary W/O/W emulsion. The resulting emulsion is transferred drop-wise to stirring 16 mL of distilled water to allow the removal of DCM by evaporation. After 3 hours, the NP suspension is washed and freeze-dried as described above.

2.2.3.2. MN incorporation- Incorporation of MN to either ester or COOH terminated PLGA-NPs was achieved by two main strategies as described in **Table 2.1**. ***The first strategy*** involved addition of MN during the process of NP formulation. In brief, an aqueous solution of MN (2 mg in100 µL PBS) was added during the first emulsification step to form the primary emulsion. The resulted formulations were designated as MN-W1-Ester and MN-W1-COOH; whereas W1 indicates that MN was added within the first aqueous phase during the formulation of ester or COOH-terminated PLGA-NPs, respectively. In addition, we have also tried an alternative method where 15 mg of MN was dissolved into the secondary aqueous phase (9% or 5% PVA), the resulted formulations were designated as MN-W2-Ester and MN-W2-COOH, respectively.

The second strategy involved attachment of MN onto the surface of the freeze dried NPs either by physical adsorption or by chemical reaction. For physical adsorption method, 50 mg of plain ester or COOH-terminated PLGA-NPs was thoroughly mixed with 100 mg of MN in 10 mL PBS (pH 5.0) and stirred at room temperature overnight. The PLGA-NPs with adsorbed MN were then collected, washed off from soluble MN by spinning at 4 °C three times (35000 × g, 15 min) and freeze-dried. NPs prepared using this method, were designated as MN-Ads-Ester or MN-Ads-COOH. On the other hand, the presence of free COOH group in the COOH terminated polymer allowed for covalent attachment of MN to PLGA-NPs. In this method, a mixture of 100 mg MN, 765 µg DCC and 2.295 mg sulfo-NHS was added to 50 mg of COOH-terminated PLGA-NPs and dispersed in 10 mL acidic PBS (pH 5.0) [35]. The mixture was then stirred at room temperature overnight. The excess reagents and soluble by-products were then washed away using cold PBS and ultracentrifugation at 35000 × g for 15 min. The NPs were then freeze-dried. NPs prepared using this method,

were denoted as MN-Cov-COOH. **Table 2.1** summarizes the different methods utilized for MN incorporation and the respective designation of the formulated NPs throughout this chapter.

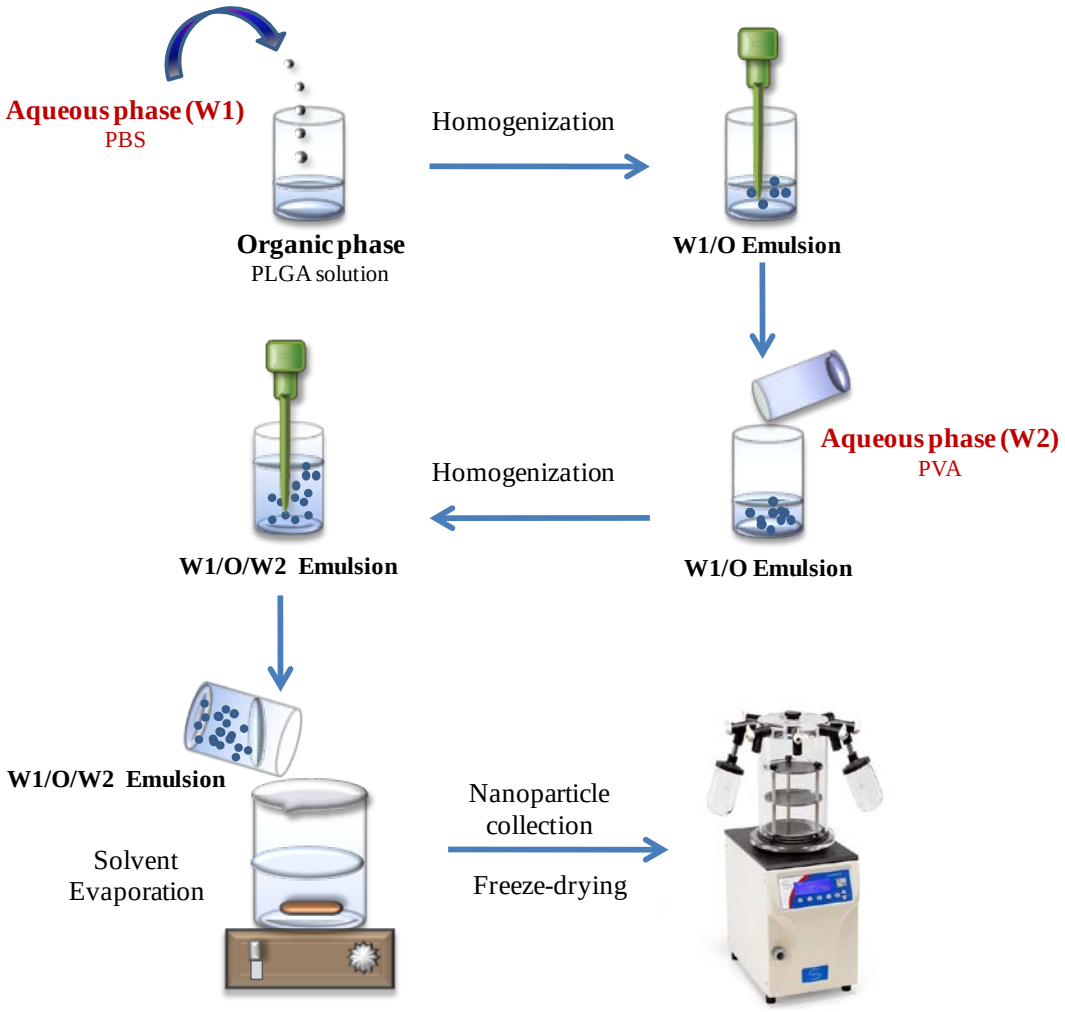

Figure 2.2: Double emulsification solvent evaporation technique for preparation of plain PLGA-NPs (ester or COOH-terminated, based on the polymer used). Addition of MN to the primary aqueous phase (W1) during the process of NP formulation resulted to MN-W1-NPs. MN-W2-NPs are the results of MN addition to the secondary aqueous phase (W2) during NP preparation. The freeze-dried plain NPs are used for attachment of MN onto the NPs either by physical adsorption (MN-Ads NPs) or by covalent conjugation (MN-Cov-NPs).

Table 2.1: Different methods of mannan incorporation and the respective designation of the formulated NPs.

Mannan incorporation	During emulsification steps		After nanoparticle preparation	
	In first aqueous phase (W1)	In second aqueous phase (W2)	Physical adsorption	Chemical binding
Ester-PLGA	MN-W1-Ester	MN-W2-Ester	MN-Ads-Ester	
COOH-PLGA	MN-W1-COOH	MN-W2-COOH	MN-Ads-COOH	MN-Cov-COOH

2.2.4. Characterization of MN-decorated NPs

NPs were characterized in terms of average particle size, size distribution and Zeta potential. In addition, the effect of polymer type and MN incorporation method on the incorporation level and release of MN was investigated by extraction and quantification of MN from different NP formulations.

2.2.4.1. Particle size- The average particle size and size distribution of prepared NPs were determined by Dynamic-Light Scattering (DLS) technique using Zetasizer 3000 (Malvern, UK).

2.2.4.2. Zeta Potential- NPs were dispersed at a concentration of 0.02 % (w/v) in distilled water. Zeta potential of each formulation was measured using Zetasizer 3000 (Malvern, UK).

2.2.4.3. Level of MN incorporation- The effect of polymer type and MN incorporation method on the incorporation level of MN was investigated by extraction and quantification of MN from different NP formulations. Physically incorporated MN was extracted from NPs using a DCM/ water extraction system. In brief, 5 mg of NPs were dissolved in 500 µL DCM in a microcentrifuge tube by vortexing and sonication. Water (700 µL) was then added and two phases were mixed very gently and thoroughly. The aqueous phase was separated and heated in a water bath to 40 °C to evaporate the remaining DCM. This was followed by centrifugation at 14000 × g for 15 min to remove the insoluble fractions and MN dissolved in the supernatant was then quantified. In MN-Cov-COOH the ester

bonds between MN and PLGA molecules were dissociated before analysis of MN. In this method, 2 ml NaOH (1 N) was added to a dispersion of MN-Cov-COOH NPs (5 mg) in 200 µL water and stirred overnight. The pH was adjusted to neutral with HCl, followed by centrifugation at 14000 × g for 15 min and MN in supernatant was then analyzed. MN quantification was accomplished by colorimetric assay using phenol-sulfuric acid method [36]. In this method, 150 µL of concentrated sulfuric acid (96%) was added rapidly to 50 µL of supernatant in a flat 96-well plate. This was followed by the addition of 30 µL of 5% (w/v) phenol and mixing. The plate was then placed in a heated static water bath for 5 min at 90 °C to allow for color development followed by cooling down to room temperature to stop the reaction. The absorbance was read at 490 nm in a microplate reader. The linear relationship between MN concentration and absorbance was investigated within the range of 15-1000 µg/mL of MN. The extent of MN incorporation in NPs was calculated from the following equation and expressed as amount of MN (in µg) per 1 mg dry weight of NPs.

$$\textbf{MN incorporation } (\mu g/mg) = \frac{\textbf{amount of incorporated MN } (\mu g)}{\textbf{initial weight of the polymer } (mg)}$$

(Equation 2-1)

The efficiency of the extraction procedures for the above methods was measured by a spiking study, where known amount of MN was added to plain NPs. Following extraction, the supernatant was assayed for MN using the colorimetric assay described above. The extraction recovery was calculated as the amount detected/ amount used in spiking □ 100.

2.2.4.4. Release of MN from NPs- Known amount of MN-decorated NPs were reconstituted in 2 mL of distilled water in a microcentrifuge tube, and kept at 37 °C in a water bath (Yamato, YB-521, Japan). In various time intervals, one of the samples was removed and centrifuged (Eppendorf microcentrifuge 5415C) at 14,000 × g for 15 min. The resulting supernatant was freeze-dried and then dissolved in 100 µL water. The released MN (in supernatant) and the MN retained

in NPs were quantified by Phenol-sulfuric acid method, as described earlier. The *in vitro* release of MN was calculated from the following equation:

$$\textbf{MN } \textit{in vitro} \textbf{ release } (\%) = \frac{\textbf{amount of released MN } (\mu\textbf{g})}{\textbf{total MN incorporated in NPs } (\mu\textbf{g})} \times \mathbf{100}$$

(Equation 2-2)

2.2.5. TMRD-loaded NPs

2.2.5.1. Preparation and characterization of TMRD-loaded NPs- Encapsulation of TMRD in MN-decorated NPs was pursued in order to achieve fluorescently labelled NPs for cell uptake studies. For the preparation of TMRD-loaded NPs, 0.5 mg TMRD (in 50 µL) was incorporated to organic solvent (chloroform or DCM based on the polymer type) during the preparation of NP formulations.

Analysis of loaded TMRD was then performed. In brief, 2 mg of TMRD-loaded NPs was dispersed in 5.0 mL of 0.1M NaOH containing 5% (w/v) SDS (pH 7.4) and stirred for 24 h in dark at room temperature until a completely clear solution was obtained. To measure the fluorescence intensity, 100 µL of the solution of degraded NPs was transferred into a black opaque 96-well plate in triplicate, and the plate was read at the emission wavelength of 582 nm using a fluorescent spectrophotometer with a microplate reader attachment (Biotek Synergy^{TM} 2, Biotek instruments, Winooski VT, USA). Analyses were performed by comparing the fluorescence intensity of each sample to a calibration curve obtained from standard solutions of TMRD in 0.1 M NaOH containing 5% (w/v) SDS.

2.2.5.2. Leaching of TMRD from NPs- To assess the release of TMRD from NPs during the cell uptake studies, 2 mg of TMRD-loaded NPs was dispersed in 0.5 mL PBS. This dispersion was added to a 100 mm cell culture plate containing 20 mL DC culture media at 37 °C. A cell culture plate was taken at 0, 0.5, 2, 6 and 20 h intervals and centrifuged at 1500 × g for 10 min. The pellet was re-suspended in 5.0 mL NaOH (0.1 M) in SDS (5% w/v) stirring overnight.

Degraded NPs were diluted with SDS/NaOH and the fluorescence intensity was measured against standard solutions made with the same solvent and used to calculate the amount of TMRD in the pellet. The collected supernatant (200 µL) was transferred to a black opaque 96-well plate and the fluorescence intensity was measured against a standard solution made with DC culture media. The fraction of TMRD was calculated by dividing the amount of TMRD in the supernatant (µg) to the sum of the TMRD in supernatant and pellet (µg).

2.2.6. Isolation and culture of murine bone marrow-derived DCs (BM-DCs)

The method for generating BM-DC was adapted from previous publications with minor modifications [9, 37]. Briefly, femurs and tibias of C57BL/6 mice were removed and purified from surrounding tissues. The bone marrow was flushed from both ends of the intact bones with PBS using an insulin syringe. Cells were triturated and filtered through a nylon screen (40 µm cell strainer) to obtain a single-cell suspension. About 3-5 $x10^7$ leukocytes were obtained per femur and tibia. Cells were washed and 2 x 10^6 cells were seeded in 100 mm non-treated cell culture dishes in 10 mL DC complete media (RPMI-1640 with L-glutamine and Gentamycin) supplemented with 20 ng/mL of GM-CSF and 10 % heat-inactivated FBS, followed by additional 10 mL fresh DC media containing 20 ng/mL GM-CSF at day 3. At day 6, culture media was replaced by fresh media containing 20 ng of GM-CSF.

2.2.7. Flow cytometry studies

2.2.7.1. Expression of CD11c - One day after pulsing DCs with NPs, i.e. at day 8 of seeding the cells, harvested semi-adherent and non-adherent cells were washed 3 times with 20 mL of PBS containing 2% FBS. To block Fcγ receptors, 200 µL of the cell suspension ($4x10^5$) was transferred into a round bottom 96-well culture plate and was incubated with 0.1 mg of anti mouse CD16/ CD32 mAb. The cells were then stained with 0.1 mg (0.5 mg/ml) FITC- labelled CD11c, as a DC-specific marker. After three washing cycles with PBS containing 2% FBS (FACS

buffer) , a live single-cell population dispersed in FACS buffer ($4x10^5$ cells) were acquired with a three-line flow cytometer (Becton-Dickinson FACSort, BD Biosciences) and analyzed for FITC- labelled CD11c using a Summit 3.1 software (DakoCytomation).

2.2.7.2. MR expression- The expression of MR was assessed by fluorescence-activated cell sorting (FACS) on different days of BM-DC culture. In brief, on days 3, 6 and 7, semi-adherent and non-adherent cells were harvested and washed twice with cold FACS buffer (PBS with 2% FBS). Then, $4x10^5$ DCs were re-suspended in FACS buffer incubated with anti mouse CD16/CD32 mAb to block Fcγ receptors before staining with biotinylated anti-mouse CD206 (MMR) mAb followed by PE-Cy5 Streptavidin. After three washes, cell suspensions were acquired on a three-line flow cytometer (Becton-Dickinson FACSort, BD Biosciences, Franklin Lakes, NJ). The data were analyzed using CELL- Quest software (Becton Dickinson).

2.2.7.3. Uptake studies- At day 7 of culture, BM-DCs were treated with different formulations of MN-decorated TMRD-loaded NPs (2 mg dispersed in 0.5 mL PBS). Control groups were treated with plain NPs, plain TMRD-loaded NPs or PBS. Semi-adherent and non-adherent cells were harvested after 20 h incubation with NPs. Harvested DCs were washed thoroughly (3 times) with cold FACS buffer to remove non-internalized NPs and soluble TMRD. A suspension of $4x10^5$ DCs was then incubated with anti mouse CD16/ CD32 mAb before staining with FITC-anti CD11c mAb and washed with FACS buffer. The isotype standard for FITC-anti CD11c antibody was used to measure background fluorescence intensity. For control, FACS studies were performed on PLGA-NPs in the absences of cells. A suspension of NPs (2 mg in 0.5 mL PBS) were added to cell culture dish containing DC media and placed at 37°C and 5% CO_2 overnight. All samples were acquired with a three-line Becton-Dickinson FACSort flow cytometer and analyzed using Summit 3.1 software (DakoCytomation). In flow cytometric studies, the region of the events, i.e. gating for the uptake of ester-

terminated and COOH-terminated NPs was chosen separately, based on the dot plot patterns of different PLGA NPs in the absence and presence of DCs.

2.2.8. Intracellular localization of NPs analyzed by Confocal Microscopy

Intracellular disposition of MN-decorated NPs was visualized using Laser Scanning Confocal Microscopy (LSCM). Briefly, $5x10^6$ of seven-day-old DCs were re-plated to a 50 mm cell culture dish, incubated at 37°C and 5% CO_2 and allowed to stabilize for 2 h prior to treatment with different MN-decorated TMRD-loaded NPs (0.2 mg NPs in 1 mL media) for 24 h. Cell suspension of each dish were collected and plated into wells of a round bottom 96-well culture plate (~$1x10^6$ cells/well). Cells were precipitated by spinning and washed twice with 250 µL PBS. Cell suspensions were then stained with FITC-labelled CD11c mAb and washed using PBS with 2% FBS. Cells were fixed for 20 min with 100 µL of 4% paraformaldehyde in PBS to each well, followed by washing with PBS and re-suspension in PBS. The nuclei were counterstained with DAPI (Gold Antifade reagent with DAPI) in cell-containing region of the slide and the cells were examined by a confocal microscope Zeiss 510 LSM NLO (Carl Zeiss, Jena, Germany) with identical settings for each confocal study. Scans from each channel were collected in multi-track mode to avoid cross-talk between channels.

Statistical analysis

The parametric data are presented as the mean ± standard deviation (SD). The data were analyzed for statistical significance ($P<0.05$) between multiple groups by one-way ANOVA followed by post-hoc comparisons with scheffe method. Comparisons between two groups were analysed by unpaired Student's t-test. The significance of r^2 was calculated from the following formula:

$t= r/ (1-r^2)/ (N-2)^{1/2}$.

2.3. RESULTS

2.3.1. Characterization of plain and MN incorporated PLGA-NPs

2.3.1.1. Particle size- Different NP formulations were characterized before and after MN incorporation in terms of their particle size and size distribution. Results are summarized in **Table 2.2**. There was a significant increase in the average diameter of most NPs after MN incorporation (analyzed by unpaired Student's t-test), with the exception of MN-W1-Ester, MN-W2-Ester and MN-W2-COOH NPs (**Table 2.2)**. While plain NPs had a mean diameter of 328 and 383 nm for COOH-terminated and ester-terminated PLGA, respectively; MN-decorated NPs showed a mean diameter in the range of 384-511 nm (for the ester-terminated PLGA-NPs) and 346-490 nm (for the COOH-terminated NPs) depending on the MN incorporation method **(Table 2.2)**. Incorporation of MN did not cause any significant change in the polydispersity of NPs.

Table 2.2: Effect of polymer type and formulation method on particle size and polydispersity Index of prepared NPs.

Nanoparticle	Mean diameter ± SD (nm)[a]	Polydispersity Index ± SD[a]
Plain-Ester	383 ± 45	0.14±0.06
MN-W1-Ester	384 ± 43	0.14±0.05
MN-W2-Ester	407 ± 41	0.13±0.08
MN-Ads-Ester	511 ± 26*	0.17±0.02
Plain-COOH	328 ± 30	0.13±0.08
MN-W1-COOH	389 ± 23*	0.10±0.08
MN-W2-COOH	346 ± 17	0.12±0.06
MN-Ads-COOH	490 ± 12*	0.19± 0.07
MN-Cov-COOH	430 ± 45*	0.17±0.07

*Statistically different from plain NPs

[a] measured by DLS technique

[b] measured by phenol-sulphuric acid colorimetric assay

NA not applicable

2.3.1.2 Zeta potential- Non-decorated PLGA-NPs showed a negative surface charge in distilled water, characterized by the Zeta potential values (-25.0 mV for the ester-terminated and -36.2 mV for the COOH-terminated PLGA-NPs, on average). Following MN incorporation, Zeta potential of NPs has dropped significantly in most cases, reaching to a maximum of -41.9 mV and -46.4 mV for ester-terminated and COOH-terminated PLGA-NPs, respectively (**Figure 2.3**). Net surface negative charge among the ester-terminated NPs followed this trend accordingly: MN-Ads-Ester> MN-W2-Ester > MN-W1-Ester = plain NPs. For the COOH-terminated NPs, maximum negative charge was observed for MN-Cov-COOH and MN-Ads-COOH. This was followed by MN-W2-COOH which showed a higher negative charge than MN-W1-COOH and plain NPs that had similar zeta potentials **(Figure 2.3)**.

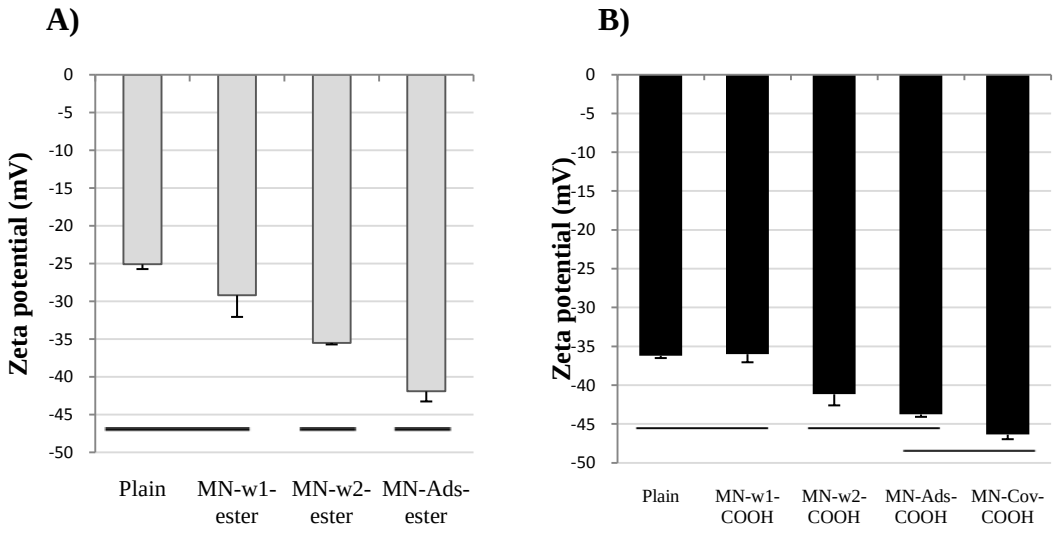

Figure 2.3: Evaluation of Zeta potential among **A)** Ester-terminated and **B)** COOH-terminated MN-decorated NPs. Continuous lines indicate lack of significance between groups encompassed by the lines; groups not encompassed within lines are significantly different from those encompassed by the lines (unpaired Student's t-test; $p<0.05$). Each bar represents mean % ± SD (n=3-5).

2.3.1.3. Incorporation of MN- The NPs were also assessed for their level of MN incorporation **(Figure 2.4).** The physically incorporated MN was efficiently extracted from NPs with an extraction efficiency of 86.2% and 87.7% for ester-terminated and COOH-terminated PLGA-NPs, respectively. . The extraction efficiency was 62.3% in the case of MN-Cov-NPs, where the extraction was achieved by the chemical bond cleavage between MN and PLGA molecules. The results showed a linear relationship between concentration of MN and the absorbance at 490 nm within the range of 15-1000 µg/mL of MN per well (r^2=0.9997) **(Figure 2.4A)**. Among all formulations, incorporation of MN was the highest for MN-Cov-COOH-NPs (365±37 µg MN/mg PLGA) **(Figure 2.4B)**. In case of formulations with physically incorporated MN, the following trend was observed for both ester and COOH-terminated PLGA-NPs: MN-Ads>MN-W2=MN-W1 **(Figure 2.4B),** (analyzed by one-way ANOVA, followed by post-hoc scheffe's analysis)**.** When identical incorporation methods were used, no significant difference in MN incorporation levels were observed between ester and COOH-terminated PLGA-NPs.

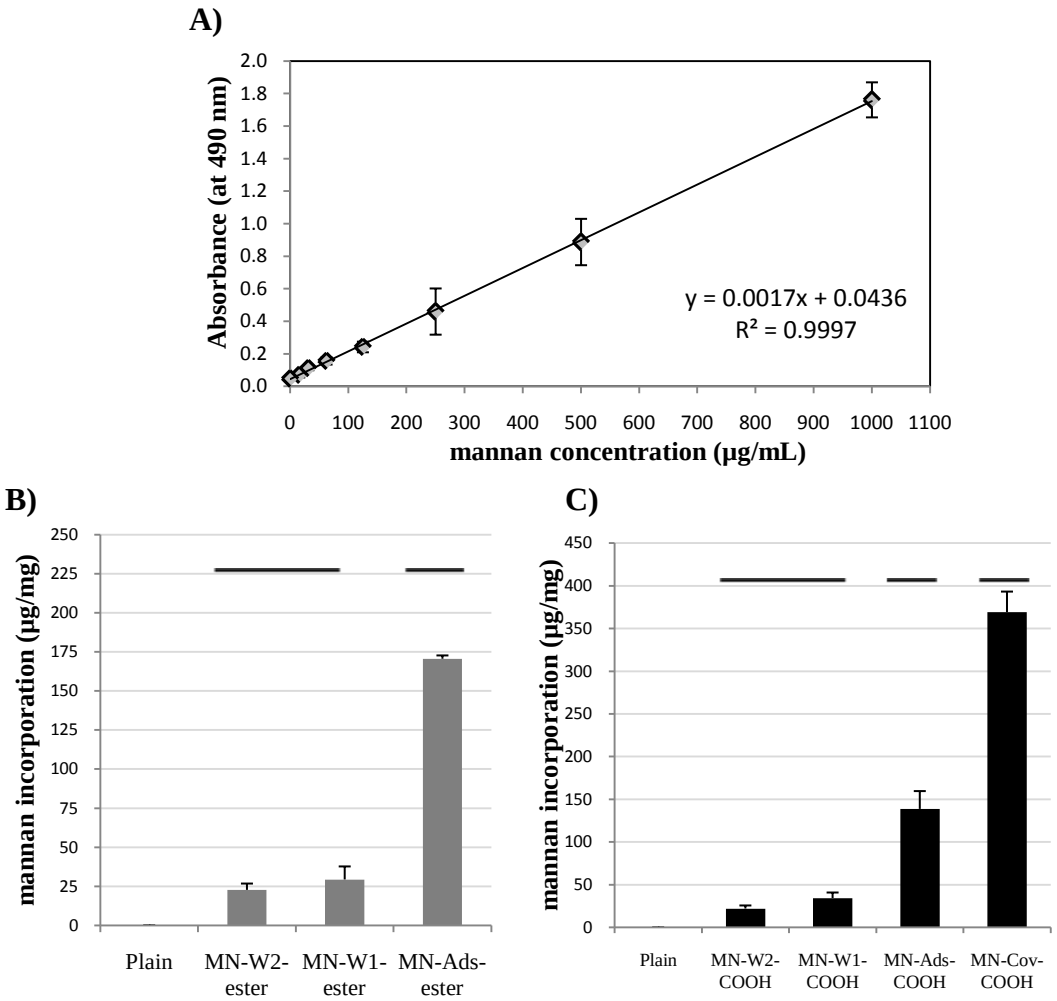

Figure 2.4: Determination of MN in various formulations using phenol-sulfuric acid colorimetric assay. **A)** Standard curve correlation.MN incorporation in **B)** ester-terminated and **C)** COOH-terminated NPs. Continuous lines indicate lack of significance between groups encompassed by the lines; groups not encompassed within lines are significantly different from those encompassed by the lines (Student's t-test; $p<0.05$). Each bar represents mean % ± SD (n=3).

2.3.2. In vitro release of MN

To verify whether MN remains incorporated in NPs during DC treatment, the *in vitro* release of MN from NPs was assessed under the same conditions of the DC uptake studies. The ester-terminated NPs showed <13±5% release of MN in the first 2 h **(Figure 2.5A).** MN release from NPs reached 27±2

% within 24 h of incubation. The COOH-terminated NPs showed 16±3% and 28±2% release of MN in the first 2 h and after 24 h, respectively **(Figure 2.5B).**

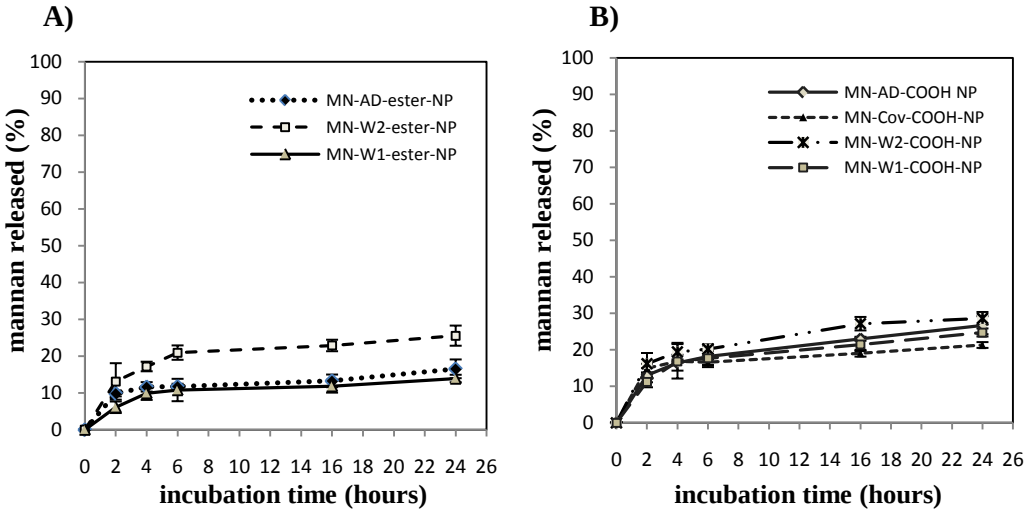

Figure 2.5: Release of MN at 37 °C from the same concentration of **A)** ester-terminated, and **B)** COOH-terminated PLGA-NPs used for the DC uptake assessment. Released MN was quantified by Phenol-sulfuric acid method and each point represents mean % ± SD (n=3).

2.3.3. Leaching of TMRD from NPs

To assess the association of TMRD with PLGA-NPs during uptake studies, the release of TMRD from NPs was performed in similar condition to uptake studies. A simple, rapid and sensitive fluorimetric method for the determination of TMRD, either released to DC culture media, or extracted from degradaded TMRD-loaded NPs by SDS/NaOH was developed. The fluorescence standard prepared in DC culture media showed a high linear correlation between TMRD and fluorescence intensity at 582 nm (r^2=0.9966) **(Figure 2.6A)**. The results showed a linear relationship between concentration TMRD and fluorescence intensity in SDS/NaOH solution (r^2=0.9982) **(Figure 2.6B).**

The results indicated that only 4.9±1.1% of TMRD loaded in ester-terminated PLGA-NPs was diffused out after 0.1 h incubation and approximately 93% of TMRD was remained inside the NPs after 20 h incubation in DC media

(Figure 2.6C). The release of TMRD from COOH-terminated PLGA-NPs was significantly higher ($P<0.05$; analyzed by student's t-test). At 0.1 h, 22.7±1.7% of incorporated TMRD leached out of the COOH-terminated PLGA-NPs. This level reached to 29.0±3.1% of the incorporated TMRD within 20 h incubation showing more than 70 % of the loaded TMRD was still incorporated in the NPs **(Figure 2.6C).**

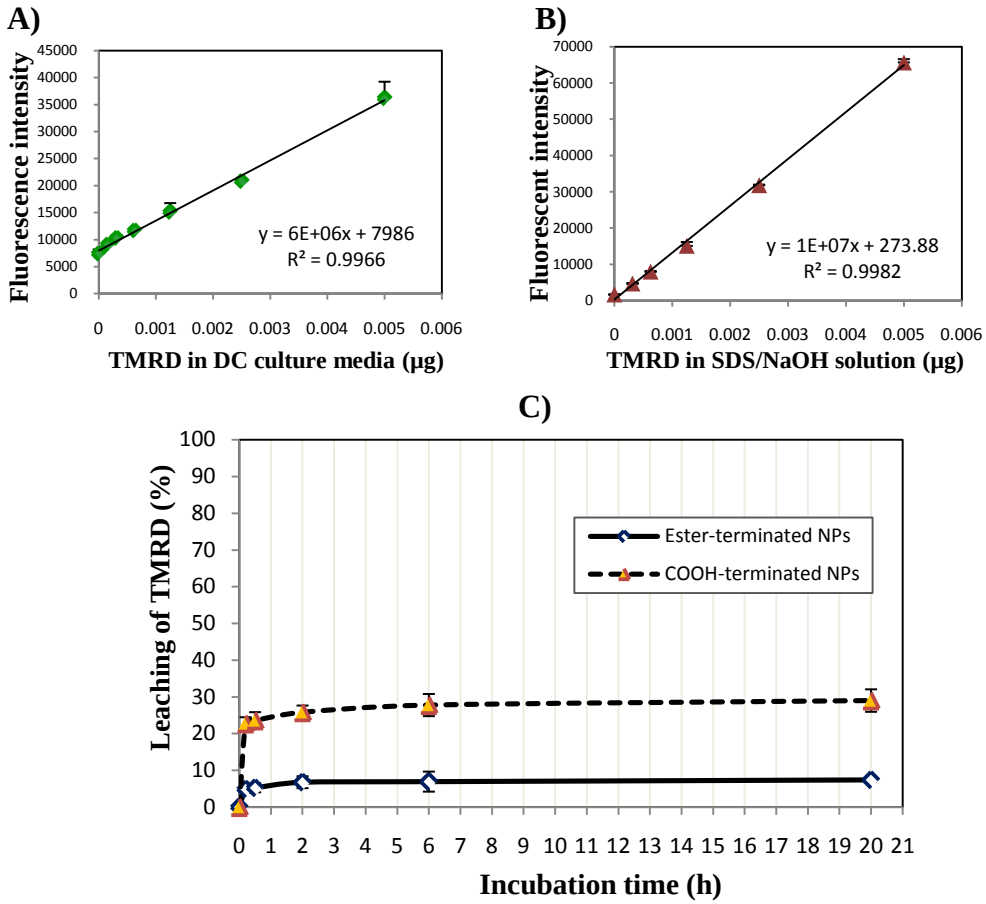

Figure 2.6: Release of TMRD from PLGA-NPs in DC culture media at 37°C, measured by fluorescent spectroscopy. **A)** Standard curve for TMRD in DC culture media. **B)** Standard curve in a SDS/NaOH solution. C) The ratio of TMRD released to the culture media and the TMRD retained in NPs was calculated against the regression line specified for the environment. Each point represents mean % ± SD (n=3).

2.3.4. The effect of MN incorporation on the uptake of NPs by DCs

2.3.4.1. MR expression- The expression of MRs on the primary culture of DCs isolated from murine bone marrow was investigated by flow cytometry. Our data showed that MR expression is age-dependent **(Figure 2.7A)**. Maximum expression of MR (42% of the whole cultured cells) was observed seven days after seeding **(Figure 2.7B)**. Based on this result, 7-day-old cultured cells were used in subsequent uptake studies. In addition, using CD11c as a DC marker, double color staining was performed to check the percentage of DCs expressing MR on Day 7. Our results showed that 36% of the cells were $CD11c^{+}/MR^{+}$.

A)

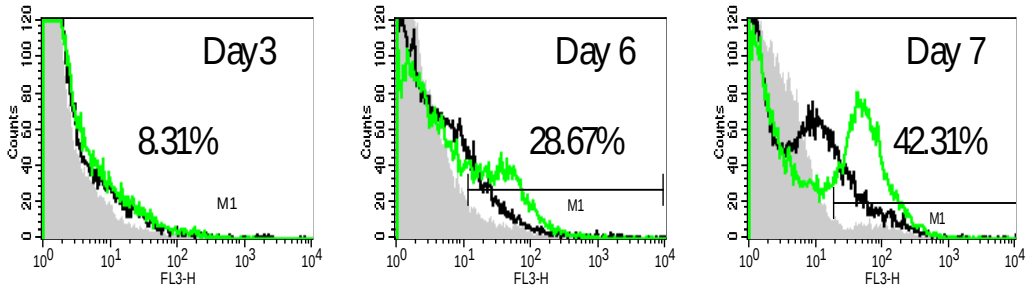

B)

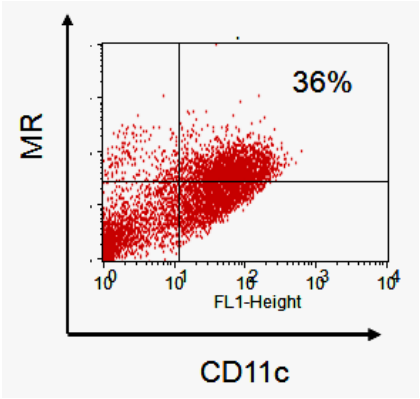

Figure 2.7: Flow cytometric characterization of live population of primary DC culture for MR expression. One representative experiment out of 3 is shown. **A)** The cells were harvested 3, 6 and 7 days after seeding; stained with biotinylated CD206 mAb followed by PE-Cy5 Streptavidin and co-stained with FITC-labelled CD11c mAb. The gray and black colors represent unstained cells and Isotype control, respectively; while MR^{+} cells are shown in green. **B)** Double color staining of 7-day-old DCs showing percentage of $CD11c^{+}/MR^{+}$ cells.

2.3.4.2. Expression of CD11c- Staining with FITC-anti CD11c mAb indicated that the population of the live cultured DCs ($CD11c^+$ cells) was 87.6±3.1% before exposure to NPs (**Figure 2.8**). Upon treatment with various formulations, this population did not significantly change (analyzed by Student's t-test) and was in the range of 85.1-91.6% and 84.7-90.7% for the ester-terminated and COOH-terminated NPs, respectively (**Figure 2.8**). No significant difference in the CD11c positivity of cells was observed between ester and COOH-terminated counterparts.

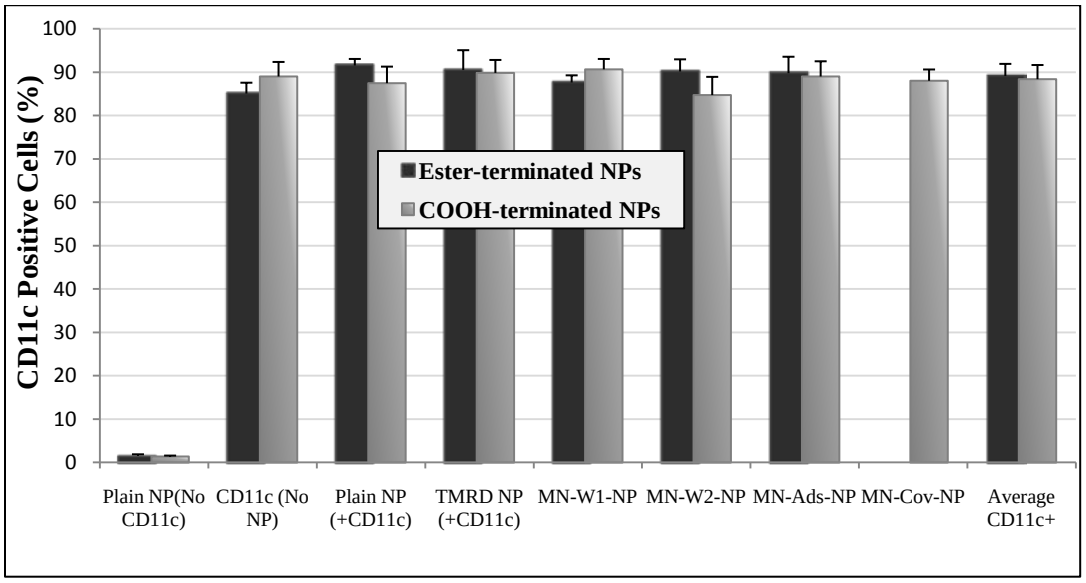

Figure 2.8: Assessment of CD11c+ cell population before and after pulsing with formulations using flow cytometry. Each bar represents mean%± SD (n=3-5).

2.3.4.3. Quantitative assessment of NP uptake by flow cytometry- Incorporation of TMRD into NP formulations allowed for quantitative estimation of the cellular uptake of NPs. Measurement of the TMRD level in NPs showed efficient encapsulation of TMRD (analyzed by unpaired student's t-test) by both ester and COOH- terminated-NPs by all encapsulation methods. For uptake studies, TMRD-loaded NPs were incubated overnight with 7-day-old DC cultures. Cells were then stained for CD11c as described in the Methods. It was shown (**Figures**

2.5 and 2.6) that after the overnight incubation with NPs, minimal amounts of MN and/or TMRD have been released into the culture media. This indicates that for all NPs prepared from different PLGAs and under various MN incorporation conditions, both MN and TMRD appeared to remain incorporated with NPs during uptake studies.

To assess the effect of MN decoration on the uptake of NPs by DCs, percentages of $TMRD^+$/ $CD11c^+$ were compared following treatment with various formulations. Fold-increase in DC-uptake was calculated for ester-terminated formulations as follows: percentages of $TMRD^+$/ $CD11c^+$ cells for test formulation/percentages of $TMRD^+$/ $CD11c^+$ cells for plain ester ended PLGA NPs. Similarly, for COOH-terminated formulations, fold-increase in DC-uptake was calculated as percentages of $TMRD^+$/ $CD11c^+$ cells for test formulation/ percentages of $TMRD^+$/ $CD11c^+$ cells for Plain COOH ended PLGA NPs. Results are represented as a bar graph in **Figures 2.9A** and **2.9B**, for ester and COOH-terminated NPs, respectively.

In general, MN incorporation into PLGA-NPs led to an increase in the level of NP uptake by DCs (one-way ANOVA followed by post-hoc scheffe's analysis), except for MN-W1-Ester and MN-W1-COOH, which showed similar uptake to that of their plain PLGA-NP counterparts **(Figures 2.9A** and **2.9B)**. Maximum uptake was observed for MN-Cov-COOH NPs containing covalently bound MN on PLGA matrix. This formulation have shown almost 2-fold increase in the level of uptake by DCs compared to plain NPs. Comparing the uptake of different formulations to plain NPs, the following rank was observed for ester-terminated PLGA-NPs: MN-Ads-ester>MN-W2-ester>MN-W1-ester. The latter showed similar uptake to that of plain ester terminated PLGA NPs. Similarly, the following trend was observed for COOH-terminated PLGA-NPs: MN-Cov-COOH=MN-Ads-COOH>MN-W2-COOH=MN-W1-COOH = plain NPs. Comparison between COOH-terminated and ester-terminated NPs did not reveal a significant difference between the two, when identical MN incorporation methods were used.

A)

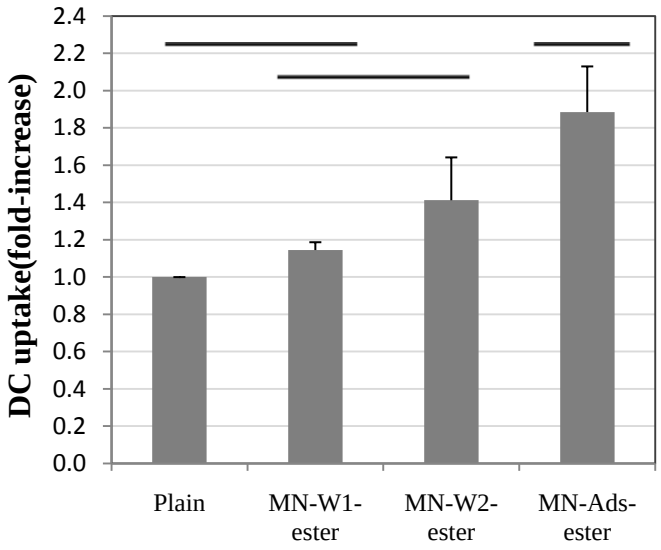

B)

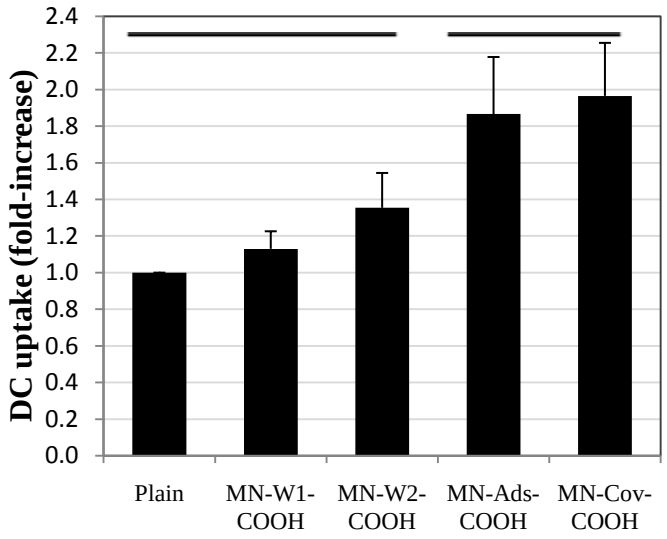

Figure 2.9: Effect of polymer type and formulation method on NP uptake by DCs as measured by flow cytometry. **A)** For ester formulations, fold-increase in DC-uptake was calculated as follow: Percentages of $TMRD^+$ /$CD11c^+$ cells for test formulation/ Percentages of $TMRD^+$/$CD11c^+$ cells for plain ester-terminated PLGA-NPs. **B)** Similarly, for COOH formulations, fold-increase in DC-uptake was calculated. Continuous lines indicate lack of significance between groups encompassed by the lines; groups not encompassed within lines are significantly different from those encompassed by the lines (one-way ANOVA followed by a post-hoc scheffe method; $p<0.05$). Each bar represents mean % ± SD (n=3-8).

2.3.4.4. Internalization of MN-decorated NPs by DCs visualized by confocal microscopy- The single cell images of the fixed cells confirmed the intracellular uptake rather than cell surface binding of MN-decorated NPs by DCs after 20 h incubation, evidenced by the presence of punctate red dots in cytoplasm of DCs **(Figure 2.10)**.

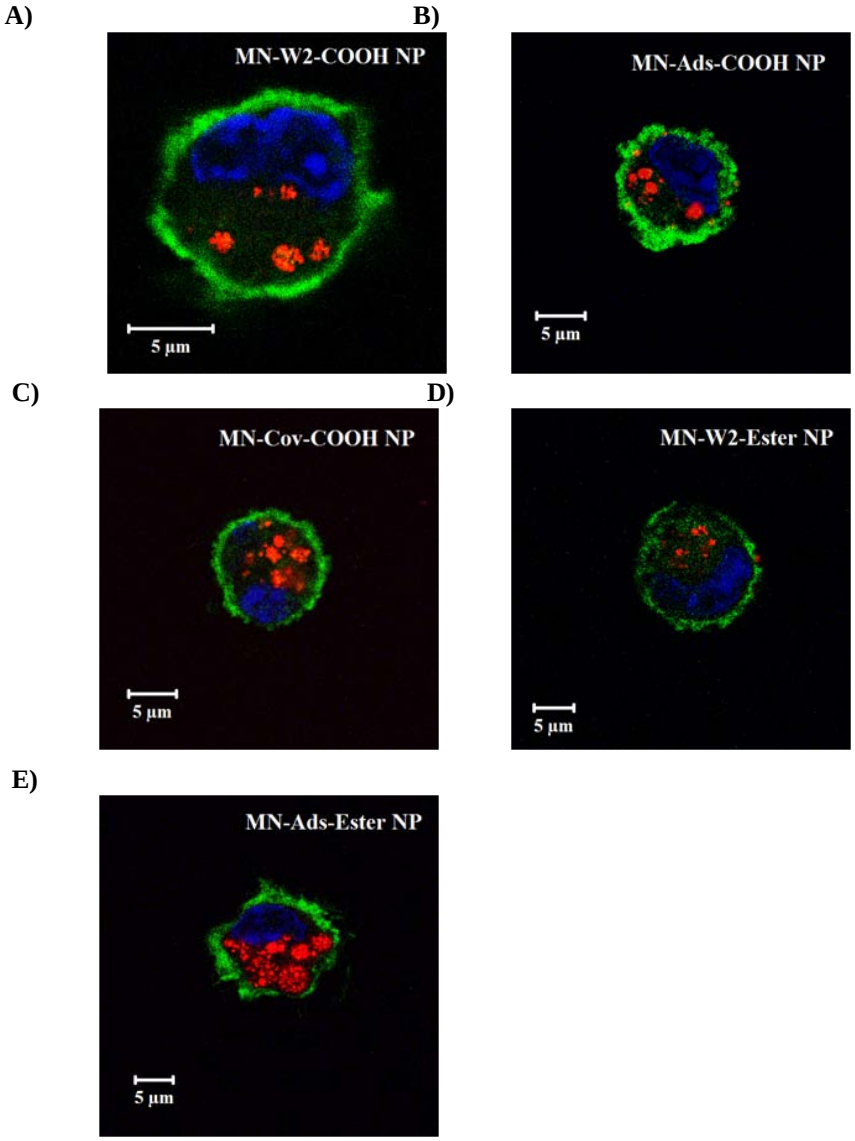

Figure 2.10: Verification of NP internalization by single cell images of fixed DCs using confocal microscopy. The red dots inside the cells show the localization of TMRD-loaded NPs in the cytoplasm. DCs are incubated with **A)** MN-W2-COOH NPs; **B)** MN-Ads-COOH NPs; **C)** MN-Cov-COOH NPs; **D)** MN-W2-ester NPs; **E)** MN-Ads-ester NPs; followed by cell membrane staining with FITC-CD11c mAb (green label) and counterstaining the nucleus with DAPI (blue label).

2.4. Discussion

Active targeting of vaccine antigens to endocytic receptors on DCs can potentially improve the efficacy of such vaccines in eliciting robust immune responses. One candidate receptor for targeting DCs is MR [13]; a member of CLR family expressed on immature murine and human monocytes-derived DC subsets as well as macrophages which are involved in antigen internalization [21, 38] and presentation to immune system [39]. Recent studies have further demonstrated that interaction with MR promoted the activation and phenotypic and functional maturation of DCs, as evidenced by up-regulation of cell surface markers (CD80, CD86, CD40, HLA-DR and CD83), increased in the level of IL-12 production and in the allostimulatory capability of DCs [40]. Therefore, MR-targeting can be a promising approach to dramatically improve the immunogenicity of vaccine formulation. One of the natural and well-identified ligands of MR is MN, a polymannose isolated from the cell wall of *Saccharomyces cerevisiae* [41]. MN is a potent ligand of both MRs and DC-SIGN (a CLR expressed on human DCs) with the capability to induce production of IL-6 (a pro-inflammatory cytokine crucial in adaptive immunity) [42] and tumour necrosis factor-α (TNF-α) by DCs from human monocytes in a TLR4-dependent manner [43]. In fact, several mannosylated antigen delivery vehicles have been formulated and evaluated for their ability to actively target DCs compared to their unmannosylated counterparts. Examples include mannosylated liposomes [44] and [45] nanoparticles [46], and niosomes [47]. Our research group has been pursuing research on the application of PLGA-NPs for the co-delivery of antigens and adjuvants as an efficient vaccination strategy for several years [9, 10, 48]. Here, we pursued decoration of PLGA-NPs by MN, the natural ligand for MR in favour of active targeting of DCs.

In the current set of studies, incorporation of MN into PLGA-NPs was accomplished using two different PLGA polymers: ester and carboxyl terminated PLGA **(Figure 2.1)**. At the same time, different methods of MN incorporation on

PLGA-NPs were used **(Table 2.1)**. All prepared PLGA-NPs were shown to be within the size range suitable for uptake by DCs (average size ranging between around 300-500 nm) [49]. Phenol-sulfuric acid assay was used to determine incorporated mannan after extraction as a reliable classical colorimetric technique for quantification of carbohydrates [36, 50] which is not sensitive to the traces of residual organic solvents [51].

The highest MN incorporation was observed in MN-Cov-COOH NPs, where MN is conjugated to the free carboxyl groups on PLGA-NPs through covalent ester bonds **(Figure 4.2)**. Adsorption of MN to pre-made ester-terminated PLGA-NPs (MN-Ads-Ester) led to slightly higher MN incorporation than its COOH-terminated counterpart (MN-Ads-COOH) **(Figure 4.2)**. This difference may be attributed to the presence of negative charge on the phosphate groups present in natural MN that disrupts the MN adsorption onto more negatively charged COOH-terminated NPs in comparison to ester-terminated ones.

The net negative surface charge of NPs characterized by the Zeta potential, increased significantly after MN incorporation in most cases except for the MN-W1 which showed similar zeta potential to that of plain NPs irrespective of the polymer type **(Figure 2.3)**. Despite similar level of MN incorporation between W1 and W2 formulations, the Zeta potential of the W2 formulations was significantly higher than that of the W1 formulations irrespective of the polymer type.

To identify the optimum NP structure, uptake of fluorescently labelled PLGA-NPs by DCs for all prepared formulations was then assessed. TMRD, the fluorochrome loaded in the NPs is a low toxic and high MW lipophilic dye and it remains associated with the polymer matrix during the uptake studies **(Figure 2.6)**. Furthermore, it has been proven that the presence of TMRD loaded in NPs does not cause MR-mediated endocytosis [6] and non-decorated TMRD-loaded NPs can be used as negative control in our uptake studies. DCs were treated with

NPs on day 7 as a maximum MR expression was observed on that day **(Figure 2.7A)**. Since MR is expected to be expressed on macrophages as well, double color staining was performed to assess number of $CD11c^+$ cells (DCs) that are expressing MR. Results in **Figure 2.7B** indicate that 36% of the cells were double positive for both DC marker (CD11c) and MR.

On the other hand, results showed that DC population ($CD11c^+$ cells) was the highly predominant cell population in our culture (85-89%) and treatment with formulations did not affect this population **(Figure 2.8).**

Assessment of the fold increase in $TMRD^+/CD11c^+$ cells following treatment with MN- decorated NPs (compared to non-decorated plain NPs) revealed that MN incorporation led to an increase in the association of PLGA-NPs with DCs, except for MN-W1-NPs (irrespective of the polymer type) that showed similar DC association to that of plain NPs **(Figure 2.9).** This observation was attributed to the encapsulation of MN rather than surface modification of NPs by MN in this formulation. Evidence for the uptake of MN-decorated NPs rather than their mere binding to cells was provided by confocal microscopy **(Figure 2.10)**.

In an attempt to identify the most important parameter(s) among simultaneously changing variables in the prepared formulations in determining the extent of NP uptake by DCs the correlation between NP characteristics (zeta potential, MN incorporation and size) and DC uptake was assessed **(Figure 2.11)**. A positive correlation between the level of MN incorporation and DC uptake of NPs was noticed (r^2= 0.8722 and r^2= 0.7589 for ester-terminated and COOH-terminated NPs, respectively) **(Figure 2.11A).** Despite approximate 3 fold increase in the level of MN incorporation in PLGA NPs containing covalently bound MN, their uptake by DCs only increased slightly when compared to the PLGA NPs with adsorbed MN. This may be due to the saturation of MRs upon which the uptake curve tends to plateau. Among different parameters in NPs affecting DC uptake, the highest and significant correlation was observed for Zeta potential of NPs (r^2= 0.9683, $p<0.05$ and r^2= 0.9603, $p<0.05$; for ester-terminated

and COOH-terminated NPs, respectively) **(Figure 2.11B).** The Zeta potential of MN incorporated PLGA NPs might serve as an indicator for the presence of MN on the surface of NPs especially for NPs containing physically incorporated MN. The presence of MN on the surface of NPs rather than its encapsulation inside NPs increases its availability to MRs. Therefore, it is not surprising that a better correlation between DC uptake and Zeta potential rather than MN total level is seen. The correlation between the average diameter of the NPs and DC uptake was positive, but weaker than the other two factors (r^2=0.899 and r^2=0.6906 for ester-terminated and COOH-terminated NPs, respectively) **(Figure 2.11C).**

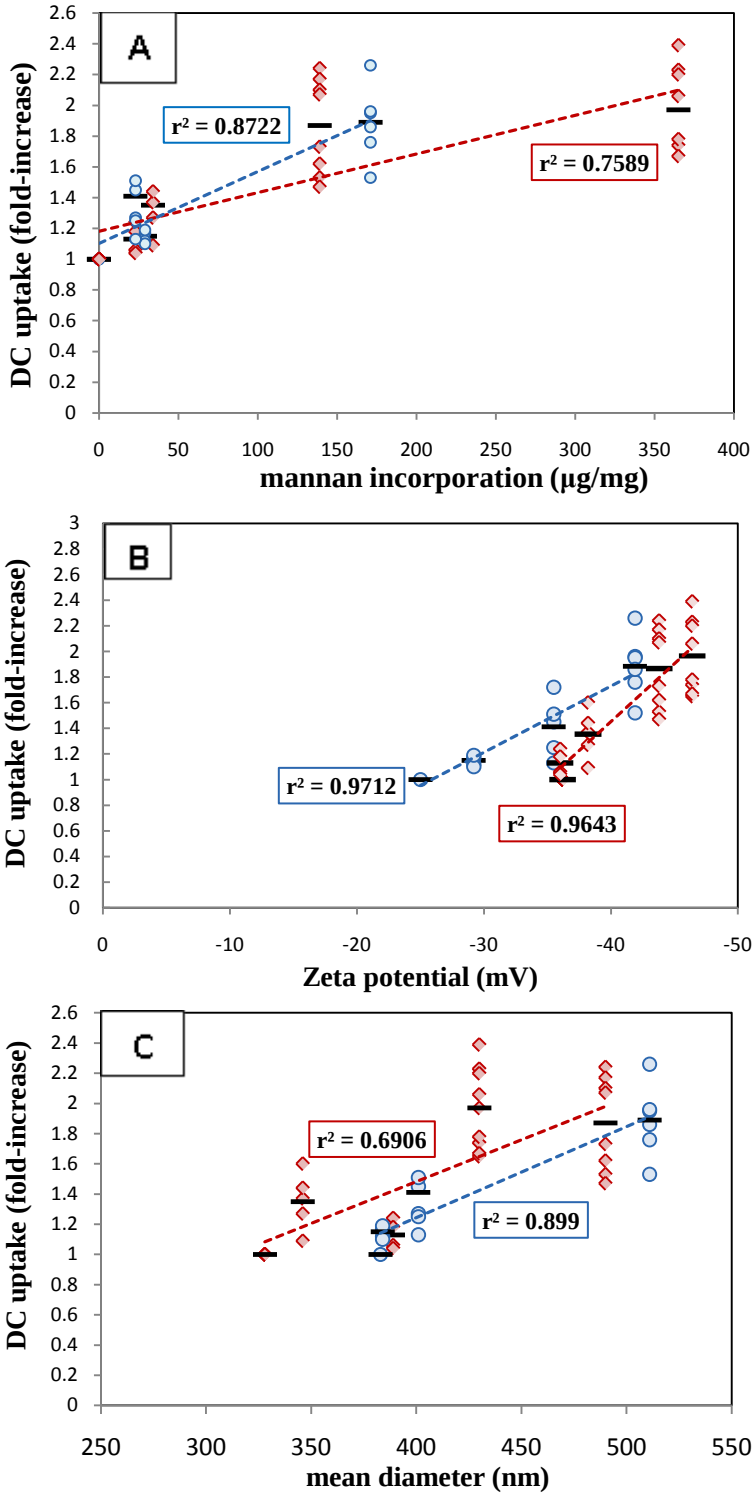

Figure 2.11: Relationship between DC uptake and **A)** Zeta potential, **B)** MN incorporation, **C)** Mean NP diameter. Circles and diamonds are representative of ester-terminated and COOH-terminated NPs, respectively.

2.5. Conclusion

Decoration of PLGA-NPs with MN can be used as a successful strategy to enhance the uptake of NPs by DCs. Among different MN incorporation strategies, covalent attachment of MN to COOH-terminated PLGA-NPs appear to provide a higher level of MN surface decoration on NPs leading to enhanced uptake of NPs by DCs and suggesting a better chance of success for this formulation as an actively targeted PLGA-based nanoparticulate vaccine.

Acknowledgements:

This study was funded by Natural Science and Engineering Council of Canada (NSERC).

References

1. Schuster, M., A. Nechansky, and R. Kircheis, *Cancer immunotherapy.* Biotechnol J, 2006. **1**(2): p. 138-47.
2. Rosenberg, S.A., J.C. Yang, and N.P. Restifo, *Cancer immunotherapy: moving beyond current vaccines.* Nat Med, 2004. **10**(9): p. 909-15.
3. Gilboa, E., *DC-based cancer vaccines.* J Clin Invest, 2007. **117**(5): p. 1195-203.
4. Steinman, R.M. and J. Banchereau, *Taking dendritic cells into medicine.* Nature, 2007. **449**(7161): p. 419-26.
5. Kleindienst, P. and T. Brocker, *Endogenous dendritic cells are required for amplification of T cell responses induced by dendritic cell vaccines in vivo.* J Immunol, 2003. **170**(6): p. 2817-23.
6. Elamanchili, P., et al., *Characterization of poly(D,L-lactic-co-glycolic acid) based nanoparticulate system for enhanced delivery of antigens to dendritic cells.* Vaccine, 2004. **22**(19): p. 2406-12.
7. Lutsiak, M.E., G.S. Kwon, and J. Samuel, *Biodegradable nanoparticle delivery of a Th2-biased peptide for induction of Th1 immune responses.* J Pharm Pharmacol, 2006. **58**(6): p. 739-47.
8. Diwan, M., et al., *Biodegradable nanoparticle mediated antigen delivery to human cord blood derived dendritic cells for induction of primary T cell responses.* J Drug Target, 2003. **11**(8-10): p. 495-507.
9. Hamdy, S., et al., *Co-delivery of cancer-associated antigen and Toll-like receptor 4 ligand in PLGA nanoparticles induces potent CD8+ T cell-mediated anti-tumor immunity.* Vaccine, 2008. **26**(39): p. 5046-57.
10. Elamanchili, P., et al., *"Pathogen-mimicking" nanoparticles for vaccine delivery to dendritic cells.* J Immunother, 2007. **30**(4): p. 378-95.
11. Fischer, S., et al., *Concomitant delivery of a CTL-restricted peptide antigen and CpG ODN by PLGA microparticles induces cellular immune response.* J Drug Target, 2009.
12. Schlosser, E., et al., *TLR ligands and antigen need to be coencapsulated into the same biodegradable microsphere for the generation of potent cytotoxic T lymphocyte responses.* Vaccine, 2008. **26**(13): p. 1626-37.
13. Xiang, S.D., et al., *Pathogen recognition and development of particulate vaccines: does size matter?* Methods, 2006. **40**(1): p. 1-9.
14. Tacken, P.J., et al., *Dendritic-cell immunotherapy: from ex vivo loading to in vivo targeting.* Nat Rev Immunol, 2007. **7**(10): p. 790-802.
15. Wei, H., et al., *Targeted delivery of tumor antigens to activated dendritic cells via CD11c molecules induces potent antitumor immunity in mice.* Clin Cancer Res, 2009. **15**(14): p. 4612-21.
16. Kempf, M., et al., *Improved stimulation of human dendritic cells by receptor engagement with surface-modified microparticles.* J Drug Target, 2003. **11**(1): p. 11-8.

17. Figdor, C.G., Y. van Kooyk, and G.J. Adema, *C-type lectin receptors on dendritic cells and Langerhans cells.* Nat Rev Immunol, 2002. **2**(2): p. 77-84.
18. Zelensky, A.N. and J.E. Gready, *The C-type lectin-like domain superfamily.* Febs J, 2005. **272**(24): p. 6179-217.
19. van Kooyk, Y., *C-type lectins on dendritic cells: key modulators for the induction of immune responses.* Biochem Soc Trans, 2008. **36**(Pt 6): p. 1478-81.
20. Engering, A.J., et al., *The mannose receptor functions as a high capacity and broad specificity antigen receptor in human dendritic cells.* Eur J Immunol, 1997. **27**(9): p. 2417-25.
21. Stahl, P.D. and R.A. Ezekowitz, *The mannose receptor is a pattern recognition receptor involved in host defense.* Curr Opin Immunol, 1998. **10**(1): p. 50-5.
22. Keler, T., V. Ramakrishna, and M.W. Fanger, *Mannose receptor-targeted vaccines.* Expert Opin Biol Ther, 2004. **4**(12): p. 1953-62.
23. Wattendorf, U., et al., *Mannose-based molecular patterns on stealth microspheres for receptor-specific targeting of human antigen-presenting cells.* Langmuir, 2008. **24**(20): p. 11790-802.
24. Lam, J.S., et al., *A model vaccine exploiting fungal mannosylation to increase antigen immunogenicity.* J Immunol, 2005. **175**(11): p. 7496-503.
25. Apostolopoulos, V., et al., *Ex vivo targeting of the macrophage mannose receptor generates anti-tumor CTL responses.* Vaccine, 2000. **18**(27): p. 3174-84.
26. Jiang, H.L., et al., *The potential of mannosylated chitosan microspheres to target macrophage mannose receptors in an adjuvant-delivery system for intranasal immunization.* Biomaterials, 2008. **29**(12): p. 1931-9.
27. Sheng, K.C., et al., *Delivery of antigen using a novel mannosylated dendrimer potentiates immunogenicity in vitro and in vivo.* Eur J Immunol, 2008. **38**(2): p. 424-36.
28. Kel, J., et al., *Soluble mannosylated myelin peptide inhibits the encephalitogenicity of autoreactive T cells during experimental autoimmune encephalomyelitis.* Am J Pathol, 2007. **170**(1): p. 272-80.
29. Apostolopoulos, V., et al., *Pilot phase III immunotherapy study in early-stage breast cancer patients using oxidized mannan-MUC1 [ISRCTN71711835]*. Breast Cancer Res, 2006. **8**(3): p. R27.
30. Cai, C., et al., *Influence of morphology and drug distribution on the release process of FITC-dextran-loaded microspheres prepared with different types of PLGA.* J Microencapsul, 2008: p. 1-12.
31. Budhian, A., S.J. Siegel, and K.I. Winey, *Production of haloperidol-loaded PLGA nanoparticles for extended controlled drug release of haloperidol.* J Microencapsul, 2005. **22**(7): p. 773-85.
32. Jaklenec, A., et al., *Sequential release of bioactive IGF-I and TGF-beta 1 from PLGA microsphere-based scaffolds.* Biomaterials, 2008. **29**(10): p. 1518-25.

33. Ueda, M. and J. Kreuter, *Optimization of the preparation of loperamide-loaded poly (L-lactide) nanoparticles by high pressure emulsification-solvent evaporation.* J Microencapsul, 1997. **14**(5): p. 593-605.
34. Haddadi, A., et al., *Delivery of rapamycin by PLGA nanoparticles enhances its suppressive activity on dendritic cells.* J Biomed Mater Res A, 2008. **84**(4): p. 885-98.
35. Kocbek, P., et al., *Targeting cancer cells using PLGA nanoparticles surface modified with monoclonal antibody.* J Control Release, 2007. **120**(1-2): p. 18-26.
36. Masuko, T., et al., *Carbohydrate analysis by a phenol-sulfuric acid method in microplate format.* Anal Biochem, 2005. **339**(1): p. 69-72.
37. Lutz, M.B., et al., *An advanced culture method for generating large quantities of highly pure dendritic cells from mouse bone marrow.* J Immunol Methods, 1999. **223**(1): p. 77-92.
38. Ezekowitz, R.A., et al., *Molecular characterization of the human macrophage mannose receptor: demonstration of multiple carbohydrate recognition-like domains and phagocytosis of yeasts in Cos-1 cells.* J Exp Med, 1990. **172**(6): p. 1785-94.
39. McKenzie, E.J., et al., *Mannose receptor expression and function define a new population of murine dendritic cells.* J Immunol, 2007. **178**(8): p. 4975-83.
40. Presicce, P., et al., *Keyhole limpet hemocyanin induces the activation and maturation of human dendritic cells through the involvement of mannose receptor.* Mol Immunol, 2008. **45**(4): p. 1136-45.
41. Vinogradov, E., B. Petersen, and K. Bock, *Structural analysis of the intact polysaccharide mannan from Saccharomyces cerevisiae yeast using 1H and 13C NMR spectroscopy at 750 MHz.* Carbohydr Res, 1998. **307**(1-2): p. 177-83.
42. Cambi, A., et al., *Dendritic cell interaction with Candida albicans critically depends on N-linked mannan.* J Biol Chem, 2008. **283**(29): p. 20590-9.
43. Sheng, K.C., et al., *Mannan derivatives induce phenotypic and functional maturation of mouse dendritic cells.* Immunology, 2006. **118**(3): p. 372-83.
44. White, K.L., et al., *Mannosylated liposomes as antigen delivery vehicles for targeting to dendritic cells.* J Pharm Pharmacol, 2006. **58**(6): p. 729-37.
45. Espuelas, S., et al., *Influence of ligand valency on the targeting of immature human dendritic cells by mannosylated liposomes.* Bioconjug Chem, 2008. **19**(12): p. 2385-93.
46. Joralemon, M.J., et al., *Synthesis, characterization, and bioavailability of mannosylated shell cross-linked nanoparticles.* Biomacromolecules, 2004. **5**(3): p. 903-13.
47. Jain, S. and S.P. Vyas, *Mannosylated niosomes as adjuvant-carrier system for oral mucosal immunization.* J Liposome Res, 2006. **16**(4): p. 331-45.

48. Hamdy, S., et al., *Enhanced antigen-specific primary CD4+ and CD8+ responses by codelivery of ovalbumin and toll-like receptor ligand monophosphoryl lipid A in poly(D,L-lactic-co-glycolic acid) nanoparticles.* J Biomed Mater Res A, 2007. **81**(3): p. 652-62.
49. Foged, C., et al., *Particle size and surface charge affect particle uptake by human dendritic cells in an in vitro model.* Int J Pharm, 2005. **298**(2): p. 315-22.
50. Dubois, M., et al., *A colorimetric method for the determination of sugars.* Nature, 1951. **168**(4265): p. 167.
51. DuBois, M., et al., Colorimetric Method for Determination of Sugars and Related Substances. Anal. Chem., 1956. 28 (3): p.350-356

Chapter Three

Assessment of the immune responses induced by DCs actively targeted with MN-decorated PLGA-NPs

3.1. Introduction

Immunotherapy against cancer mainly centres on the induction of CTLs against tumour specific antigens. This points toa particular interest on DC-targeted vaccine strategies due to the critical role of DCs in the induction of CTL responses. Activation of DCs by pro-inflammatory cytokines does not produce equivalent response to that achieved by PRRs and possibly DCs activated by cytokines induce tolerance rather than immunity [1]. A direct approach is needed to target antigens to cell-specific receptors on DCs *in vivo* for initiation of anti-tumour responses.

The DC surface molecule to be targeted should be as DC-specific as possible to prevent unwanted side effects and also to be an endocytic receptor involved in initial recognition and subsequent uptake of antigens by DCs [2]. CLRs are interesting candidates because of their cell-restricted expression pattern and their function to facilitate antigen uptake in DCs as well as a powerful role in the modification modulation of immune reactions to enhance antigen presentation [3, 4]. CLRs can also determine whether the antigen is presented in the context of MHC-I or MHC-II molecules or both [5]. The signalling processes are complex and sometimes depend on the cross-talk with other PRRs (particularly TLRs), the ligand (or carbohydrate specific signalling pathway) and the DC subset [3]. TLR activation in turn leads to the up-regulation of maturation markers and the production of pro-inflammatory cytokines. Several studies have demonstrated that targeting antigens to CLRs can result in $CD8^+$ T cell responses and strong anti-tumour outcomes.

MR was primarily identified as an endocytic/ phagocytic receptor with a focus on its role in the innate immune system and its involvement in intracellular signalling in adaptive immunity was further shown [6, 7]. In higher organisms, there is evidence for MR to play a role in antigen processing [8]. MR has been demonstrated to take part in antigen presentation following uptake, as the mannosylated antigens are better internalized and presented to T cells [6, 9]. *In vivo* and *ex-vivo* targeting of MR with oxidized mannan-MUC1 fusion induces potent MHC-restricted CTL responses and tumour protection in mouse [6].

Moreover, Pilot phase III immunotherapy study in early-stage cancer patients supported the effectiveness of this strategy [10].

Recent studies show a cross-talk between MR and TLRs, particularly TLR4 and TLR2 on the induction of a cell-mediated immune response [11]. The close link between MR and TLR2 tends to the enhanced production of TNF-α and IL-12 [11, 12]. When MR and TLR ligands are delivered together in a vaccine, the tolerogenic response could be suppressed [3].

Exclusively, antigens internalized through MR, do not require intracellular diversion to access the cross-presentation pathway, because they enter the pathway during the endocytosis [13, 14]. It is suggested that MR functions on DCs as an antigen uptake receptor targeting its cargo to intracellular compartments where it is processed for further presentation to T cells.

Interaction between the MN incorporated in PLGA-NPs and MR could improve the specificity of NPs for DCs [4, 15]. The decoration of MN as targeting moieties on PLGA surface can not only facilitate the uptake of NPs by DCs, but also enhance DC maturation and ultimately lead to improving the effectiveness of vaccine formulation. PLGA-NPs as a vehicle also provide the possibility of simultaneous delivery of MR and TLR ligands along with the antigen in vaccine formulations.

In previous chapters we investigated the effect of MN incorporation on the uptake of PLGA NPs by DCs. In this chapter, the influence of targeting MR on DCs by the PLGA-based NPs decorated with MN on the maturation and stimulation of DCs is investigated by analyzing the DC surface phenotype and function. In addition, the capability of the formulations to induce production of immunostimulatory cytokines would have been evaluated. Moreover, the influence of MN-decorated NP formulations on the immunostimulatory activity of DCs was assessed during interaction of DCs treated with NPs and T cells.

3.2. Materials and methods

3.2.1. Materials

MN derived from S. Cerevisiae, was purchased from Sigma-Aldrich (St. Louis, MO, USA). Gibco RPMI-1640 with L-glutamine, Gentamycin, Fetal Bovine Serum (FBS), were supplied by Invitrogen (Carlsbad, CA, USA). Recombinant murine granulocyte–macrophage colony-stimulating factor (GM-CSF) was purchased from Peprotech (Rockville, IL). Anti-mouse FITC labeled anti-CD86 and its respective Isotype control, PE-Cy5 labeled anti-CD40 were purchased from BD Biosciences-Pharmingen (San Diego, CA, USA). IL-12, IL-6 and TNF-α assay enzyme-linked immunosorbent assay (ELISA) kits were purchased from eBiosciences, USA. [^{3}H]-Thymidine was purchased from Amersham (Oakville, ON, Canada). EasySep® mouse T cell enrichment kit was purchased from Stem Cell Technologies, Vancouver, BC, Canada. C57Bl/6 and BALB/c mice were purchased from the Jackson Laboratory (Bar Harbor, ME, USA).

3.2.2. Assessment of the effect of MN decoration on the surface phenotype of DCs

DC primary cultures were generated from murine bone-marrow precursors in complete DC media using femurs and tibias of C57BL/6 mice as reported earlier in **Section 2.2.6***.*

Seven-day old DC cultures were treated either with different concentrations of soluble MN, (0.03, 0.3, 3, 9 or 18 mg) or 50 μg of MN-decorated NP formulations, including MN-Cov-COOH, MN-Ads-COOH, MN-W1-COOH, MN-W2-COOH, MN-Ads-Ester, MN-W1-Ester and MN-W2-Ester (**Section 2.2.3**) after reconstitution in 1 mL PBS. Untreated DCs and DCs treated with plain NPs were used as controls. All cell culture dishes were kept in an incubator in 37°C and 5% CO_2. After 24 h, the semi-adherent and non-adherent cells were harvested and washed twice by adding PBS (pH=7.4) and centrifugation at 500 × g for 5 minutes. Cell suspensions consisting of 2 × 10^6

cells/ mL were prepared in FACS buffer (PBS containing 2 % FBS). The cells were then stained with 0.25 μg of either FITC labeled anti-CD86 or PE-Cy5 labeled anti-CD40. The threshold for sample acquisitions were set based on the background staining observed with the appropriate isotype control mAbs. Samples were acquired on a Becton-Dickinson FACSort and analyzed by CELL-Quest software (Becton Dickinson).

3.2.3. Assessment of the effect of MN-decorated NPs on DC cytokine secretion

The supernatants from the DC cultures of the previous experiment (after harvesting) **(Section 3.2.2)** were collected and analyzed for the presence of IL-12, IL-6 and TNF-α cytokines. The production of cytokines was measured by a sandwich ELISA, using the commercially available ELISA kits, in a 96-well microplate and the plate was read at the OD of 450 nm using a microplate reader (Powerwave with KC Junior software; Bio-Tek, Winooski, VT, USA) according to the manufacturer's directions.

3.2.4. Assessment of the effect of MN- decorated NPs on mixed lymphocyte reaction (MLR)

DCs were isolated from the bone marrow of C57BL/6 mice and treated with different formulations of MN-decorated NPs. Untreated DCs and DCs treated with plain NPs were used as controls. After incubation for 24 h, DCs were irradiated with 3000 rads (radiation absorbed dose) using a ^{137}Cs irradiator, washed and plated at graded doses in triplicates in 96-well microtiter plates (Costar, Cambridge, MA). T cells from the spleens of BALB/c mice were isolated by negative selection using the EasySep® mouse T cell enrichment kit, according to the manufacturer's instructions. Irradiated DCs were co-cultured with spleen T cells (2×10^5 cells/ well) as responders in RPMI-1640 complete medium for 72 h at 37^oC. T cell proliferation was then assessed by [^{3}H]-Thymidine incorporation following a final 24 h pulse (1 μCi/well). Incorporation of [^{3}H]-Thymidine into DNA was measured by liquid scintillation counting.

Statistical Analysis

The parametric data are presented as the mean ± SD throughout this chapter. The data were analyzed for statistical significance differences ($P<0.05$) by unpaired Student's t-test, unless otherwise stated.

3.3. Results

3.3.1. Expression of DC surface markers upon treatment with soluble MN

The results of flow cytometry analysis for the expression level of CD86 and CD40 on DCs, showed an increase following the treatment of seven-day-old DCs with soluble MN (0.03, 0.3, 3, 9 or 18 mg/dish) (**Figure 3.1A**). Compared to untreated DCs (4.9%), soluble MN-treated DCs showed a minimum of four-fold increase in the percentage of positive cells for CD 86 (starting from at least 20% for 0.03 mg to 49% for 18 mg) (**Figure 3.1B**). The expression of CD40 was upregulated from 14% for the untreated to a minimum of 22% for MN (0.03 mg) treated DCs. The CD40 expression was further increased to 48% for the highest concentration of MN (**Figure 3.1C**).

It has also been observed that the expression of CD86 and CD40 markers on DCs is dose-dependent and reach to a plateau upon treatment with MN. As shown in **Figures 3.1B and 3.1.C** there is no increase in either CD86 or CD40 expression, when the concentration of MN increases from 9 mg to 18 mg.

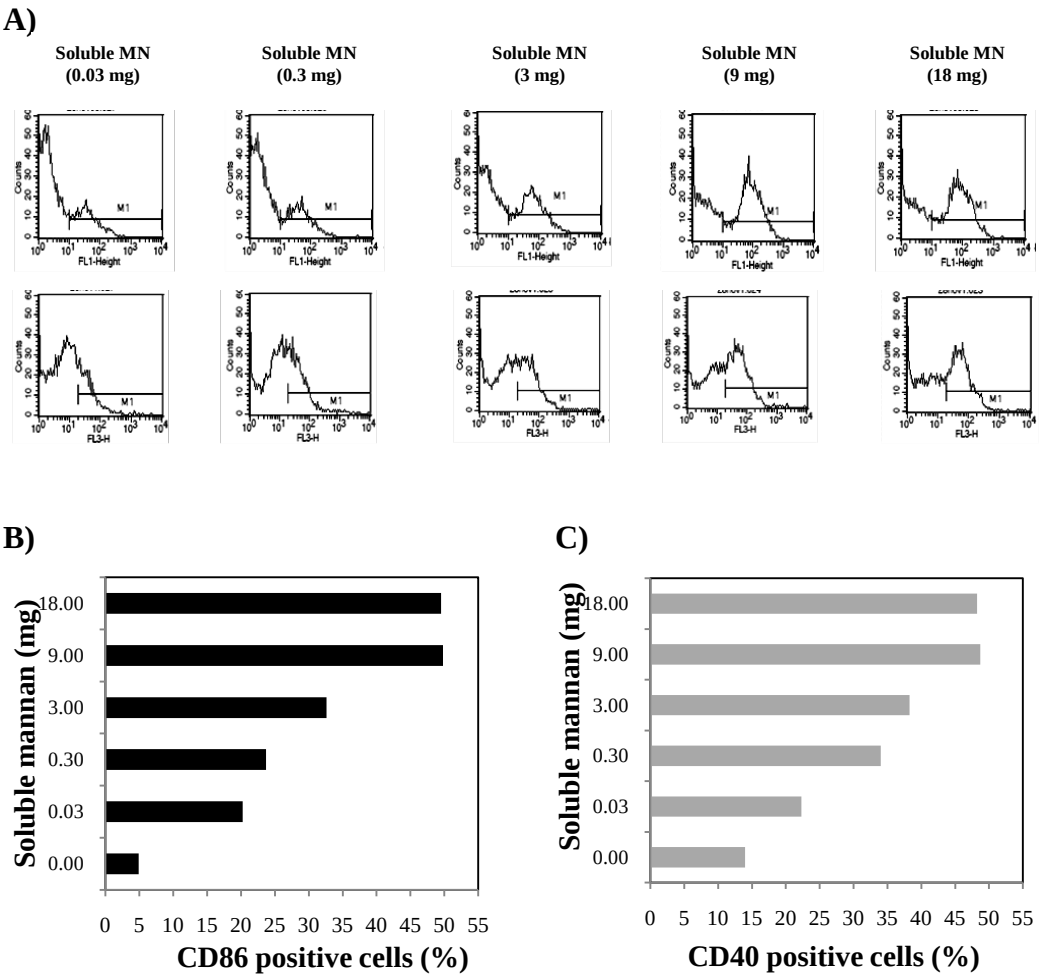

Figure 3.1: Dose-dependent expression of CD86 and CD40 on DCs after treatment with soluble MN. **A**) Antibody staining of specific treatment is represented by solid line histograms for CD86 (top row) and CD40 (bottom row). **B**) Up-regulation of CD86 and **C**) CD40 by soluble MN shown as a bar graph.

3.3.2. Up-regulation of surface markers in DCs treated with MN–decorated NPs

The flow cytometry showed the percentage of CD86 and CD40 positive cells following treatment with various ester-terminated MN-decorated formulations (**Figure 3.2.A).** The percentage of positive cells for both CD86 and CD40 positive cells upon treatment with COOH-terminated NPs are illustrated as histograms in **Figure 3.2B**. The bar graphs also show the magnitudes of the data for a better comparison. (**Figure 3.3)**

The results showed that the CD86 expression induced by MN-W1-Ester NP formulation was increased (1.5 fold) relative to the plain NPs (**Figures 3.2A**

and **3.3A**). However, MN-W2-Ester and MN-Ads-Ester had no superiority to plain-Ester NPs on the up-regulation of CD86 (**Figures 3.2A** and **3.3A**). **Figures 3.2A** and **3.3B** demonstrated that MN-decorated Ester-terminated NPs had no effect on the expression of CD40 on DCs compared to the plain-NPs.

In the case of COOH-terminated NPs, it has been shown that MN-W1-COOH NPs and MN-W2-COOH NPs had no effect on the expression of CD86 on DCs compared to the undecorated NPs (**Figures 3.2B** and **3.3A**). However, MN-Ads-COOH and MN-Cov-COOH showed a significant influence on the level of CD86 expression compared to the plain-COOH NPs (2.3 and 2.8 fold-increase, respectively) (**Figures 3.2B** and **3.3A**).

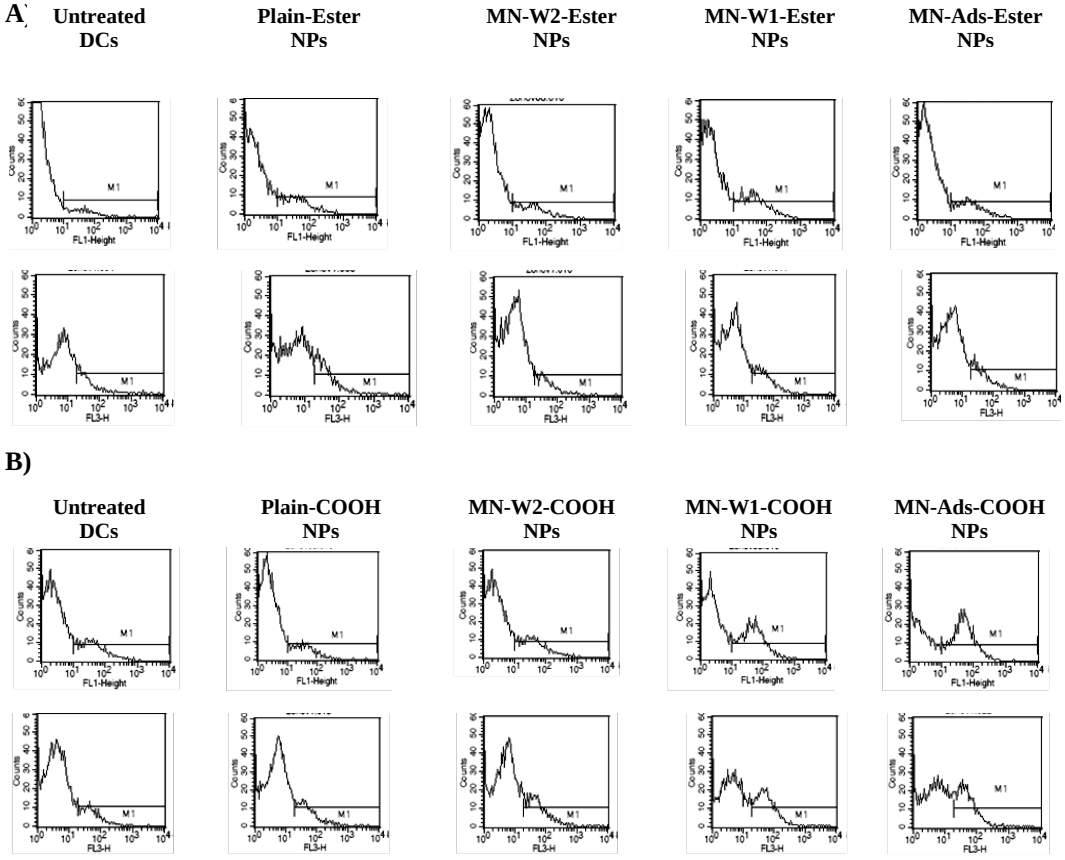

Figure 3.2: Expression of CD86 and CD40 on DCs after different treatments of MN- decorated NPs. Antibody staining of specific treatment is represented by solid line histogram. Expression of CD86 (upper row) and CD40 (bottom row) influenced by **A)** ester-terminated PLGA-NPs and **B)** COOH-terminated PLGA-NPs. Results are representative of 3 separate experiments.

The results showed that all the COOH-terminated formulations had a considerable effect on the up-regulation of CD40, with the exception of MN-W2-COOH-NPs. MN-W1-COOH, MN-Ads-COOH and MN-Cov-COOH NPs increased expression of CD40 on DCs up to 1.5, 2 and 2.3 folds in comparison to plain NPs.

A)

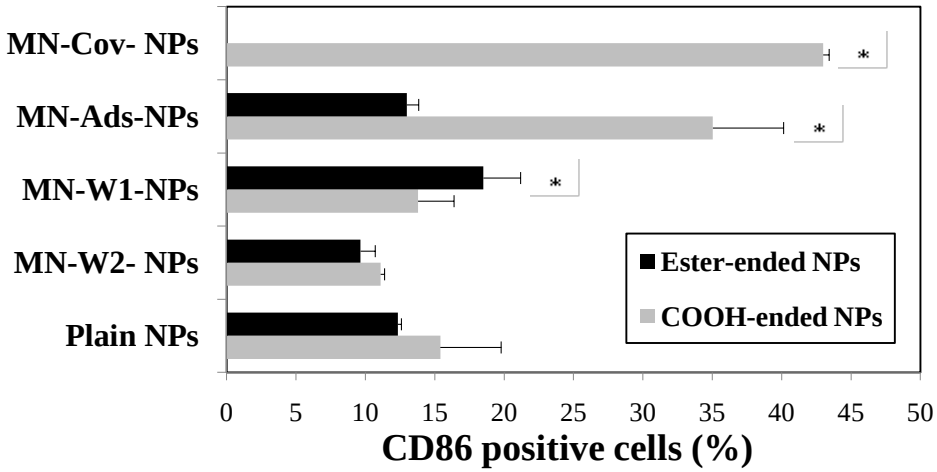

B)

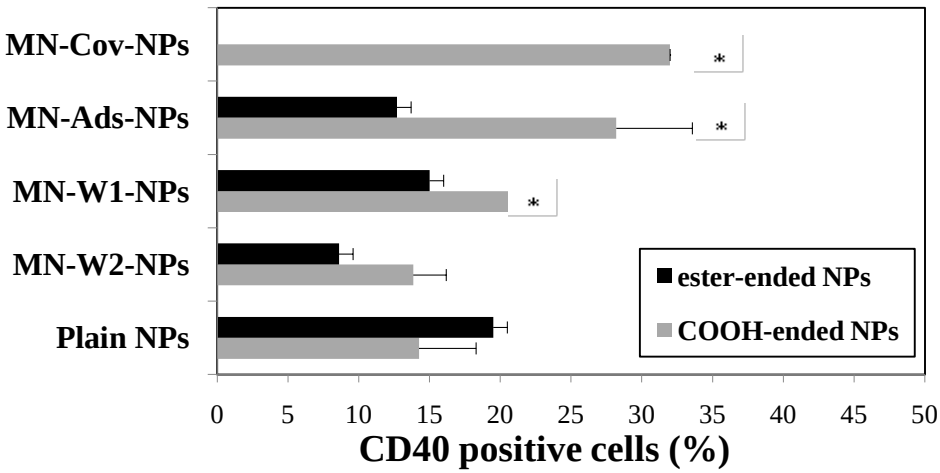

Figure 3.3: Expression of DC surface markers after treatment with different MN-decorated NP formulations. Bar graphs have shown the **A)** CD86 expression and **B)** CD40 expression. Significant groups are shown by (*) ($p<0.05$), analyzed by unpaired Student's t-test. Each bar represents mean ± SD (n=3).

3.3.3. Cytokine production by DCs upon treatment with soluble MN

The analysis of cytokines (IL-12, IL-6 and TNF-α) secreted from seven-day-old DCs treated with different concentration of soluble MN revealed a dose-

dependent profile. As shown in **Figure 3.4A**, IL-12 secreted from DCs following the treatment with 0.03, 0.3, 3, 9 or 18 mg/dish of soluble MN was observed to be 17.4 ± 5.1, 25.6 ± 1.3, 42.7 ± 5.9, 54.8 ± 1.1 and 58.6 ± 1.3 pg/mL, respectively.

Figure 3.4B illustrates the production profile of IL-6 from DCs upon treatment with different concentrations of soluble MN (0.03, 0.3, 3, 9 or 18 mg/dish) in a dose-dependent mode: 43.2 ± 2.2, 64.6 ± 0.8, 175.6 ± 0.1, 497 ± 27 and 722 ± 10 pg/mL, respectively.

The treatment of DCs with the same concentrations of soluble MN resulted in dose-dependent production of TNF-α starting from 258 ± 12, 437 ± 47, 1016 ± 15, 1912 ± 58 and 1978 ± 16 pg/mL for 0.03, 0.3, 3, 9 or 18 mg/dish, respectively (**Figure 3.4C)**.

A) **B)**

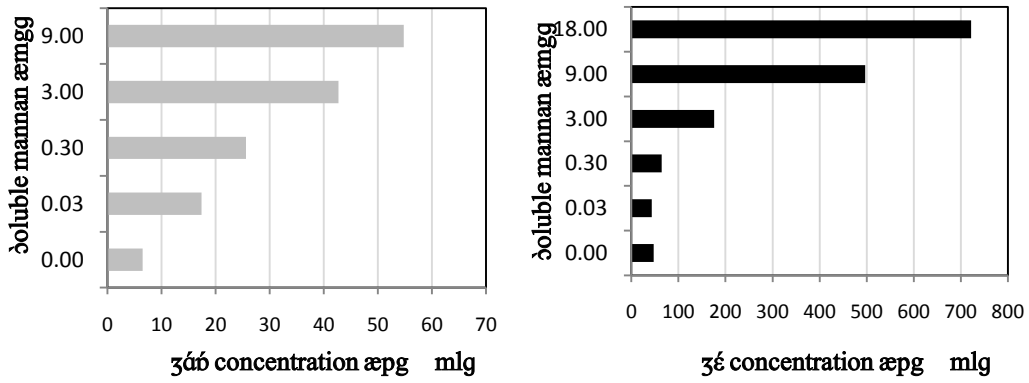

C)

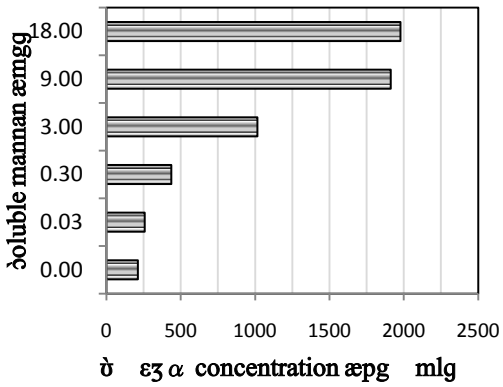

Figure 3.4: Production of different cytokines from DCs induced by various concentration of soluble MN: **A)** IL-12, **B)** IL-6 and **C)** TNF- α.

3.3.4. Effect of MN decoration on the level of cytokine production by DCs

Seven-day old DCs treated with different formulations of MN–decorated-NPs at a concentration of 50 μg/mL, were subjected to assay for secretion of IL-12, IL-6 and TNF-α.

The production of different cytokines from DCs following treatment with ester and COOH-terminated MN-decorated NP formulations is illustrated in **Figure 3.5**.

The Ester-terminated NP formulations decorated with MN had no or little effect on secretion of IL-12 from DCs, compared to plain NPs (**Figure 3.5A**). In the case of COOH-terminated NPs, it has been observed that secretion of IL-12 following the treatment with MN-W1-COOH and MN-W2-COOH NPs did not show any change compared to plain PLGA-COOH NPs, whereas MN-Cov-COOH NPs and MN-Ads--COOH induced the IL-12 production up to 2 and 2.5 folds, respectively (**Figure 3.5A**).

Amongst the ester-terminated formulations only MN-W2-ester NPs showed 1.3 fold-increase in the level of IL-6 production by DCs, relative to plain-ester NPs (from 70.5 ± 6.6 to 92.6 ± 11.6 pg/mL) (**Figure 3.5B**).

As shown in **Figure 3.5B**, MN-W1-COOH and MN-W2-COOH NPs did not affect on the secretion of IL-6 compared to the plain-COOH NPs. However, MN-Ads-COOH and MN-Cov-COOH NPs highly induced IL-6 production by 2.5 and 4.7 fold-increases, respectively.

The measurements of TNF-α production by DCs are illustrated in **Figure 3.5C**. Ester-terminated PLGA formulations decorated with MN showed no effect on the secretion of TNF-α from DCs. However, COOH-terminated PLGA formulations show the ability to induce the production of TNF-α considerably, with the exception of MN-W2-COOH NPs (**Figure 3.5C)**.

A)

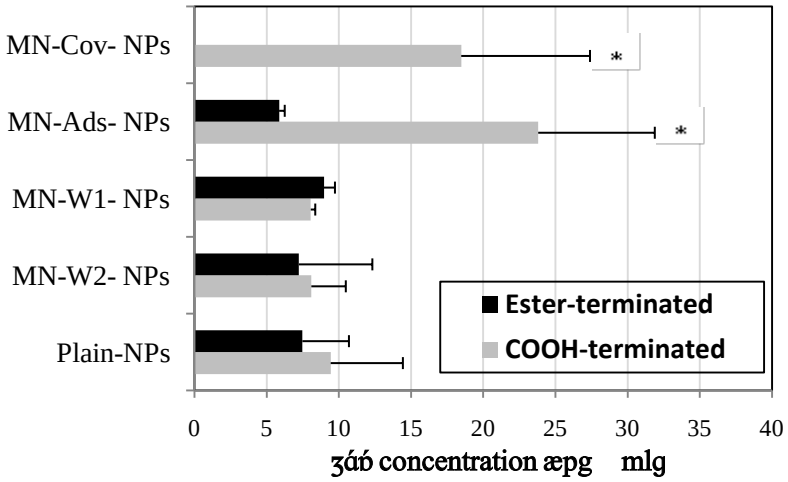

B)

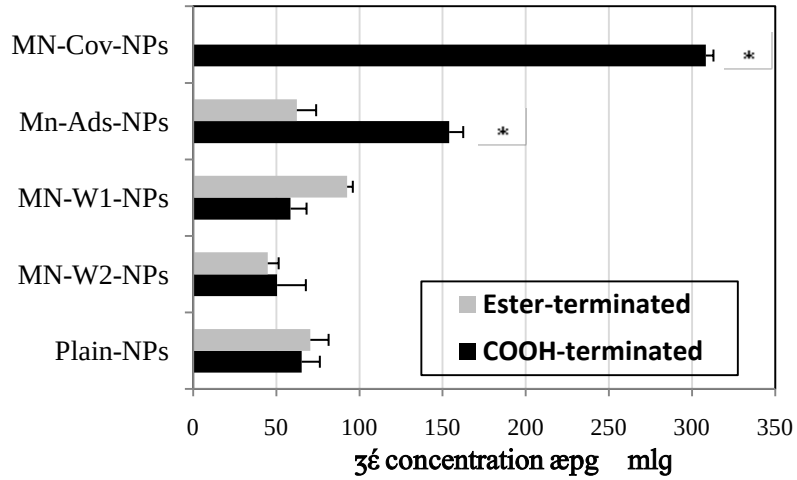

C)

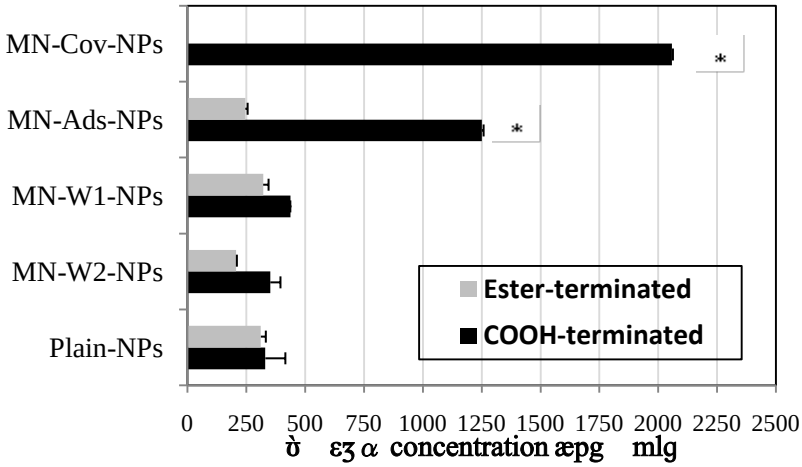

Figure 3.5: Secretion of cytokines from DCs induced by MN-decorated NPs as the bar graphs: **A)** IL-12, **B)** IL-6, **C)** TNF- α. Significant groups are shown by (∗) ($p<0.05$), analyzed by Student's t-test. Each bar represents mean ± SD (n=3).

3.3.5. Effect of MN-decorated-NPs on the allostimulatory activity of DCs

The effect of MN-decorated NPs on immunostimulatory function of DCs was evaluated by MLR assay. The formulations were added during DC propagation from C57BL6 BM-derived DCs in the presence of GM-CSF. After incubation, DCs were irradiated and co-cultured with purified T cells obtained from the spleens of BALB/c mice. DCs were treated with soluble MN at 4 or 18 mg/dish as the control.

Figure 3.6 shows that DCs treated with 4 mg of soluble MN had no influence on allostimulatory activity compared to untreated DCs, whereas DCs treated with 18 mg/dish showed 3-fold-increase in allostimulation. Treatment of DCs by ester-terminated PLGA formulations resulted in amplification of allostimulation by MN-Ads-ester NPs up to 1.8 folds. However, no effect was observed from other ester-terminated formulations **(Figure 3.6)**.

Although MN-W1-COOH and MN-W2-COOH NPs had no influence on the allostimulatory function of DCs, MN-Ads-COOH and MN-Cov-COOH NPs increased the DCs immunostimulatory capacity up to 1.5 and 2.4 folds, respectively **(Figure 3.6)**.

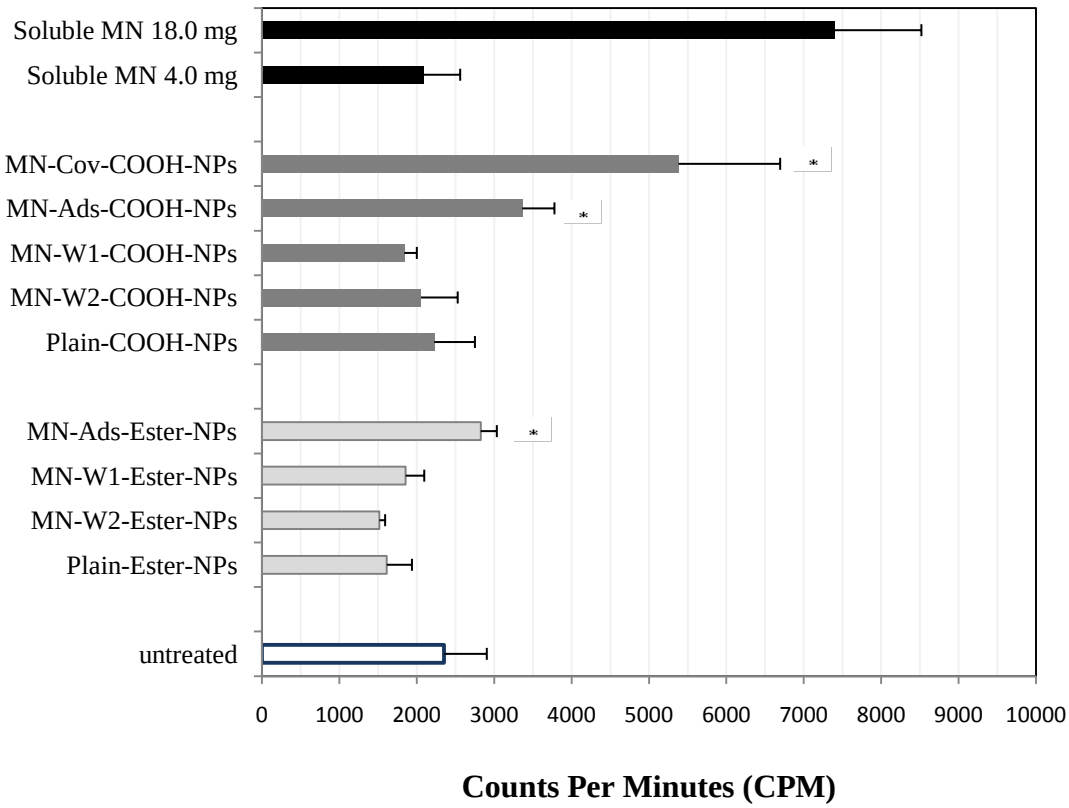

Figure 3.6: Effects of the soluble MN and the MN-decorated NPs on mixed lymphocyte reaction of DCs. Significant groups are shown by (*) ($p<0.05$), analyzed by unpaired Student's t-test. Each bar represents mean ± SD (n=3).

3.4. Discussion

The recent studies suggest a role in immunology for MR beyond the classical function of antigen recognition and internalization. It is evidenced that MRs are also capable of intracellular signalling in the APCs. It has been demonstrated that interaction with MR upgraded the activation and phenotypic status as well as functional maturation of DCs, as evidenced by up-regulation of DC surface markers (CD86, CD40, CD80, HLA-DR and CD83), increase in the level of IL-12 and IL-6 production and in the allostimulatory potential of DCs [16, 17]. Moreover, the MR in human supplied an early endosomal compartment distinct from lysosomes committed to cross-presentation, suggesting a primary role for DCs in MR-mediated cross-priming [14]. As a result, MR-targeting can

be a promising approach to improve immune responses sufficient to induce tumour immunity in vaccine formulation.

In this study, the influence of MR targeting by soluble MN derived from *Saccharomyces Cerevisiae* and MN incorporated PLGA-based NPs on DC surface phenotype and function was investigated.

Our results showed the capability of soluble MN in up-regulation of CD40 and CD86 in a dose-dependent manner (r^2=0.7034 and r^2=0.8115 for CD40 and CD86, respectively) **(Figure 3.1)**. Reaching to a plateau at 18 mg of MN implies the saturation of the receptor by the ligand. COOH-terminated formulations incorporated with MN were shown to be able to induce DC maturation demonstrated by the noticeable up-regulation of both CD40 and CD86.

Amongst the formulations, the highest up-regulation was observed with MN-Cov-COOH NPs **(Figure 3.3)**, where MN is conjugated to the free carboxyl groups on PLGA-NPs through covalent ester bonds. Adsorption of MN to COOH-terminated PLGA-NPs (MN-Ads-COOH) also led to upgraded expression of both CD40 and CD86 **(Figure 3.3)**. The extent of CD40 and CD86 up-regulation induced by MN-Cov-COOH is equivalent with the effect of ~2.5 and ~6 mg soluble MN, respectively. In the case of MN-Ads-COOH this ability is equivalent to addition of ~1.5 and ~3.5 mg soluble MN, respectively. Considering the magnitude of MN incorporated in MN-Cov-COOH-NP (365 μg) and MN-Ads-COOH-NP (171 μg) formulations, this suggests a stronger effect on up-regulation of DCs induced by the MN incorporated in a PLGA particulate system than the MN in soluble form.

The incorporation of MN on ester-terminated PLGA counterpart did not show any influence on the DC surface phenotype **(Figure 3.3**), with the exception of MN-W1-ester, suggesting that the effect of MN-decorated NPs on the expression of DC surface markers is polymer-dependent.

The formulations were also characterized by their ability to promote the production of immunostimulatory cytokines including IL-12, IL-6 and TNF-α. Soluble MN was been shown to increase the production of cytokines dose-dependently (r^2=0.7937 for IL-12, r^2=0.9766 for IL-6 and r^2=0.9784 for TNF-α.

production) **(Figure 3.4)**. The secretion of IL-12 and TNF-α upon DC treatment with 18 mg soluble MN reached to a plateau, but not in the case of IL-6 secretion.

The level of IL-12 secretion by MN-Cov-COOH NPs and MN-Ads-COOH-NPs was increased to a similar extent, whereas treatment with MN-Cov-COOH NPs led to noticeably stronger IL-6 and TNF-α production than what achieved by MN-Ads-COOH-NPs (2 folds and 1.7 folds, respectively) (**Figure 3.5**). The level of the observed effects on the production of TNF-α by MN-Cov-COOH and MN-Ads-COOH are comparable with the ~9.5 and ~5.1 mg of soluble MN. Accordingly, the induced IL-6 secretion by these formulations is weighted as the effect of ~6.3 and ~2.4 mg of MN in the soluble form, respectively. Although this magnitude is less in the case of IL-12 secretion, still is more than the MN incorporated in these formulations, suggesting the superiority of NP formulations of MN to the soluble form.

Similar to what observed in DC surface markers up-regulation, the ester-terminated NPs showed no or a slight influence on production of cytokines **(Figure 3.5)**.

Compatible with DC maturation, the assessment of immunostimulatory activity of DCs on the proliferation of T cells demonstrated MN-Cov-COOH-NPs as the superior formulation **(Figure 3.6)**. The MN-Ads-NPs also enhanced the on the allostimulatory activity of DCs (regardless of the polymer) when compared to plain NPs (**Figure 3.6)**. It is worth to mention that the total amount of MN in the NPs added to the culture was less than 0.36 mg, while with 4.00 mg of soluble MN no effect was observed.

The findings showing the influence of MN-decorated-COOH NP formulations on DC maturation are consistent with the ability of these NPs on the enhancement of DC uptake (**Chapter 2**). However, the effect of ester-terminated formulations on DC maturation is not completely consistent with the results of DC uptake studies (**Chapter 2**). It can be attributed to the different fates of PLGAs following the active internalization of NPs by DCs and their transport to intracellular compartments. The hydrophilic COOH-terminated PLGA and its hydrophobic ester-terminated counterpart may have different susceptibility and

outcomes in low-pH intracellular compartments, which in turn could affect the intracellular signalling events. This needs further investigations.

3.5. Conclusion

MN-decorated NPs are able to induce up-regulation of co-stimulatory molecules, DC maturation and immunostimulatory activity of DCs mostly observed by MN-Cov-NPs and MN-Ads NPs with a superiority of nanoparticulate formulations to the same concentration of the soluble form of MN.

In general, COOH-terminated PLGA showed to be a better choice to decorate MN on the surface of NPs, compared to its ester-terminated counterpart formulations. These findings suggest the capability of PLGA-based NPs incorporated with MN as vehicles to boost immune responses in antigen delivery in vaccines.

References

1. Joffre, O., et al., *Inflammatory signals in dendritic cell activation and the induction of adaptive immunity.* Immunol Rev, 2009. **227**(1): p. 234-47.
2. Burgdorf, S., et al., *Distinct pathways of antigen uptake and intracellular routing in CD4 and CD8 T cell activation.* Science, 2007. **316**(5824): p. 612-6.
3. Geijtenbeek, T.B. and S.I. Gringhuis, *Signalling through C-type lectin receptors: shaping immune responses.* Nat Rev Immunol, 2009. **9**(7): p. 465-79.
4. Reddy, S.T., M.A. Swartz, and J.A. Hubbell, *Targeting dendritic cells with biomaterials: developing the next generation of vaccines.* Trends Immunol, 2006. **27**(12): p. 573-9.
5. Aarnoudse, C.A., et al., *Recognition of tumor glycans by antigen-presenting cells.* Curr Opin Immunol, 2006. **18**(1): p. 105-11.
6. Apostolopoulos, V., et al., *Ex vivo targeting of the macrophage mannose receptor generates anti-tumor CTL responses.* Vaccine, 2000. **18**(27): p. 3174-84.
7. Gazi, U. and L. Martinez-Pomares, *Influence of the mannose receptor in host immune responses.* Immunobiology, 2009.
8. East, L. and C.M. Isacke, *The mannose receptor family.* Biochim Biophys Acta, 2002. **1572**(2-3): p. 364-86.
9. Taylor, P.R., S. Gordon, and L. Martinez-Pomares, *The mannose receptor: linking homeostasis and immunity through sugar recognition.* Trends Immunol, 2005. **26**(2): p. 104-10.
10. Apostolopoulos, V., et al., *Pilot phase III immunotherapy study in early-stage breast cancer patients using oxidized mannan-MUC1 [ISRCTN71711835]*. Breast Cancer Res, 2006. **8**(3): p. R27.
11. van Vliet, S.J., et al., *Innate signaling and regulation of Dendritic cell immunity.* Curr Opin Immunol, 2007. **19**(4): p. 435-40.
12. Tada, H., et al., *Saccharomyces cerevisiae- and Candida albicans-derived mannan induced production of tumor necrosis factor alpha by human monocytes in a CD14- and Toll-like receptor 4-dependent manner.* Microbiol Immunol, 2002. **46**(7): p. 503-12.
13. Backer, R., et al., *CD8- dendritic cells preferentially cross-present Saccharomyces cerevisiae antigens.* Eur J Immunol, 2008. **38**(2): p. 370-80.
14. He, L.Z., et al., *Antigenic targeting of the human mannose receptor induces tumor immunity.* J Immunol, 2007. **178**(10): p. 6259-67.
15. Foged, C., A. Sundblad, and L. Hovgaard, *Targeting vaccines to dendritic cells.* Pharm Res, 2002. **19**(3): p. 229-38.
16. Presicce, P., et al., *Keyhole limpet hemocyanin induces the activation and maturation of human dendritic cells through the involvement of mannose receptor.* Mol Immunol, 2008. **45**(4): p. 1136-45.

17. Cambi, A., et al., *Dendritic cell interaction with Candida albicans critically depends on N-linked mannan.* J Biol Chem, 2008. **283**(29): p. 20590-9.

Chapter Four

Development of PLGA nanospheres decorated with hydrophobized mannan for active targeting of dendritic cells

A version of this chapter presented as a poster in
11th Canadian Society for Pharmaceutical Sciences (CSPS)
Banff, Alberta Canada, May 30-June 02, 2007

Ghotbi, Z.[1], Haddadi, A.[1], Hamdy, S.[1], Samuel, J.[1] and Lavasanifar, A.[1,2].

[1], Faculty of Pharmacy and Pharmaceutical Sciences, 3133 Dentistry/Pharmacy Centre, University of Alberta, 4119 Dent/Pharm Centre, Edmonton, Alberta T6G 2N8, Canada.
[2], Faculty of Engineering, Department of Chemical and Material Engineering, University of Alberta

4.1. Introduction

As a vehicle for vaccine delivery, PLGA-NPs show natural affinity towards the DCs and passively targeted to them; yet inclusion of the DC receptor(s) specific ligands may significantly enhance the rates and extent of NP uptake by these cells. It is expected that ligand-mediated active targeting to the DCs significantly increase the rate and extent of DC internalization and subsequent immune responses.

Mannan (MN) is a natural polymannose with a high affinity for MR [1] expressed on DCs and macrophages. The proved effect as an adjuvant makes MN an excellent candidate for targeting DCs in the form of MN-decorated PLGA-NPs, as discussed earlier in **Chapter 2**. However, a major difficulty primarily associated with coupling ligands to the capped (ester-terminated) PLGA-NPs has been the lack of functional chemical groups on the aliphatic polyester backbone of PLGA for linking to ligands **(Figure 4.1)**. This severely hinders the application of traditional chemical conjugation methods to the capped PLGA surface. To introduce functionality into PLGA surfaces several approaches have been studied such as a) synthesis of PLGA polymers with carboxylate or amine terminated groups [2]; b) blending or adsorption of functional polymers into PLGA [3, 4]; c) incorporating fatty acids (such as palmitic acid) conjugated with proteins into PLGA-NPs [5].

However, polysaccharides such as MN have a drawback resulting from their hydrophilic nature. The difference in physio-chemical properties between the hydrophobic PLGA matrix and the hydrophilic MN leads to a lower incorporation efficiency of MN in NPs. In fact, if the MN is physically adsorbed or anchored on the surface of NPs, its hydrophilic molecule could be washed off the NPs to some extent while surrounded with water or body liquids.

It is assumed shifting the physio-chemical characteristics of MN towards a more hydrophobic molecule, would play a substantial role in facilitated incorporation of the resulted hydrophobized MN in PLGA-NPs.

Conjugation of polysaccharides with fatty acids have been emerged earlier in liposomal formulations with the aim of improving the biochemical and physical stability of liposomes and the ability of targeting certain cells and organs [6]. Polysaccharides including MN, pullulan and amilopectin hydrophobized with fatty acids moieties, such as palmitoyl and cholestroyl have been designed for coating liposomal surface. The palmitoyl and cholesteroyl moieties behave as a hydrophobic anchor for the polysaccharides to bind tightly to the exterior of liposomal membranes [7].

This approach has also been exploited in coating the surface of oil droplets in oil-in-water lecithin emulsion with polysaccharides such as MN bearing a cholesterol moiety to target macrophages [8]. Moreover, palmitoylated molecules have been commonly used for surface modification of various nanocarriers [9].

Self-assembled nanospheres and nanoparticulate hydrogels of cholesterol-bearing hydrophobized pullulan also have been used as drug delivery systems [10, 11] or as active targeting tools aimed DCs [12]. In the context of DC targeting, it is believed that cholesterol-bearing hydrophobized pullulan NPs behave like chaperones, compelling DCs towards cross-presentation [12].

In the current study, we are investigating an approach with potential to improve MN incorporation to ester-capped PLGA NPs with no negative influence on the avidity of MN for MR. This approach was based on introducing a palmitoyl chain in MN structure by a substitution nucleuphilic reaction resulting in O-Palmitoyl mannan (OPM). The palmitoyl tail of OPM act as a hydrophobic component to preferentially partition into the hydrophobic PLGA matrix, driving the hydrophilic MN on display toward the aqueous external environment to be recognized by DC-expressed MR. Moreover, it is probable that this approach confer stability and better structure integrity against harsh bio-environments encountered after *in vivo* administration.

4.2. Materials and methods

4.2.1. Materials

N,N-Dimethyl formamide (DMF), dichloromethane (DCM) and chloroform were purchased from Caledon Laboratories Ltd. (Toronto, ON, Canada). Anhydrous diethyl ether, tetrahydrofuran (THF), acetonitrile, methanol, chloroform and absolute ethanol were purchased from Fisher Scientific (Ottawa, ON, Canada). Pyridine purchased as extra dry (< 50 ppm H_2O) from ACROS organics (Geel, Belgium). Mannan derived from S. Cerevisiae, Deuterated dimethyl sulfoxide (DMSO-d_6), PVA (MWt 31-50KDa), SDS and palmitoyl chloride (hexadecanoyl chloride, 98%) were purchased from Sigma-Aldrich (St. Louis, MO, USA). Ester-terminated PLGA copolymer (average MWt of 7KDa; lactide to glycolide ratio of 50:50) and COOH-terminated PLGA (Inherent viscosity range of 0.15-0.25 dL/g and lactide/ glycolide ratio of 50:50) were purchased from LACTEL®, Birmingham polymers (DURECT Corporation, USA). TMRD, MWt 40KD and Gold Antifade reagent with DAPI were purchased from Invitrogen (Carlsbad, CA, USA). Black opaque 96-well plate was from Costar®. Recombinant murine GM-CSF was purchased from Peprotech (Rockville, IL). FITC-conjugated CD11c mouse mAb were purchased from E-Bioscience (San Diego, CA, USA). Biotinylated anti-mouse CD206 (MMR) Ab was purchased from BioLegend (San Diego, CA, USA). C57BL/6 mice were purchased from the Jackson Laboratory (Bar Harbor, ME). All experiments were performed using 6 to 12 week old female mice.

4.2.2. Synthesis of OPM

The modified polysaccharide, OPM, was synthesized by esterification of the yeast MN through a nucleuphilic substitution reaction under extra anhydrous catalytic condition [13, 14]. The nomenclature denotes replacement of the hydrogen atom of the alcoholic hydroxyl groups of MN by palmitoyl **(Figure 4.1)**. Briefly, 1000 mg MN dried in vacuum-oven overnight at room temperature was dissolved in 20 mL extra-dried DMF in 50-60 °C. 1.2 mL extra dry pyridine was added drop-wise to stirring MN solution following by drop-wise addition of

1.5 mL of anhydrous palmitoyl chloride ($CH3(CH_2)_{14}COCl$), mixed with 1.5 mL extra-dried DMF. The reaction was allowed to proceed in 6 h at 60 °C while stirring under argon in a rubber-capped flask. The combination of product and reactants were slowly poured into 150 mL of cold (2-8 °C) absolute ethanol under vigorous stirring for 0.5 h. The precipitate of OPM was then collected by centrifugation at 700 × g for 10 minutes followed by washing off the un-reacted remaining reagents and other impurities with another 100 mL of cold absolute ethanol by two more centrifugation cycles. The purification process was then carried out by washing the pellet with 40 mL of anhydrous diethyl ether (dried by metallic sodium and distillation for 1-2 h at 60-70 ºC). The desired product was then dried under vacuum at 60 °C overnight. The product was practically insoluble in various solvents including chloroform, DMF, THF, acetone, DCM, diethyl ether, acetonitrile and methanol; partially soluble in water and practically soluble in DMSO.

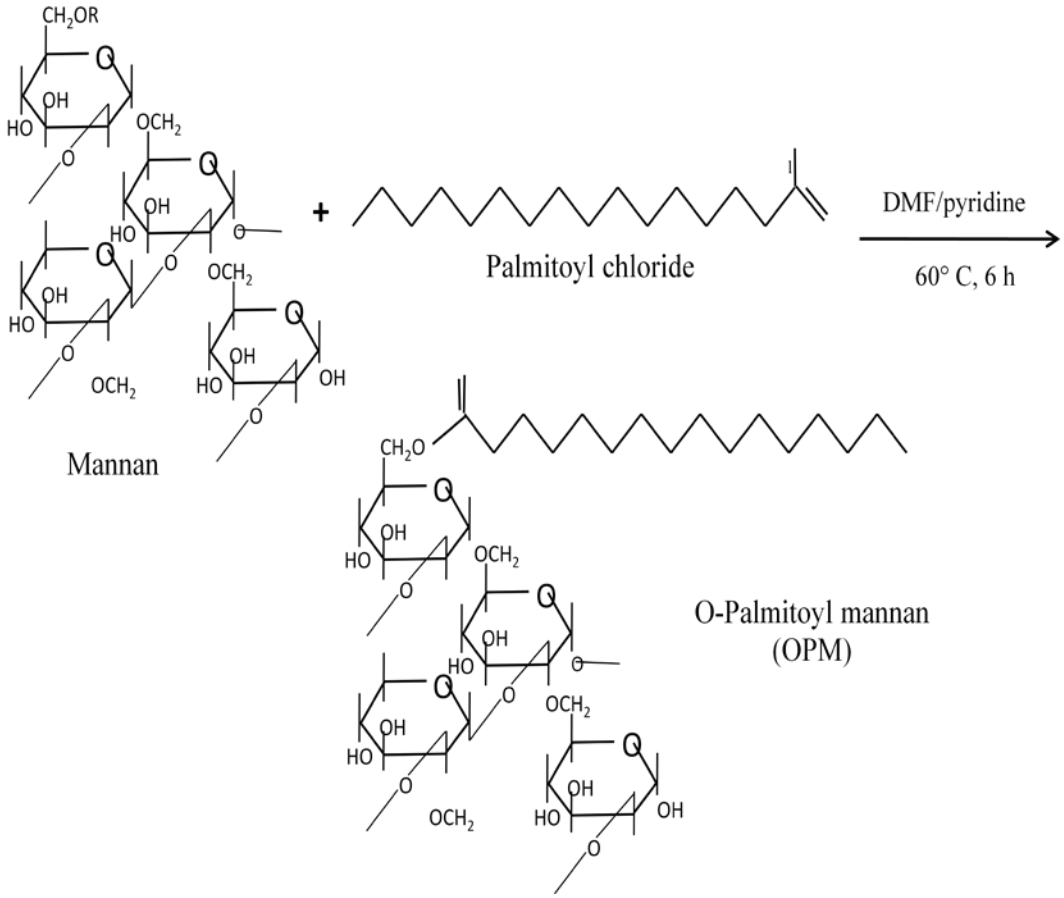

Figure 4.1: Illustration of the OPM synthesis from the starting materials.

4.2.4. Characterization of OPM

The reaction product was dissolved in DMSO-d_6 and the palmitoyl substitution in esterification reaction was elucidated by ^{1}H nuclear magnetic resonance (^{1}H-NMR) spectroscopic analysis at 500 MHz (INOVA 500 (4 Channel) with a Direct Drive Varian 600 HX (NANUC)). To assess the substitution of hydrogen atoms with palmitoyl, the OPM spectra were compared with the one for MN to verify the presence of corresponding peaks.

4.2.4. Preparation of ester-terminated NPs

4.2.4.1 Plain NPs- Plain PLGA-ester NPs were prepared using double-emulsion solvent evaporation technique [15] as described in **Section 2.2.4.1** and **Figure 2.2**. In brief, PBS (W1) was emulsified in the organic phase (PLGA solution in

chloroform) and emulsified followed by the addition of PVA solution (W2) as stabilizer. The resulted emulsion was transferred to stirring PVA and NPs collected after evaporation of chloroform, washed and freeze-dried.

4.2.4.2 OPM-decorated PLGA-NPs- OPM incorporation into ester-terminated PLGA NPs was accomplished using the above procedure. OPM was added during or after the NP formation by three different approaches and resulted NPs were designated as OPM-W1-Ester, OPM-W2-Ester and OPM-Ads-Ester NPs, respectively **(Table 4.1)**.

OPM-W1-Ester NPs were prepared by addition of the OPM solution into the primary aqueous phase (W1). In brief, the aqueous phase containing 100 µL of a 15 mg/mL solution of OPM in 1:2 DMSO-deionized water mixture (v/v) was emulsified into the organic phase (containing 100 mg PLGA dissolved in 300 µL chloroform) to form the w/o emulsion. This was followed by addition of the primary (w/o) emulsion to 8 mL of stirring 9% PVA solution and NP formation as described earlier in **Section 2.2.4.1**.

OPM-W2-Ester NPs were prepared by introducing OPM to the secondary aqueous phase (W2) containing 9% PVA solution in PBS. A solution of 10 mg/mL OPM in 1:5 DMSO-deionized water mixtures was prepared by heating up to 40 °C. The NP preparation was accomplished by mixing 1 mL of the OPM solution with 1 mL 9% PVA/PBS followed by sonication and NP purification as described earlier.

OPM-Ads-Ester NPs were prepared by physical adsorption of OPM onto the surface of NPs. This was accomplished by adjoining OPM solution to freeze-dried formulation of plain NPs, prepared in **Section 4.2.4.1**. Briefly, 60 mg of OPM was thoroughly mixed with a suspension of 30 mg of ester-terminated plain NPs in 8 mL PBS (pH 5). The adsorption process was allowed to proceed by gently stirring at room temperature overnight. The ester-terminated PLGA-NPs with adsorbed OPM were then collected, washed off from non-adsorbed OPM using cold PBS (pH 7.4) by spinning at 4 °C with an ultracentrifuge (35000 × g, 15 min for three times) and freeze-dried for 48 hours.

Table 4.1- Designated names to different methods used for physical incorporation of OPM in PLGA-NPs.

Physical incorporation of OPM	Ester-terminated PLGA	COOH-terminated PLGA
In primary aqueous phase (W1)	OPM-W1-Ester NPs	OPM-W1-COOH NPs
In secondary aqueous phase (W2)	OPM-W2-Ester NPs	OPM-W2-COOH NPs
Adsorption after NP preparation	OPM-Ads-Ester NPs	OPM-Ads-COOH NPs

4.2.5. Preparation of TMRD-loaded ester-terminated NPs

4.2.5.1 TMRD-loaded plain NPs- Encapsulation of TMRD in NPs was pursued in order to achieve fluorescently labelled NPs for cell uptake studies. Plain TMRD-loaded NPs were prepared using the procedure described above for plain NPs, by addition of 50 µL (0.5 mg) of a TMRD solution in PBS to organic phase (a solution of 100 mg PLGA in 300 µL chloroform), and further emulsification, solvent evaporation, NP collection and freeze-drying in dark (**Section 4.2.4.1**).

4.2.5.2 TMRD-loaded OPM-W1-Ester NPs- OPM-W1-PLGA-ester NPs loaded with TMRD were prepared with minor modifications to the procedure described for OPM-W1-PLGA-Ester NPs. Briefly, a mixture of 50 µL of a TMRD solution (10 mg/mL) in PBS and 100 µL of OPM (1.5 mg) in 1:2 DMSO-deionized water solution was emulsified with the PLGA solution in chloroform, followed by secondary emulsification and NP purification, as described earlier (**Section 4.2.4.2**).

4.2.5.3 TMRD-loaded OPM-W2-Ester NPs- TMRD incorporated NPs with OPM in the secondary aqueous phase were accomplished using identical procedure described for OPM-W2-PLGA-ester NPs accompanied by the addition of 0.5 mg TMRD (50 µL) to PLGA solution in organic solvent.

4.2.5.4 TMRD-loaded OPM-Ads-Ester NPs- Preparation of OPM-Ads-Ester NPs loaded with TMRD was carried out using TMRD-loaded plain ester-terminated NPs instead of plain-ester- terminated NPs (**Section 3-2-4-2**).

4.2.6. Preparation of COOH-terminated NPs

4.2.6.1 Plain NPs- Plain PLGA-COOH NPs were prepared using a double-emulsion solvent evaporation technique with some modifications from the method for ester-terminated PLGA. The preparation technique is previously reported in **Section 2.2.4.1,** and involved using DCM as the organic solvent, a different concentration of the secondary aqueous phase (5% PVA in PBS) and solvent evaporation in stirring distilled water.

4.2.6.2 OPM-decorated COOH-terminated NPs- Similar to ester-terminated PLGA-NPs, OPM incorporation into COOH-terminated PLGA-NPs was accomplished by three methods as described above in **Section 4.2.4.2**, with respect to the alterations for preparation of COOH-terminated NPs (**Section 4.2.6.1 and 2.2.4.1**). Resulted NPs were designated as OPM-W1-COOH, OPM-W2-COOH and OPM-Ads-COOH NPs, respectively. **Table 4.1** summarizes the different methods utilized for each formulation.

4.2.7. Preparation of TMRD-loaded COOH-terminated NPs

Preparation of TMRD incorporated NPs were accomplished using identical procedures ***(Section* 4.2.6**) accompanied by the addition of 0.5 mg TMRD (50 µL) to PLGA/DCM solution.

4.2.8. Characterization of OPM-decorated PLGA NPs

4.2.8.1. Particle size analysis- The mean hydrodynamic diameter and polydispersity index of the NPs used in cell uptake studies was determined by Zetasizer 3000 utilizing DLS-based methodology. The measurements were performed at a scattering angle of 90° and at 25°C, using NPs approximately diluted 100 fold with filtered deionized water (0.22 lm GV, Millipore).

4.2.8.2. Zeta potential measurements- Plain and OPM-decorated NPs used for the cell uptake studies were examined for their net surface charge. NPs were dispersed in deionized water to a final concentration of 0.02 % (w/v) and Zeta potential was measured by streaming potential with a Zetasizer 3000 in 3 serial measurements.

4.2.8.3. TMRD loading- Analysis of TMRD-loaded NPs was performed for the extent of loading and for the leaching TMRD from NPs during cell uptake studies as previously reported in **Section 2.2.5**.

4.2.9. Generation and characterization of murine BM-DCs

DC primary cultures were generated from murine bone-marrow precursors in complete DC media using femurs of C57BL/6 mice as reported earlier in ***Section 2.2.6.*** Cultured BM-DCs were characterized for the expression of CD11c (DC specific cell surface marker) and MR.

4.2.9.1 Expression of CD11c- The 8-day-old semi-adherent and non-adherent cultured cells were characterized for the expression of CD11c with FITC- labelled CD11c mAb using flow cytometry (**Section 2.2.7.1*.*).**

4.2.9.2 MR expression- As described earlier in **Section 2.2.7.2**, the level of MR expression on semi-adherent and non-adherent cells were assessed on days 3, 6 and 7 of culture by anti- CD206 (MMR) mAb using flow cytometry.

4.2.10. Assessment of the effect of OPM-decoration on DC uptake of NPs

At day7 of culture 2 mg of freeze-dried TMRD-loaded NPs were added to DC cultures after reconstitution in 0.5 mL PBS followed by 1-5 seconds sonication at level 2 using a microtip sonicator. All cell culture dishes were kept in a CO_2 incubator in 37 °C and 5% CO_2.

At day 8 of culture and 20 h after treatment with OPM-decorated or plain NPs, semi-adherent and non-adherent cells were harvested and collected by adding 20 mL cold PBS (pH 7.4) and centrifugation at 500 × g for 5 minutes. The cells were washed thoroughly (3 times) with cold FACS buffer (PBS with 2% FBS) to remove soluble TMRD and non-internalized NPs. Cells were diluted with FACS buffer at a concentration of $2x10^6$ cells per ml. 200 µL of the cell suspension ($4x10^5$) was transferred into a U-shaped 96-well culture plate and incubated with 0.5 µg of anti mouse CD16/ CD32 mAb to block Fcγ receptors, washed and re-dispersion in 200 µL FACS buffer. The CD11c surface marker was stained with 0.1 µg (10 µL) FITC- labelled anti-mouse CD11c Ab and then washed with 200 µL FACS buffer by centrifugation and supernatant aspiration

between washes. A live single-cell suspension were then acquired with a three-line flow cytometer (Becton-Dickinson FACSort, BD Biosciences) and analyzed for FITC- labelled CD11c using a Summit 3.1 software (DakoCytomation).

4.2.11. Intracellular localization of OPM-decorated NPs

Intracellular location of OPM-decorated NPs was assessed by LSCM images of a fixed cell population stained with FITC- labelled CD11c (DC- cell membrane stain) and counterstained with DAPI (fluorescent nuclear label) as previously described in **Section 2.2.8**.

Statistical analysis

Complied data are presented as the mean ± standard deviation (SD) throughout this chapter. The data were analyzed for statistical significance differences ($P<0.05$) by unpaired Student's t-test, unless otherwise stated.

4.3. Results

4.3.1. Synthesis and characterization of OPM

OPM was produced under anhydrous catalytic reaction by replacement of the hydrogen atom(s) of the alcoholic group(s) of MN by palmitoyl and was purified.

The palmitoyl substitution in esterification reaction was elucidated by ^{1}H-NMR spectra of the reaction product in DMSO-d_6. The results showed the presence of characteristic peaks for -CH_3, -$(CH_2)_{13}$- and -CO-CH_2- groups, with the corresponding chemical shifts [δ 0.85(3H), δ 1.24 (26H) and δ 1.58 (2H)] , compared to the MN **(Figure 4.2)**.

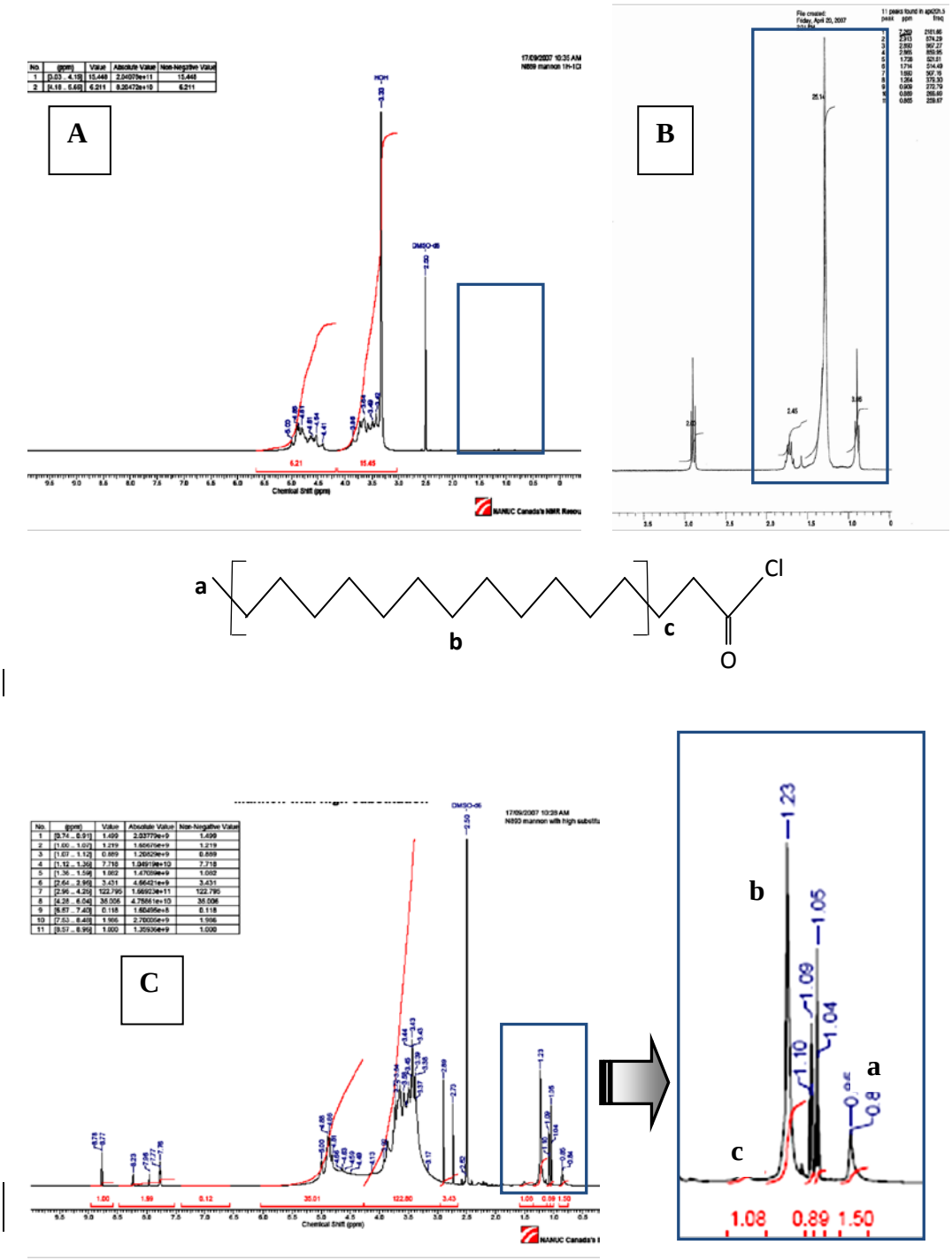

Figure 4.2: ^{1}H-NMR spectrum and peaks of **A)** mannan (non-substituted), **B)** palmitoyl chloride and **C)** OPM (corresponding palmitoyl peaks are highlighted). The ^{1}H-NMR spectra are obtained in DMSO-d_6.

4.3.2. Characterization of OPM-decorated PLGA NPs

4.3.2.1. Particle size analysis- Decoration of NPs (either ester-terminated or COOH-terminated) with OPM, did not cause any significant change in NP size (unpaired Student's t-test; $P<0.05$), except for OPM-Ads-NPs (**Table 4.2**).

While plain ester-terminated PLGA-NPs had a mean diameter of 344, OPM-decorated NPs showed a mean diameter in the range of 383-523 nm; depending the incorporation method (**Table 4.2)**. As the result of OPM incorporation in COOH-terminated NPs, the NP size changed from 328 nm to a range size of 354-434 nm (**Table 4.2)**.

Incorporation of OPM in both ester and COOH-terminated PLGA-NPs resulted in no significant increase in polydispersity index of NPs (Student's t-test, $P<0.05$) (**Table 4.2**).

Table 4.2: Mean diameter and polydispersity index of OPM-decorated PLGA-NPs.

Nanoparticles	**Mean diameter ± SD (nm)** [a]	**Polydispersity Index ±SD**
PLGA-Ester NPs	344±45	0.12±0.06
OPM-W1- Ester NPs	383±11	0.14±0.07
OPM-W2- Ester NPs	365±37	0.17±0.05
OPM-Ads- Ester NPs	523±13*	0.18±0.11
PLGA-COOH NPs	328±30	0.13±0.04
OPM-W1- COOH NPs	354±21	0.09±0.07
OPM-W2- COOH NPs	355±27	0.13±0.05
OPM-Ads- COOH NPs	434±17**	0.15±0.05

[a] measured by DLS technique
*Statistically different from PLGA-Ester NPs
** Statistically different from PLGA-COOH NPs

4.3.2.2 Zeta potential of NPs- Plain PLGA-NPs demonstrated a negative Zeta potential of -25.0±0.5 for ester-terminated and -36.2±0.3 for COOH-terminated polymers, respectively. Following surface-decoration with OPM, Zeta potential dropped significantly (**Figure 4.3**), due to the partially or complete screening of

the polymer surface by OPM; reaching -34.1 to -46.2 mV for ester-terminated and -44.4 to -50.3 mV for COOH-terminated PLGA-NPs **(Figure 4.3).**

The following trend was observed for net negative surface charge of both ester and COOH-terminated PLGA-NPs: OPM-Ads>OPM-W2>plain NPs.

A)

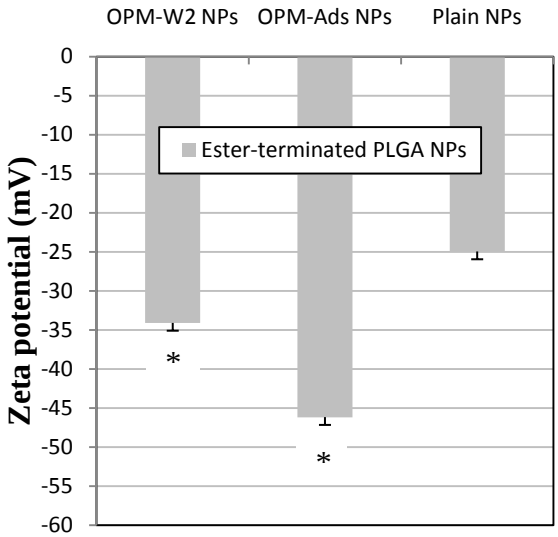

B)

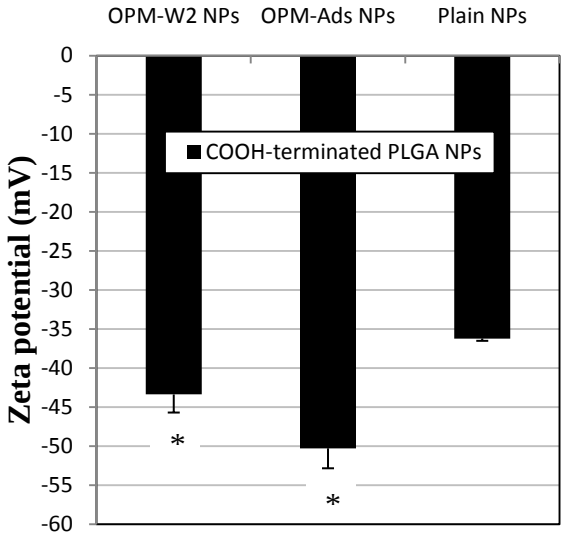

Figure 4.3: The extent of Zeta potential upon OPM incorporation for **A)** ester-terminated and **B)** COOH-terminated PLGA-NPs; compared to plain PLGA-NPs. Significant groups are shown by (*) ($p<0.05$), analyzed by unpaired Student's t-test. Each bar represents mean± SD (n=3).

4.3.3. Characterization of DCs used in uptake studies

4.3.3.1. MR expression- Based on the maximum expression of MR (36% of $CD11c^+/MR^+$ cells), 7-day old DCs were used in subsequent uptake studies **(Section 2.4.4.1)**.

4.3.3.2. Expression of CD11c- Staining with FITC-anti CD11c mAb indicated that the population of the live cultured DCs ($CD11c^+$ cells) was 87.6±3.1% before exposure to formulations (**Figure 4.4**). Upon treatment with various OPM-decorated or non-decorated NPs, this population did not significantly changed (analyzed by Student's t-test) and was in the range of 84.6-89.4% (for the ester-terminated PLGA-NPs) and 86.1-90.9% (for the COOH-terminated NPs) (**Figure 4.4**). After treatment with NPs, no significant difference was observed between CD11c positivity of the cells treated with ester and COOH-terminated counterparts.

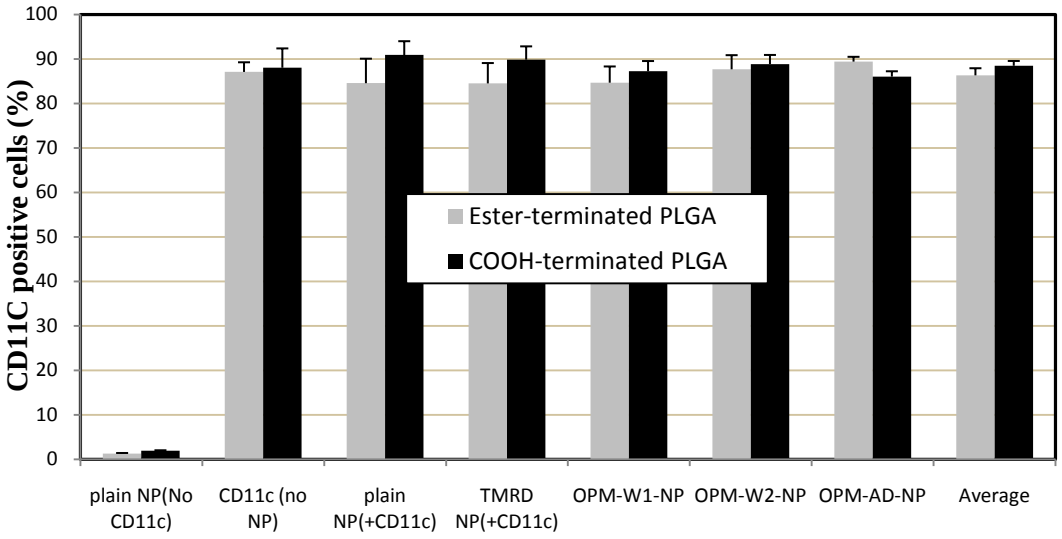

Figure 4.4: CD11c+ cell population before and after pulsing with various formulations using flow cytometry. Each bar represents mean%± SD (n=3-5).

4.3.4. Quantitative assessment of NP uptake by DCs using flow cytometry

In flowcytometry studies, the COOH-terminated and ester-terminated TMRD loaded NPs appeared with different patterns on dot plots in the absence of DCs (**Figure 4.5A** and **B**). To exclude the non-internalized NPs from the DC

population (**Figure 4.5**), the region of the events (gating) for the uptake of ester-terminated and COOH-terminated NPs was chosen separately, based on the dot plot patterns of different PLGAs in the absence (**Figure 4.5A**) and presence of DCs**.**

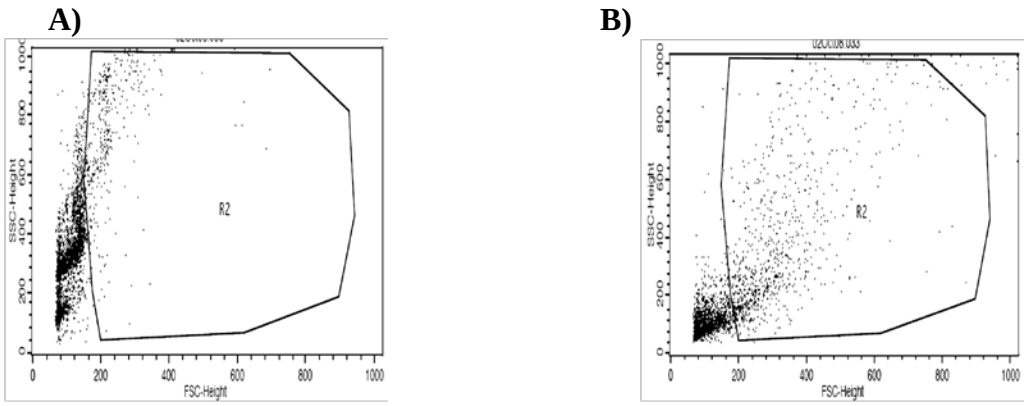

Figure 4.5: Flow cytometric dot plots forward scatter (FCS) and size scatter (SSC) profiles of NPs in the absence and presence of DCs. FCS and SSC profiles of **A)** ester-terminated NPs, and **B)** COOH-terminated NPs in the absence of DCs. TMRD-loaded NPs spinned at the same time and rate as for the cells (500g for 15 min) and acquired with the same setting. The gated regions for 7-day-old DCs treated with C) PBS in the absence of NPs, **D)** ester-terminated NPs, and **E)** COOH-terminated NPs. The dot plots of DCs treated with NPs represent increase in cellular granularity of cells due to uptake.

To evaluate the effect of OPM decoration on the *in vitro* DC uptake of PLGA-NPs, 7-day-old DC cultures were treated with various formulations of fluorescent-loaded NPs, analyzed after 20h incubation and the percentages of $TMRD^{+}$/ $CD11c^{+}$ cells were compared. Fold-increase in DC-uptake was calculated for TMRD-labelled ester-terminated formulations as follows:

$$\textbf{Fold} - \textbf{increase in DC uptake} = \frac{\textbf{TMRD}/_{\textbf{CD11c}}\ \textbf{positive cells for OPM decorated formulation}\ (\%)}{\textbf{TMRD}/_{\textbf{CD11c}}\ \textbf{positive cells for plain PLGA NPs}\ (\%)}$$

(Equation 4-1)

Similarly, for COOH-terminated formulations, fold-increase in DC-uptake was calculated as percentages of $TMRD^+$/ $CD11c^+$ cells for test formulation/ percentages of $TMRD^+$/ $CD11c^+$ cells for plain COOH-terminated PLGA-NPs.

The fold-increase in the level of DC uptake for ester-terminated OPM-decorated NPs is shown in **Figure 4.6A.** The results demonstrated the level of NP uptake by DCs was elevated following OPM incorporation, in general; with the exception of OPM-W1-Ester-NPs (analyzed by student's t-test; $p<0.05$) which shows similar uptake to that of the control (plain PLGA-NPs). The following trend was observed for the level of uptake of ester-terminated NPs: OPM-Ads-Ester>OPM-W2-Ester>OPM-W1-Ester=plain-Ester NPs.

In the case of COOH-terminated formulations, a significant fold-increase in DC uptake was observed only by OPM-Ads-COOH-NPs (analyzed by student's t-test; $p<0.05$) (**Figure 4.6B)**.

Overall, the maximum DC uptake among all formulations was observed for OPM-Ads-COOH NPs which showed 1.67 ± 0.12 fold increase in the level of uptake, compared to plain NPs.

A)

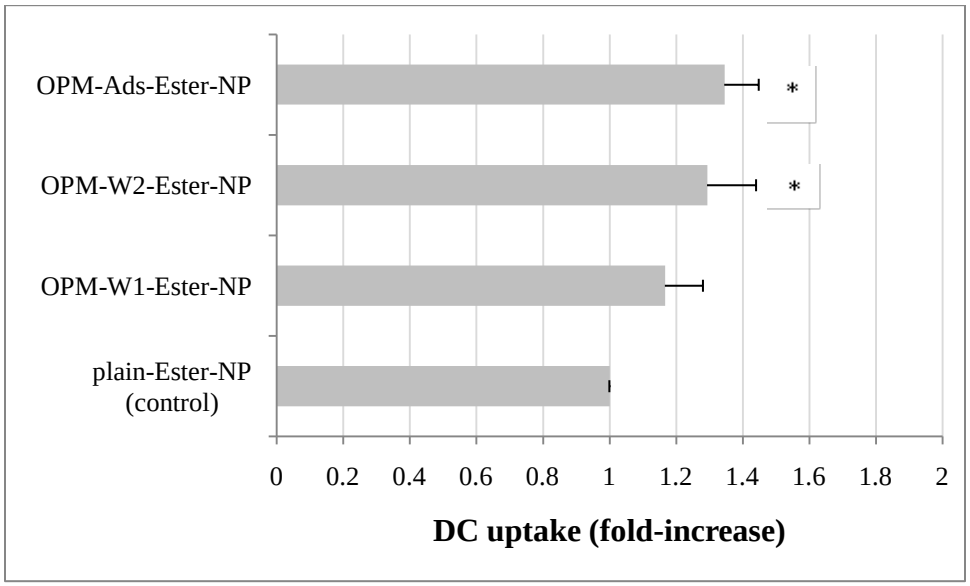

B)

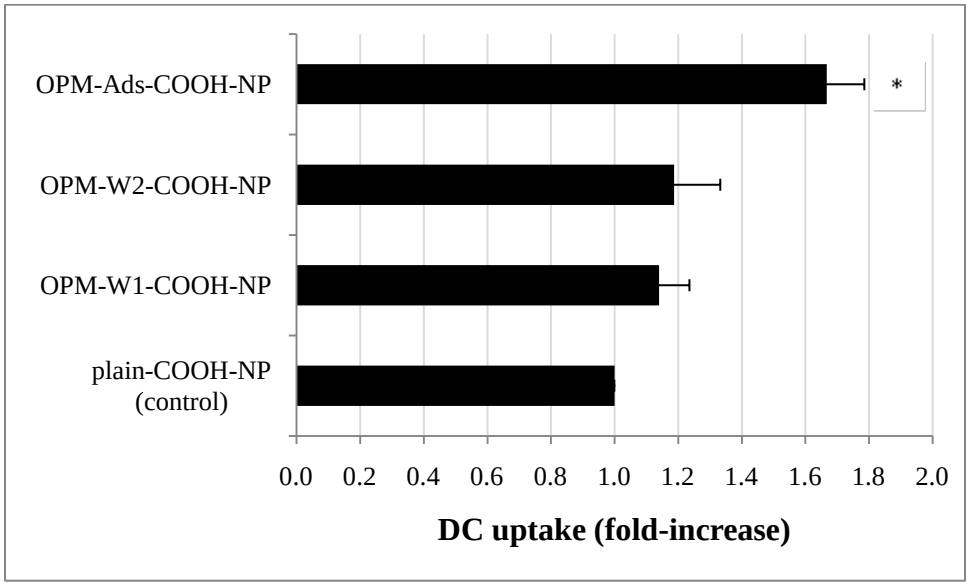

Figure 4.6: Effect of OPM- decoration, formulation method and polymer type on NP uptake by DCs, measured by flow cytometry and expressed as the fold-increase in the level of uptake relative to plain NPs (control) for **A)** ester-terminated and **B)** COOH-terminated formulations. Significant groups are shown by ($*$) ($p<0.05$), analyzed by unpaired Student's t-test. Each bar represents mean ± SD (n=3-4).

4.3.5. Intracellular localization of OPM-decorated NP

A three-color single cell images of the fixed cells was obtained to verify the intracellular uptake of various OPM-decorated NPs by DCs. DCs have been visualized specifically by cell membrane staining with FITC-conjugated anti-CD11c Ab and intracellular localization of TMRD-loaded NPs was evidenced by punctate red dots inside the cytoplasm **(Figure 4.7)**.

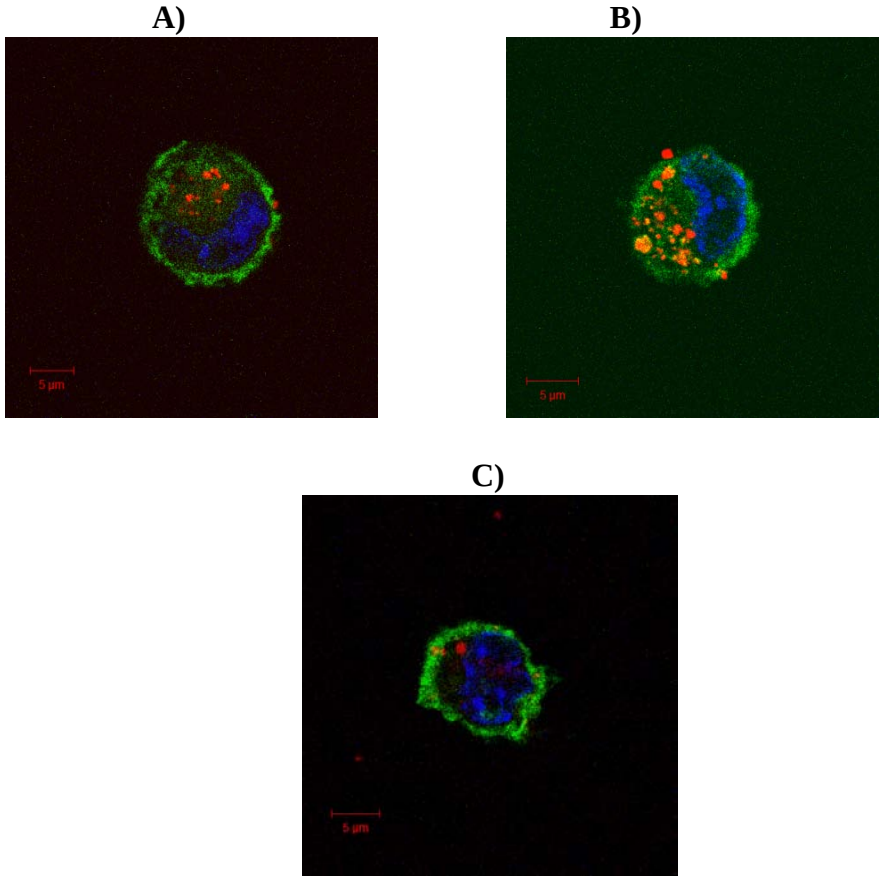

Figure 4.7: Confirmation of OPM-decorated NPs internalization by single cell images of confocal microscopy. The red dots inside DCs show the localization of TMRD-loaded NPs in the cytoplasm. DCs are incubated for 20 h with **A)** OPM-AD-COOH NPs; **B)** OPM-AD-ester NPs ; **C)** OPM-W2-ester NPs; followed by cell membrane staining with FITC-CD11c mAb (green label) and counterstaining of nucleus with DAPI (blue label).

4.4. Discussion

Development of particle-based cancer vaccines that actively target DC-expressed receptors and deliver cancer antigens and adjuvants to DCs can induce improved immune responses against vaccination [16, 17]. One candidate receptor for targeting DCs is MR [18]; a member of CLR family expressed on immature murine and human monocytes-derived DC subsets. MR is involved in antigen internalization, in particular and eventually presentation to immune system [19-21]. One of the well-identified ligands of MR is MN, a hydrophilic branched polymannose isolated from *Saccharomyces cerevisiae* with affinity towards both MR and DC-SIGN [22], and also the capability to induce production of TNF-α in a TLR4-dependent manner [23]. However, the accessibility of the ligand to MR which is a cell surface endocytic receptor is crucial. To target APCs through MR using polymeric delivery systems, the physio-chemical characteristics of MN should be shifted towards a more hydrophobic molecule for a facilitated and strong incorporation of MN to polymeric NPs.

This approach has been exploited earlier in targeting macrophages by liposomes anchored with hydrophobized MN [14]. Chemical modification of MN by its conjugation to a palmitoyl chain (resulting to OPM) was hypothesized to allow for facilitated and more stable physical anchoring of MN into PLGA NPs. This strategy allows the interaction of available mannose moieties with endocytic MR.

In the current study, MN was esterified by a substitution reaction **(Figure 4.1),** and incorporation of the resulted OPM into PLGA-NPs was accomplished using different methods **(Table 4.1)** on both ester and COOH-terminated PLGA in parallel. All prepared PLGA-NPs were shown to be within the size range suitable for uptake by DCs (average size between around 300-500 nm) [24].

Upon OPM decoration, the net negative surface charge of NPs increased significantly characterized by the Zeta potential. The level of change in Zeta potential was higher for OPM-Ads-NPs (for both PLGAs) **(Figure 4.3)** compared to plain NPs. Since OPM possesses a negative charge, possibly due to the

presence of phosphate groups on MN molecule, its incorporation into NPs led to further increase in the Zeta potential of negatively charged PLGA-NPs.

Moreover, OPM incorporation led to an increase in the association of OPM-Ads-COOH and OPM-W2-COOH PLGA-NPs with DCs **(Figure 4.6B).** However, in ester-terminated counterparts, a significant increase in uptake was only observed in OPM-Ads-ester formulations **(Figure 4.6A)**. The highest fold-increase in uptake was observed for OPM-Ads-COOH NPs (1.67±0.12). The intracellular localization rather than surface binding of NPs to DCs was also confirmed by confocal microscopy images (**Figure 4.7**).

The correlation between NP characteristics and DC uptake is summarized in **Figure 4.8**. A high correlation was observed for Zeta potential of NPs (r^2= 0.9635 and r^2= 0.8822 for COOH-terminated and ester-terminated NPs, respectively) **(Figure 4.8A).** In fact, the higher the negative Zeta potential of OPM incorporated NPs, the more the likelihood of OPM presence on the surface of NPs. The presence of OPM on the surface of NPs rather than inside NPs increases its availability to MR. Therefore; it is not surprising that a better correlation between DC uptake and Zeta potential is seen. However, the correlation between the average size of the NPs and DC uptake was weak (r^2= 0.4165) **(Figure 4.8B).** These observations are consistent with what observed for MN-decorated NPs **(Section 2.4)**.

A)

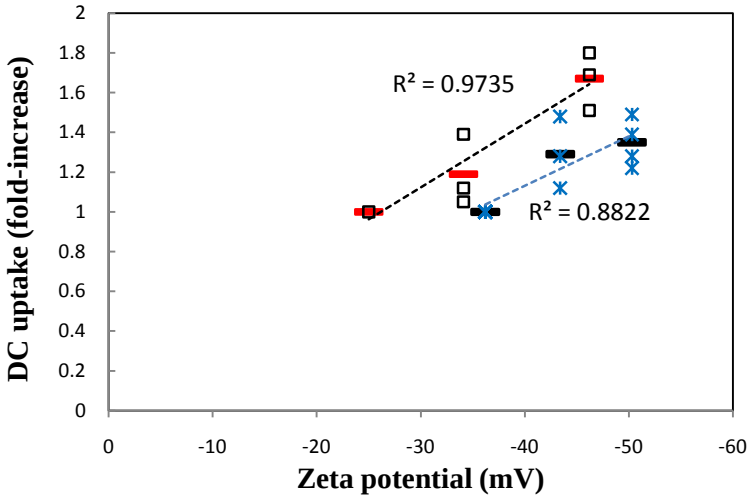

B)

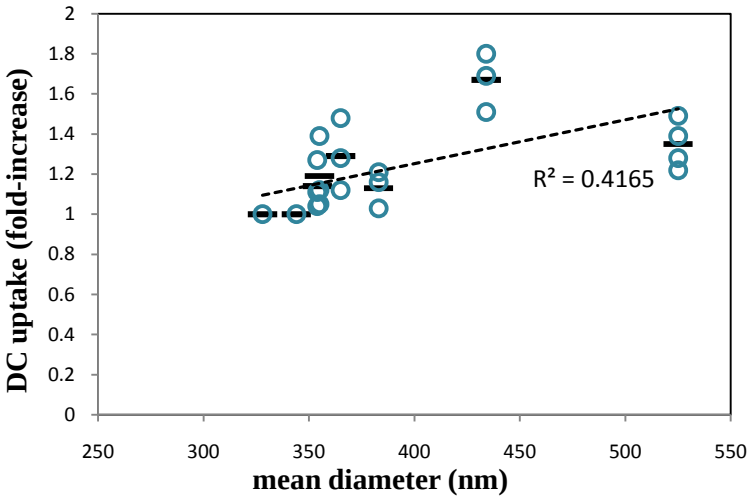

Figure 4.8: Relationship between DC uptake of NPs and various characteristics of different OPM-decorated formulations under study. **A)** Zeta potential versus DC uptake. **B)** Mean NP diameter versus DC uptake. Stars and squares are representative of ester-terminated and COOH-terminated NPs, respectively, while circles are representative of both groups together.

4.5. Conclusion

OPM-decorated NPs showed capability to enhance DC uptake relative to non-decorated NPs. However, the effect of OPM incorporation in DC uptake of NPs is less significant than what observed for the MN-incorporated PLGA-NPs **(Chapter 2)**.

References

1. Apostolopoulos, V., et al., *Ex vivo targeting of the macrophage mannose receptor generates anti-tumor CTL responses.* Vaccine, 2000. **18**(27): p. 3174-84.
2. Caponetti, G., et al., *Microparticles of novel branched copolymers of lactic acid and amino acids: preparation and characterization.* J Pharm Sci, 1999. **88**(1): p. 136-41.
3. Zheng, J. and P.J. Hornsby, *Production of microspheres with surface amino groups from blends of Poly(Lactide-co-glycolide) and Poly(epsilon-CBZ-L-lysine) and use for encapsulation.* Biotechnol Prog, 1999. **15**(4): p. 763-7.
4. Faraasen, S., et al., *Ligand-specific targeting of microspheres to phagocytes by surface modification with poly(L-lysine)-grafted poly(ethylene glycol) conjugate.* Pharm Res, 2003. **20**(2): p. 237-46.
5. Fahmy, T.M., et al., *Surface modification of biodegradable polyesters with fatty acid conjugates for improved drug targeting.* Biomaterials, 2005. **26**(28): p. 5727-36.
6. Sihorkar, V. and S.P. Vyas, *Potential of polysaccharide anchored liposomes in drug delivery, targeting and immunization.* J Pharm Pharm Sci, 2001. **4**(2): p. 138-58.
7. Sunamoto, J. and K. Iwamoto, *Protein-coated and polysaccharide-coated liposomes as drug carriers.* Crit Rev Ther Drug Carrier Syst, 1986. **2**(2): p. 117-36.
8. Iwamoto, K., et al., *Polysaccharide-coated oil droplets in oil-in-water emulsions as targetable carriers for lipophilic drugs.* J Pharm Sci, 1991. **80**(3): p. 219-24.
9. D'Souza, G.G., et al., *Surface modification of pharmaceutical nanocarriers with ascorbate residues improves their tumor-cell association and killing and the cytotoxic action of encapsulated paclitaxel in vitro.* Pharm Res, 2008. **25**(11): p. 2567-72.
10. Jeong, Y.I., et al., *Self-assembling nanospheres of hydrophobized pullulans in water.* Drug Dev Ind Pharm, 1999. **25**(8): p. 917-27.
11. Akiyoshi, K., Y. Sasaki, and J. Sunamoto, *Molecular chaperone-like activity of hydrogel nanoparticles of hydrophobized pullulan: thermal stabilization with refolding of carbonic anhydrase B.* Bioconjug Chem, 1999. **10**(3): p. 321-4.
12. Wang, L., et al., *Bone marrow-derived dendritic cells incorporate and process hydrophobized polysaccharide/oncoprotein complex as antigen presenting cells.* Int J Oncol, 1999. **14**(4): p. 695-701.
13. Hammerling, U. and O. Westphal, *Synthesis and use of O-stearoyl polysaccharides in passive hemagglutination and hemolysis.* Eur J Biochem, 1967. **1**(1): p. 46-50.
14. Vyas, S.P., et al., *Ligand directed macrophage targeting of amphotericin B loaded liposomes.* Int J Pharm, 2000. **210**(1-2): p. 1-14.

15. Ueda, M. and J. Kreuter, *Optimization of the preparation of loperamide-loaded poly (L-lactide) nanoparticles by high pressure emulsification-solvent evaporation.* J Microencapsul, 1997. **14**(5): p. 593-605.
16. Elamanchili, P., et al., *"Pathogen-mimicking" nanoparticles for vaccine delivery to dendritic cells.* J Immunother, 2007. **30**(4): p. 378-95.
17. Hamdy, S., et al., *Co-delivery of cancer-associated antigen and Toll-like receptor 4 ligand in PLGA nanoparticles induces potent CD8+ T cell-mediated anti-tumor immunity.* Vaccine, 2008. **26**(39): p. 5046-57.
18. Xiang, S.D., et al., *Pathogen recognition and development of particulate vaccines: does size matter?* Methods, 2006. **40**(1): p. 1-9.
19. Stahl, P.D. and R.A. Ezekowitz, *The mannose receptor is a pattern recognition receptor involved in host defense.* Curr Opin Immunol, 1998. **10**(1): p. 50-5.
20. Kel, J., et al., *Soluble mannosylated myelin peptide inhibits the encephalitogenicity of autoreactive T cells during experimental autoimmune encephalomyelitis.* Am J Pathol, 2007. **170**(1): p. 272-80.
21. Apostolopoulos, V., et al., *Pilot phase III immunotherapy study in early-stage breast cancer patients using oxidized mannan-MUC1 [ISRCTN71711835]*. Breast Cancer Res, 2006. **8**(3): p. R27.
22. Adams, E.W., et al., *Carbohydrate-mediated targeting of antigen to dendritic cells leads to enhanced presentation of antigen to T cells.* Chembiochem, 2008. **9**(2): p. 294-303.
23. Sheng, K.C., et al., *Mannan derivatives induce phenotypic and functional maturation of mouse dendritic cells.* Immunology, 2006. **118**(3): p. 372-83.
24. Foged, C., et al., *Particle size and surface charge affect particle uptake by human dendritic cells in an in vitro model.* Int J Pharm, 2005. **298**(2): p. 315-22.
25. Elamanchili, P., et al., *Characterization of poly(D,L-lactic-co-glycolic acid) based nanoparticulate system for enhanced delivery of antigens to dendritic cells.* Vaccine, 2004. **22**(19): p. 2406-12.

Chapter Five

Development of a micro-Positron Emission Tomography (PET) probe loaded in PLGA nanospheres for dendritic cell tracking

A version of this chapter presented as a poster in

Canadian Society for Pharmaceutical Sciences (CSPS), Montréal, Québec Canada

May 30-June 02, 2007

Ghotbi, Z.[1], Haddadi, A.[1], Samuel, J.[1] and Lavasanifar, A.[1,2].

[1], Faculty of Pharmacy and Pharmaceutical Sciences, 3133 Dentistry/Pharmacy Centre, University of Alberta, 4119 Dent/Pharm Centre, Edmonton, Alberta T6G 2N8, Canada.
[2], Faculty of Engineering, Department of Chemical and Material Engineering, University of Alberta

5.1. INTRODUCTION

Cancer immunotherapy has captured the interest of numerous immunologists and clinicians since 1970s. In immunotherapy, it is important to be able to measure an "effective," tumor specific immune response. Imaging modalities that reveal the combat in tumor microenvironment would provide vital information on infiltrating immune cells, their functional status, and their interaction with tumor cells upon vaccination, *in vivo.* This would assist the development of immunotherapeutic strategies that can shift the balance in favor of the immune system in its battle against cancer [1]. Development of more sensitive and less invasive methods to detect and monitor a minimal number of immune cells *in vivo* is; therefore, a research priority.

Dendritic cells (DCs) are of particular interest in cancer vaccination, either as cells manipulated *ex-vivo* for vaccination [2] or cells targeted by *in vivo* vaccination strategies [3, 4], due to their exclusive role in initiation and maintenance of cell-mediated immune responses. This study predominantly aimed for the development of probes for non-invasive *in vivo* monitoring of DCs among other immune cells. It is expected that advances in live imaging techniques to provide opportunities to elucidate the phenotypic and activation status as well as dynamics of recruitment, differentiation, mobilization, and fate of DCs.

Among different imaging techniques, positron emission tomography (PET) is particularly of interest for our purpose. This is owed to the potential high detection sensitivity and specificity offered by PET [5] [6] [7]. PET is based on the special decay of positron emitting (β^+) nuclides [8]. To date, most PET studies have used ^{18}F as the radiotracer. However, the rapid radioactive decay of ^{18}F ($T_{1/2}$ 109 min) has limited its benefit for *in vivo* imaging of immune cells including DCs. Recent studies have used ^{64}Cu as another option [7]. Considering the time required for the DC tracking, ^{124}I with a relatively long half-life has been preferred as an alternative in this study. The comparatively long half-life ($T_{1/2}$ 4.18 days) makes it suitable for transporting labelled compounds even to destinations very far away *in vivo*. ^{124}I is an isotope with a decay of 25% β^+ (2.1

Mev) and 75% electron capture [8]. The β^+ decay makes it suitable for PET applications.

Polymer-based nanoparticles (NPs) have recently emerged as important platforms for a variety of immunological applications such as cancer vaccination [3] and molecular imaging [9]. Poly (D, L-lactide-co-glycolide) (PLGA) NPs, in particular, have received our attention for this study as they are shown to be biocompatible and biodegradable and primarily target DCs (or other phagocytic cells) as they are readily taken up by phagocytic cells including DCs [10].

In this chapter, loading of a PET probe, [^{124}I] 5-iodo-2, 4-difluro-1-(2-deoxy-b-D-ribofuranosyl) benzene ([^{124}I] 5-IDFPdR), into PLGA-NPs has been examined as means for *in vivo* monitoring of DCs by PET. 5-IDFPdR (MWt 357 Da) is a thymidine analog [11] that can be radiolabeled by ^{124}I through an isotope exchange reaction ***(Figure 5.1)*** resulting to a PET probe [12]. 5-IDFPdR was chosen for this study due to its appropriate physiochemical and biochemical characteristics including high lipophilicity (logP 2.8), low toxicity, biochemical inertness and *in vivo* stability, i.e. resistance to metabolic deiodination [11]. It was hypothesized that [^{124}I] 5-IDFPdR to be efficiently loaded in PLGA-NPs (due to its lipophilic nature) and form an appropriate nanoprobe for PET- image after NP capturing by DCs. Because of the similarity in the chemical characteristics of ^{124}I and ^{125}I, the radioisotope ^{125}I has been used for initial *in vitro* experiments in this chapter.

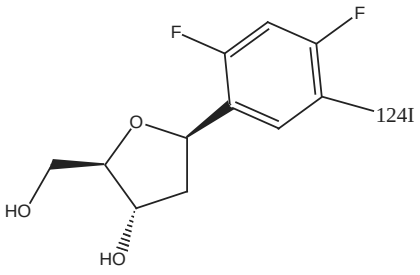

Figure 5.1: Chemical structure of radioiodinated 5-iodo-2, 4-difluro-1-(2-deoxy-b-D-ribofuranosyl) benzene ([^{124}I] (5-IDFPdR).

5.2. Materials and methods

5.2.1. Materials

Poly (D, L-lactide-co-glycolide) (PLGA) copolymer with an average molecular weight of 45,000-70,000 Da and D, L-lactide to glycolide ratio of 50:50 was purchased from LACTEL® (Birmingham polymers, Inc., USA). [^{125}I] NaI, Sodium Iodide in 0.01 M NaOH solution (100 mCi/ ml, 15 Ci/mg Iodide, carrier free) was purchased from GE Healthcare. Polyvinyl alcohol (PVA), MW 31,000-50,000 Da, was purchased from Sigma-Aldrich (St. Louis, MO, USA). 5-iodo-2, 4-difluoro-1-(2-deoxy-β-D-ribofuranosyl) benzene (5-IDFPdR) was kindly provided by Dr. L. Wieb (Faculty of pharmacy and Pharmaceutical Sciences, University of Alberta). Solvents and reagents are analytical grade and used without further treatment.

5.2.2. Radioiodination of [^{125}I] 5-IDFPdR

1-(2-deoxy-β-D-ribofuranosyl)-2, 4-difluoro-5-[^{125}I] iodobenzene ([^{125}I] 5-IDFPdR) was radiolabeled through an "iodine- radioiodine exchange reaction". This was accomplished by a nucleuphilic substitution reaction in an acidic environment using a mixture of non-radioactive 5-iodo-2, 4-difluoro-1-(2-deoxy-β-D-ribofuranosyl) benzene (5-IDFPdR) as the precursor, and [^{125}I]NaI, in the presence of Cu^{2+} as the catalyst (***Figure 5.2***) as described in literature [13] with some modifications. Briefly, 100 µL $CuSO_4.5H_2O$ (0.36 mM, 0.036 mmol) and 100 µL $(NH_4)_2SO_4$ (3.6 mM, 0.36 µmol) were added to a 2 mL reaction vial containing 5-IDFPdR (in the range of 150-250 µg) in a methanolic solution (2 mg/mL). The solvent was removed by nitrogen flow and 0.7 mCi [^{125}I] NaI (0.007 mL) was added to the vial and gently mixed. The mixture then was dried by nitrogen flow at room temperature. The closed vial was heated in oil bath at 130 °C for 2 h, and then was left at room temperature for one hour to cool down.

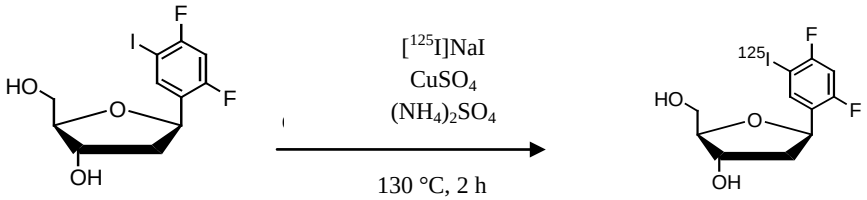

Figure 5.2: Synthetic scheme for the radioiodination of 5-IDFPdR.

5.2.3. Recovery and purification of [^{125}I] 5-IDFPdR

To estimate the yield of the radioiodination reaction, [^{125}I] 5-IDFPdR was collected, purified and analyzed as the main product of the reaction. To accomplish this, two systems were developed and compared. In the first system, the radiolabeled [^{125}I] 5-IDFPdR was collected and purified in two steps by leaching in a total of 1.5 mL chloroform for 45 minutes at room temperature. Extraction with a chloroform/water (1:1) mixture followed by 2 minutes sonication was used as the alternative system. The efficiency of extraction of both approaches was then compared.

The radiochemical and chemical purity of the resulted [^{125}I] 5-IDFPdR was examined by liquid chromatography. A radio-thin-layer chromatography (radio-TLC) system was established using a mixture of ethyl acetate: methylene chloride (6:1) as eluent, with an R_f value in the range of 0.35-0.4 for the separation of [^{125}I] 5-IDFPdR from non-reacted components or by-products. Quantitative analysis was then carried out by Reverse-Phase High Performance Liquid Chromatography (RP-HPLC) (Waters 501, USA) equipped with Waters µBundapak C18 (10 µm 3.9 × 300 mm) analytical column, using both Ultraviolet (UV) and radioactive detectors. Isocratic elution with methanol/water (50:50) at a flow rate of 1.0 mL/min of the recovered radiolabeled product with UV detection at 286 nm and a retention time (RT) of 8.0 min was applied to obtain the purity of the extracted [^{125}I] 5-IDFPdR. The linear relationship between 5-IDFPdR concentration and the peak area was investigated within the range of 1.5-100 µg/mL of 5-IDFPdR.

5.2.4. Radiation yield and specific activity of [^{125}I] 5-IDFPdR

The concentration of the isolated [^{125}I] 5-IDFPdR was determined by the HPLC system as described earlier in **Section 5.2.3**. The radioactivity of a diluted sample of the recovered [^{125}I] 5-IDFPdR was measured by a Gamma solid scintillation counter (Wellec® 1480, USA) and expressed as counts per minutes (CPM) after correction for the radioactivity of empty vial. The radiation yield was calculated as the ratio of the net activity of radioiodinated [^{125}I] 5-IDFPdR (CPM) to the total activity used for the reaction. The specific activity was determined from the following formula:

$$Specific\ activity\ \left({}^{Ci}/_{mol}\right) = \frac{(radioactivity of\ extracted\ [125I]5\text{–}IDFPdR\ \times radiochemical\ purity)}{amount\ of\ the\ recovered\ compound\ (mol)}$$

(Equation 5-1)

5.2.5. Preparation of 5-IDFPdR-nanoprobe based on PLGA

5.2.5.1. Oil-in-water emulsion (single emulsion)- PLGA-NPs containing either [125I] 5-IDFPdR or cold 5-IDFPdR were prepared using an oil-in-water (o/w) single-emulsion solvent evaporation technique as described in previous publications from our laboratory [14]. Briefly, PLGA copolymer (100 mg) was dissolved in 150 µL chloroform. To load the radioactive probe in the polymer, a sample containing 7,000,000- 11,000,000 CPM [125I] 5-IDFPdR in 300 µL chloroform was transferred to the vial containing polymer resulting to a final PLGA concentration of 22.2% w/v (organic phase).

Loading of cold probe into PLGA-NPs was achieved by addition of 500 or 1000 µg of a 5-IDFPdR solution in 300 µL chloroform to a vial containing PLGA to final PLGA concentration of 22.2% w/v (organic phase).

A 9% PVA solution in PBS (2 mL) was added as the stabilizer to the organic phases containing PLGA (either with radioactive or cold probe) and emulsified with microtip probe sonicator (Model XL2010, Heat Systems, Farmingdale, NY) at high shear stress on ice. The resulted emulsion was

immediately transferred to 8 mL stirring PVA solution in a drop-wise manner and the solvent was evaporated while stirring at room temperature for 2 h (**Figure 5.3.A**). The unhardened NPs were collected by centrifugation (Beckman L8-55, USA) at 4 °C (35000 × g, 15 min), resuspended in cold deionized water and centrifuged for two more cycles (overall three cycles).

The NPs loaded with the cold probe were freeze-dried for 40 h (VirTis Lyo-Centre, VWR international, USA) and stored at -20°C .The radioactive probe was stored at 2-8 °C as a wet suspension without any further treatment. Plain NPs were prepared using identical procedures as described above without addition of [^{125}I] 5-IDFPdR.

5.2.5.2. Water-in-oil-in-water emulsion (double emulsion)- Preparation of PLGA-NPs loaded with 5-IDFPdR was accomplished using a water-in-oil-in-water (w/o/w) emulsion solvent evaporation technique as described in Chapter 3, with some modifications. In summary, 100 µL of an aqueous solution of cold 5-IDFPdR (250) µg was added to a vial containing a solution of PLGA in chloroform (100 mg in 300 µL) and emulsified using a microtip probe sonicator. The resulting w/o emulsion was then mixed and emulsified with 2 mL of 9% PVA solution in PBS to form the secondary emulsion (Figure 5.3.B). The w/o/w emulsion was transferred to 8 mL of stirring PVA solution in PBS (9%) and the NPs were collected, washed, freeze-dried and stored as described in Section 5.2.5.1. Plain NPs were prepared using similar procedure without 5-IDFPdR addition.

A)

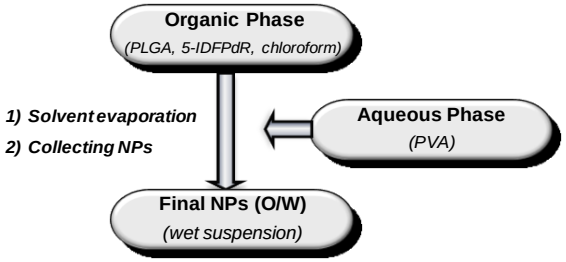

B)

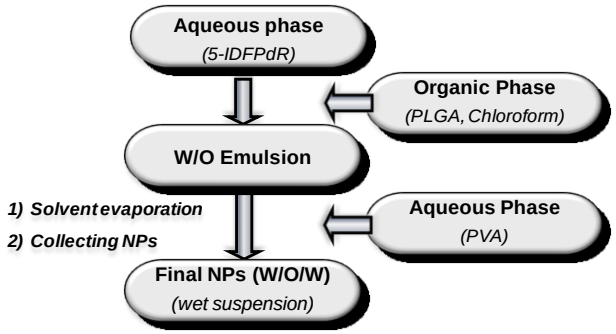

Figure 5.3: Brief illustration of nanoprobe preparation: **A)** water-in-oil (single) emulsion and **B)** water-in-oil-in-water (double) emulsion.

5.2.6. Characterization of 5-IDFPdR- loaded PLGA-NPs

5.2.6.1. Particle size analysis- The mean hydrodynamic diameter and polydispersity of the 5-IDFPdR- loaded NPs was determined by Zetasizer 3000 (Malvern, UK) at 25°C, using Dynamic-Light Scattering (DLS)-based methodology. The measurements were performed at a scattering angle of 90° using NPs loaded with [^{125}I] 5-IDFPdR or cold 5-IDFPdR diluted 100 fold with filtered deionized water (0.22 lm GV, Millipore).

5.2.6.2. 5-IDFPdR-to-PLGA-loading ratio- The [^{125}I] 5-IDFPdR content in NPs was obtained based on the radioactivity measurements in a sample of NPs. Briefly; a suspension of loaded NPs (1 mL) was dried under nitrogen flow at room temperature overnight. The dehydrated NPs were weighed and measured for radioactivity by a Gamma solid scintillation counter. The specific activity

(Equation 5-1) was applied to convert the radioactivity (µCi) of the [^{125}I] 5-IDFPdR to the equivalent weight (µg) in 1 mg of dried NPs.

Cold 5-IDFPdR was extracted from freeze-dried NPs using a mixture of chloroform and methanol following by quantification with HPLC. Briefly, 100µL chloroform was added to 10-25 µg of probe-loaded NPs and sonicated for 4-5 minutes until a completely clear solution was obtained. The resulted solution was mixed with 900 µL methanol by vortexing. The mixture was then centrifuged (Shelton Scientific-VSMC-13, USA) at 14,000 × g for 15 min to precipitate PLGA. The supernatant was separated and dried under nitrogen flow at room temperature. The dried cold 5-IDFPdR was concentrated 4-folds by dissolving in 250 µL methanol and analyzed by RP-HPLC as described in **Section 5.2.3**.

To evaluate the efficiency of extraction, chloroform was added to a mixture of the known amount of 5-IDFPdR and plain NPs and the extraction process was carried out as described above. The proportion of 5-IDFPdR loaded in PLGA-NPs (w/w) was calculated based on the following equation:

$$5\text{–}IDFPdR\text{–}to\text{–}PLGA\ weight\ ratio\ (^{w}/_{w}) = \frac{amount\ of\ loaded\ 5\text{–}IDFPdR\ (\mu g)}{initial\ weight\ of\ the\ PLGA\ (mg)}$$

(Equation 5-2)

The "Encapsulation Efficiency" was calculated from the following formulas for radiolabeled and cold iodine probes:

$$[125I]5\text{–}IDFPdR\ encapsulation\ efficiency\ (\%) = \frac{total\ activity\ of\ a\ suspension\ of\ [125I]5\text{–}IDFPdR\text{–}NPs\ (CPM)}{initial\ radioactivity\ of\ [125I]5\text{–}IDFPdR\ added\ to\ formulation\ (CPM)} \times 100$$

(Equation 5-3)

$$5\text{–}IDFPdR\ encapsulation\ efficiency(\%) = \frac{amount\ of\ 5\text{–}IDFPdR\ loaded\ in\ NPs\ (mg)}{initial\ 5\text{–}IDFPdR\ added\ to\ formulation\ (mg)} \times 100$$

(Equation 5-4)

The effect of the initial probe added to the formulation and the emulsification method on encapsulation efficiency was also investigated.

5.2.7. In vitro release of 5-IDFPdR from PLGA-NPs

The wet, unhardened NPs were directly subjected to the release experiment. “Short term” and “Long term” release behavior of the nanoprobe was studied in a wet suspension of [^{125}I] 5-IDFPdR-loaded NPs in a 24 h and 10 day time frame, respectively. In summary, after preparation and collection of NPs and immediately following the completion of three washing cycles, 1.0 mL of a mixture of suspended NPs and fresh PBS (1:10 v/v) were transferred into a microcentrifuge tube. The NPs were incubated at 37ºC in a water bath rotary shaker (Yamato, YB-521, and Japan) under continuous mild shaking. In various time intervals, one of the samples was removed and centrifuged at 15,000 × g for 15 minutes and the radioactivity of both pellet and the supernatant were measured by Gamma solid scintillation counter. The *cumulative* release of [^{125}I] 5-IDFPdR was determined from the following equation:

$$[125I]5\text{–}IDFPdR\ in\ vitro\ release\ (\%) = \frac{radioactivity\ of\ the\ supernatant\ (CPM)}{sum\ of\ the\ radioactivity\ of\ supernatant\ and\ pellet\ (CPM)} \times 100$$

(Equation 5-5)

The effect of NPs washing on the release of [^{125}I] 5-IDFPdR from NPs was evaluated by applying variable number of washing cycles (3-5 cycles) after solvent evaporation and before conduction of release experiment. Each washing cycle included 15 min washing with 25 mL of cold deionized water and further centrifugation at 15,000 × g for 15 minutes.

Release of cold 5-IDFPdR from the freeze-dried NPs was also investigated. Briefly, 50 mg of NPs were dispersed in 2.5 mL PBS then transferred to a centrifuge tube and incubated as described above. At each time interval, the tubes were centrifuged (Mistral 2000, USA) at 5000 × g for 10 min, and an aliquot of 500 µL was withdrawn from the supernatant and transferred to a microcentrifuge tube. The pellet was resuspended and returned to the tube in water bath rotary shaker. The supernatant was once again centrifuged (Shelton Scientific-VSMC-13, USA) at 15000 × g for 15 min, while the pellet was again returned to the tube in rotary shaker after resuspension in 500 µL PBS. The final resulting supernatant

was concentrated 10-folds by freeze-drying then dissolved in methanol (50 µL). The extent of released 5-IDFPdR was determined by RP-HPLC, as described in **Section 5.2.3** and the cumulative release of 5-IDFPdR was calculated using the following equation:

$$5\text{–}IDFPdR\ in\ vitro\ release(\%) = \frac{sum\ of released\ 5\text{–}IDFPdR\ (\mu g)}{5\text{–}IDFPdR\ loaded\ in\ NPs\ (\mu g)} \times 100$$

(Equation 5-6)

To calculate the overall release for each time point (except for the first one), the numerator of the following equation is the sum of the probe released in present time point together with the previous ones.

Statistical analysis

Data are expressed as mean ± standard deviation (SD) and were analysed by unpaired Student's t-test. Significance of difference among groups was determined by $P<0.05$.

5.3. RESULTS

5.3.1. Radioiodination, recovery and purification of [^{125}I] 5-IDFPdR

[^{125}I]-IDFPdR was radioiodinated using different quantities of 5-IDFPdR in the range of 150-250 µg. Maximum specific activity was obtained (665±31 µCi/µmol) with a radiation yield of 49.2±4.5 % with 200 µg of 5-IDFPdR. The radiolabeled [^{125}I]-IDFPdR was efficiently recovered from un-reacted compounds and by-products as evidenced by RP-HPLC and radio-TLC analysis. The results showed a linear relationship between the concentration of 5-IDFPdR analyzed by HPLC and the peak areas detected by UV at 286 nm within the range of 1.5-100 µg/mL of 5-IDFPdR (R^2=0.9997) (**Figure 5.4**). The chemical purity of the recovered probe using chloroform/Water (1:1) extraction system was 83.5±2.4%, as detected by RP-HPLC and radio-TLC. The radiochemical purity of the probe was 85.3±1.4%. The chemical and radiochemical purity achieved from chloroform-leaching system was 94.71±1.3% and 93.92±1.8%, respectively.

Therefore, the chloroform-leaching system was chosen for the extraction of [^{125}I] 5-IDFPdR, due to the more efficient recovery of the probe.

A)

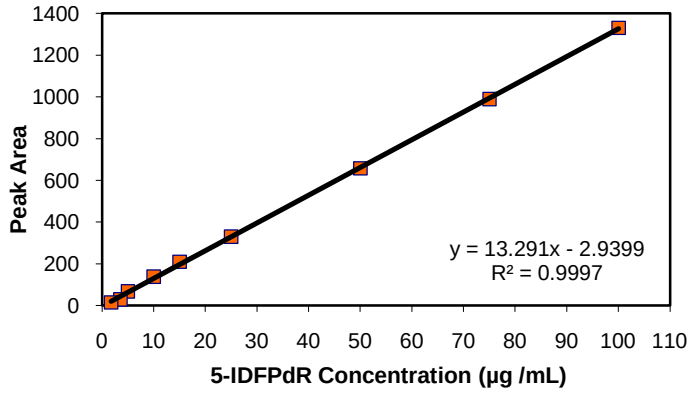

B)

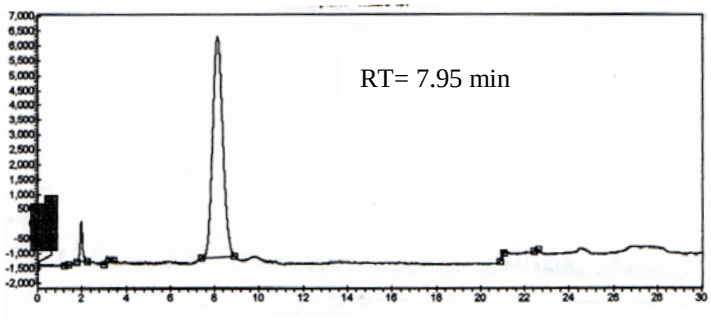

C)

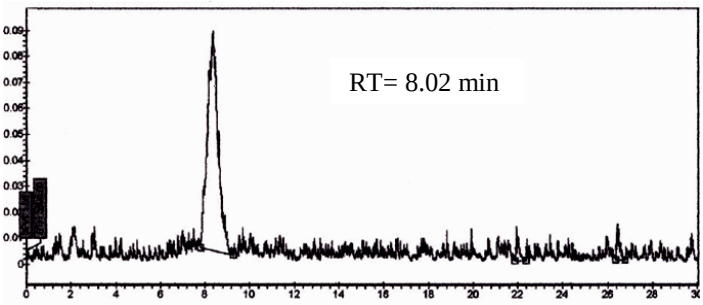

Figure 5.4: Analysis of [^{125}]5-IDFPdR recovered in chloroform by RP-HPLC: A) Standard curve correlation B) peak area of UV detection at 286 nm, and C) peak area from radioactive detector.

5.3.2. Characterization of 5-IDFPdR -loaded PLGA-NPs

5.3.2.1. Particle size analysis- Probe-loaded PLGA-NPs prepared by either single emulsion or double emulsion methods showed a narrow polydispersity index (PI) with a mean diameter in the range of 310- 380 nm **(Figure 5.5, Table 5.2)**. Loading of the probe by double-emulsion method resulted in an increase in NP size ($P<0.05$), whereas no significant difference between unloaded and loaded NPs was observed when single-emulsion method was applied.

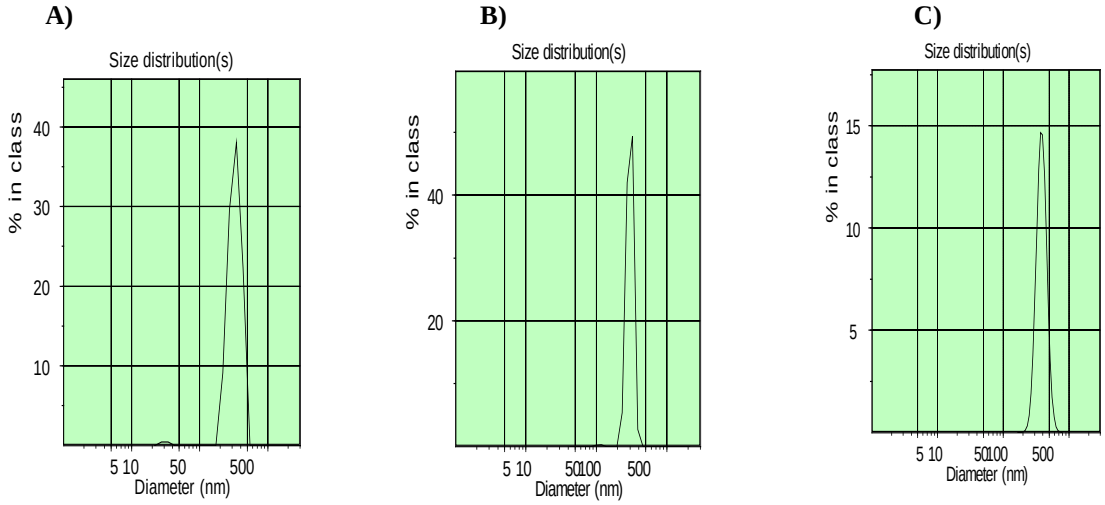

Figure 5.5: Mean diameter before freeze-drying for 5-IDFPdR-loaded PLGA-NPs**. A)** [^{125}I] 5-IDFPdR-loaded PLGA-NPs prepared by single-emulsion technique, **B)** cold 5-IDFPdR-loaded PLGA-NPs prepared by single-emulsion technique and **C)** cold 5-IDFPdR-loaded PLGA-NPs prepared by double-emulsion technique.

Table 5.2: Particle size analysis of 5-IDFPdR-loaded PLGA-NPs, measured by DLS technique

Nanoprobe	***Emulsification Technique***	***Mean diameter (nm± SD)***	***PI ± SD***
Plain PLGA-NPs	Single emulsion	312±11	0.054±0.001
[^{125}I] 5-IDFPdR-loaded PLGA-NPs	Single emulsion	310±4	0.160±0.110
5-IDFPdR-loaded PLGA-NPs	Single emulsion	309±7	0.085±0.060
Plain PLGA-NPs	Double emulsion	325±22	0.050±0.030
5-IDFPdR-loaded PLGA-NPs	Double emulsion	381±13*	0.030±0.140

*Statistically different from plain NPs

5.3.2.2. [^{125}I] 5-IDFPdR and cold 5-IDFPdR content- The 5-IDFPdR-to-PLGA-loading ratios and encapsulation efficiencies are summarized in Table 5.3. The encapsulation efficiency of cold 5-IDFPdR in NPs did not improve by increasing the initial amount of probe fed into the formulation. Comparing to w/o/w emulsion, NPs prepared with w/o emulsification method showed a significant increase in the encapsulation efficiency ($P<0.05$) **(Table 5.3).**

Table 5.3: Level of radioiodinated and cold 5-IDFPdR loaded in PLGA-NPs

Nanoprobe	Method of analysis	Emulsification method	Initial probe in formulation	probe-to-PLGA ratio (µg/mg)	Encapsulation efficiency (%)
Cold IDFPdR loaded NPs	HPLC (UV detector)	Single emulsion	1000 µg	0.38±0.12	3.8±2.0
Cold IDFPdR loaded NPs	HPLC (UV detector)	Single emulsion	500 µg	0.22±0.08	4.5±1.4
Cold IDFPdR loaded NPs	HPLC (UV detector)	Double emulsion	250 µg	0.12±0.05	4.7±1.7
[^{125}I] IDFPdR loaded NPs	Gamma solid scintillation	Single emulsion	11,000,000 cpm	0.56±0.08	6.3±0.8
[^{125}I] IDFPdR loaded NPs	Gamma solid scintillation	Single emulsion	7,000,000 cpm	0.33±0.04	9.5±1.2

5.3.3. In vitro release profile of probe-loaded NPs

5.3.3.1. In vitro release profile of a suspension of NPs- The "short-term" release studies of a suspension of [^{125}I] –IDFPdR-loaded NPs, just retrieved from solvent evaporation and purification without further treatment, demonstrated a relatively high "burst release" within the first hours and [^{125}I] –IDFPdR release from NPs reached "steady state" within 24 h (**Figure 5.6A**). Evaluation of the long-term [^{125}I] –IDFPdR release from NPs showed the prolongation of the plateau part of the [^{125}I] –IDFPdR release for the next 10 days **(Figure 5.6B)**.

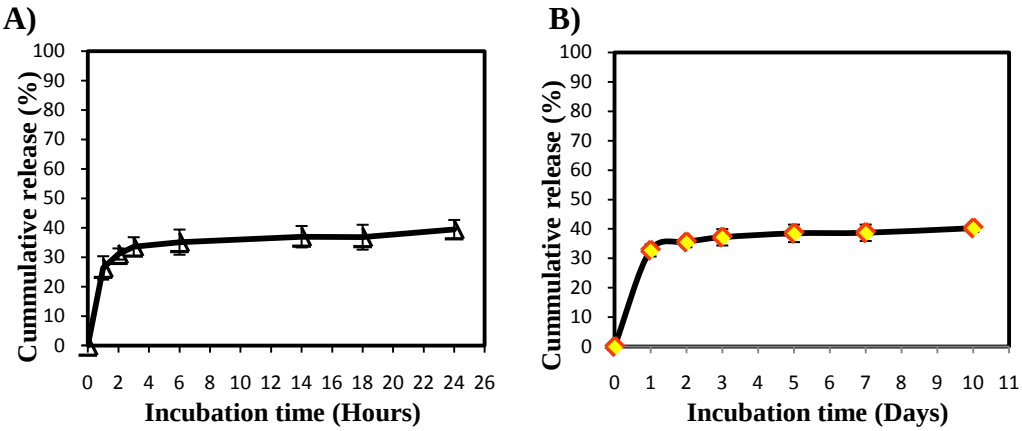

Figure 5.6: A) Short term and **B)** Long-term *in vitro* release profile of a suspension of [^{125}I] 5-IDFPdR-loaded NPs prepared by single emulsion method (n=3).

5.3.3.2. Effect of washing cycles on release profile- In previous studies, it was assumed that the initial burst release was primarily caused by the presence of encapsulated drug in the vicinity of the surface region of the hydrated NPs [15]. To minimize this possible cause, the wet NPs were washed with various numbers of centrifugation/ resuspension cycles after completion of solvent evaporation process. The results for the NPs prepared by single emulsion method indicated no significant change in release profile as a result of an increase in the number of washing cycles for NPs. The burst release of probe from NPs after 4 washing cycles was 25.0± 0.5% in the first hour, which reached to 39.3± 4.2% within 24 h **(Figure 5.7**). After 5 washing cycles 22.1± 4.1% and 36.6± 4.3% of the probe was released within the first and 24 h, respectively.

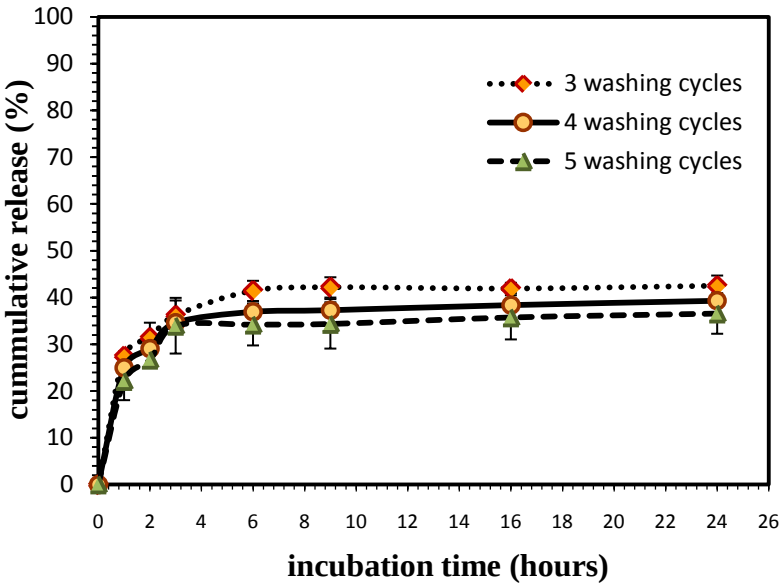

Figure 5.7: Effect of various number of centrifugation/resuspension (washing) cycles on *in vitro* release profile of a suspension of [^{125}I] 5-IDFPdR-loaded NPs prepared by single emulsion method (n=3).

5.3.3.3. Release profile of suspension vs. freeze-dried NPs- Release profiles of freeze-dried and suspended NPs were compared, as well. The release studies on freeze-dried NPs were performed only on NPs loaded with cold 5-IDFPdR, due to the lack of access to a freeze-dryer for radioactive use.

The results indicated the probe was released from lyophilized NPs with a high initial release of 36.6% after 3 hours, followed by a plateau and reaching to 45.8% within 120 hours. This was comparable to the burst release of 33.6± 3.2% and maximum release of 38.5± 3.0% within the same time for a wet suspension of NPs **(Figure 5.8)**. In other words, freeze drying of NPs did not affect the rate of probe release.

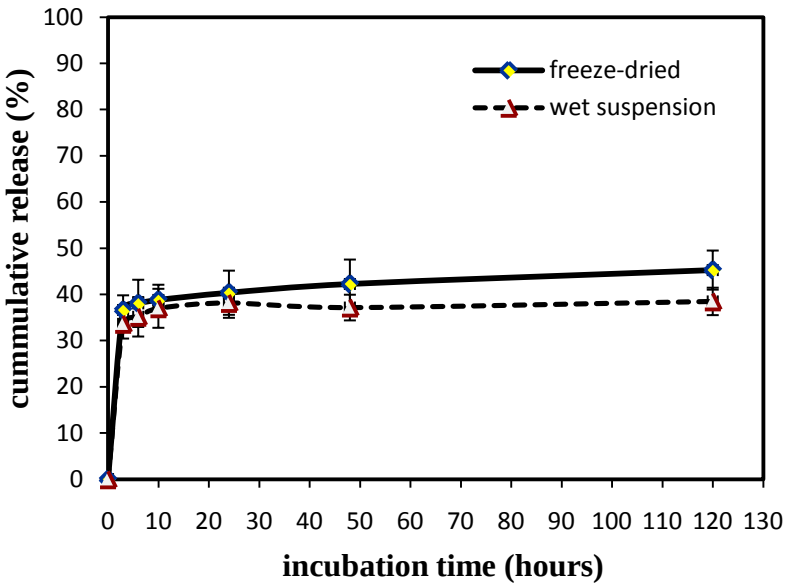

Figure 5.8: Comparing *in vitro* release profile of freeze-dried cold 5-IDFPdR-loaded NPs with a wet suspension of [^{125}I] 5-IDFPdR-loaded NPs prepared by single emulsion method (n=3). The released cold 5-IDFPdR and the labeled 5-IDFPdR were determined by HPLC and gamma scintillation measurement, respectively.

5.3.3.5. Effect of emulsification method on release profile- Oil-in-water (single emulsion) emulsification, which is usually used for the encapsulation of lipophilic compounds, resulted in a burst release of probe either in wet suspension form or freeze-dried form. Applying water-in-oil-in-water (double emulsion) emulsification method as an alternative for the preparation of nanoprobes showed a significantly higher burst release (56.9%) than o/w emulsion ($P<0.05$), followed by a plateau (**Figure 5.9**). It reached up to 66.3% release within 120 hours (**Figure 5.9**), which is less favorable than the oil-in-water emulsification method.

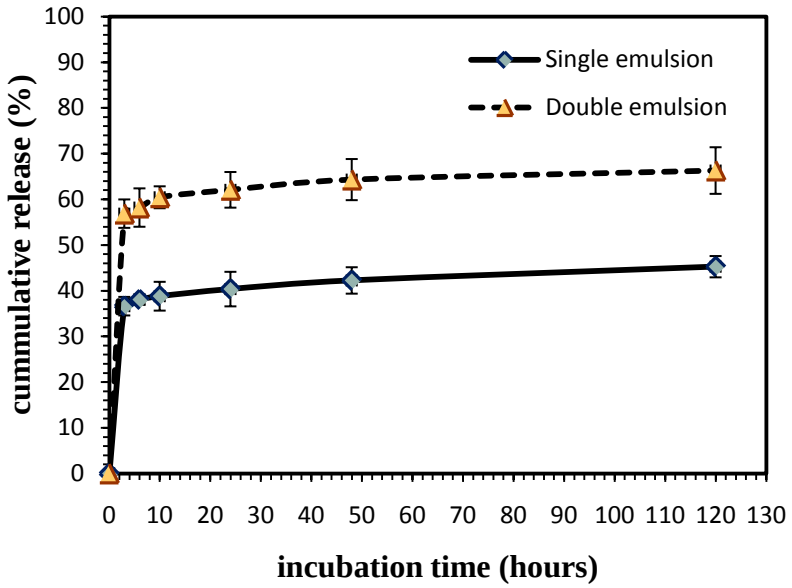

Figure 5.9: Comparing the *in vitro* release profile of freeze-dried cold 5-IDFPdR-loaded NPs prepared by single emulsion and double emulsion method.

5.5. DISCUSSION

In this study, the lipophilic thymidine analog, 5-IDFPdR, was radiolabeled, purified and loaded in PLGA-NPs to produce a nanoprobe appropriate for *in vivo* DC monitoring by PET imaging. Since there is a limitation in the extent of the *in vivo* administration of the probe, specific activity of the radiolabeled probe must be as high as possible. As specified in our results, the specific activity seems to be high enough to produce detectable signals with an acceptable radiolabeling yield.

The radiolabeled probe was then purified from the possible sources of impurity including non-reacted Iodide ion (I^-), hydrophilic and lipophilic by-products, I_2 and/or various complexes of Iodine. Leaching by chloroform in several steps along with sonication was shown to be an efficient method for the recovery of [^{125}I] 5-IDFPdR. The [^{125}I] 5-IDFPdR is fairly soluble in chloroform, while the Iodide ion (I^-) is insoluble in chloroform and can be removed from [^{125}I] 5-IDFPdR using this method. The possible problem would be the presence of I_2 and lipophilic by-products along with extracted solute in chloroform. To assess the extent of these impurities the extracted radiolabeled probe was analyzed by

RP-HPLC showing high level of purity (less than 5% chemical and 6% radiochemical impurity). The chloroform-leaching system is also advantageous from a practical point of view as well, since a solution of the probe in chloroform will be directly used for the preparation of [^{125}I] 5-IDFPdR-loaded PLGA-NPs.

A propitious nanoprobe should be able not only to encapsulate high levels of the radio labeled probe, but also to retain its content inside DCs for several hours, providing the possibility to map the journey DCs take using PET. On the other hand, the accumulation of radioactivity in blood or other tissues should be minimal to produce a high signal-to-noise ratio. To improve the efficiency of loading and the retention of [^{125}I] 5-IDFPdR inside NPs, the PET-nanoprobe was prepared using the high molecular weight (45,000-70,000 Da) PLGA. Theoretically, the higher MWt of the polymer is expected to retard biodegradation of PLGA and also slow down the diffusion of small molecules out of PLGA-NPs [15] [16]. Owing to a low porosity and surface area in NPs prepared from high MWt PLGA, encapsulated 5-IDFPdR will be less accessible to the media, thus, the release or diffusion from the matrix of NPs will reduce [17] [18].

Loading NPs with [^{125}I] 5-IDFPdR either by single emulsion or double emulsion solvent-evaporation technique forms a nanoprobe with a size below 400 nm (**Table 5.2**) optimal for DC uptake [19]. However, the encapsulation of the probe in NPs was not as efficient as expected. Changes in the encapsulation procedure barely elevated the level of encapsulation (**Table 5.3**). The encapsulation efficiency did not increase with increasing the concentration of probe initially fed into the formulation implying the saturation of PLGA-NPs by [^{125}I] 5-IDFPdR. In addition, a burst release of the probed from NP was observed within a few hours after incubation in buffer (**Figure 5.6**). The rapid release of probe from PLGA-NPs indicates a predominant diffusion dependent mode of release for [^{125}I] 5-IDFPdR probe from PLGA-NPs rather than the degradation (hydrolysis) of the PLGA (See Section 1.5). Given that the time required until the onset of PLGA degradation ranges from days to months, control over the burst release of probe from PLGA-NPs will depend on controlling its diffusion [18]. In

this context, several formulation strategies were attempted in this study to make the probe unavailable for immediate diffusion and release from the nanocarrier.

For instance the number of washing cycles of wet semi-solid NPs right after solvent evaporation process was increased to remove the level of non-encapsulated probe adsorbed to the surface of NPs, but little success was achieved in controlling the burst release (**Figure 5.7**). In the next effort, the rate of NP drying was changed. The rate of drying is known to influence the morphology and porosity of NPs as well as probe recrystallization inside the spheres [15] . Migration of drugs during air or vacuum drying process results in a heterogeneous drug distribution in the polymer matrix [20]. In fact, when water flows to the matrix surface before evaporation, drug also diffused toward the surface by convection. It seems that convection-induced drug migration can be reduced by freeze-drying of the NPs [21] resulting to a lower burst release [22]. Several previous studies supports this assumption, where freeze-drying of PLGA microspheres has attenuated the burst release of Bovine Serum Albumin [23] and FITC-Dextran [24]. On the other hand, freeze-drying process is not always effective in preventing the burst release. The volume expansion of encapsulated water during the freezing stage can cause additional cracks in the NPs and induce a large initial burst [18]. In the current study freeze- drying of NPs slightly reduced burst release, possibly as a result of the suppressed migration of the probe and hardening of the NP surface (**Figure 5.8**). However, the reduction in burst release was still insufficient for the purpose of a nanoprobe development.

Finally, altering the emulsification method (single emulsion vs. double emulsion) was applied to enhance the encapsulation of radio labeled probe in PLGA-NPs and modifying its release profile. The results demonstrated a higher initial burst release from nanoprobes prepared by double emulsion method (**Figure 5.9**). This may be attributed to the tendency of the internal aqueous phase in double emulsion method to unite with the adjacent aqueous continuous phase leading to the rapid release of the small molecule of the 5-IDFPdR.

Unsuccessful approaches to improve the loading efficiency and reduce the initial burst release by both single and double emulsion methods, implies that 5-

IDFPdR is practically neither lipophilic enough to be loaded efficiently by single emulsion method, nor adequately hydrophilic for a successful loading by double emulsion method.

5.5. CONCLUSION

A favorable micro-PET nanoprobe for DC monitoring is supposed to be internalized by DCs and remained in the cells for several hours. The purified lipophilic molecule of radiolabeled [^{125}I] 5-IDFPdR was encapsulated poorly into PLGA-NPs and released rapidly due to its inadequate physio-chemical properties. The present study demonstrated that altering the emulsification method, freeze-drying of the NPs and extending number of washing cycles cannot diminish the burst release of ^{125}I] 5-IDFPdR from nanocarriers or lead to its improved encapsulation. In conclusion, due to the high burst release on one hand, and the low encapsulation efficiency on the other, the [^{125}I] 5-IDFPdR loaded in PLGA-NPs cannot be considered as an acceptable nanoprobe for DC tracking by micro-PET imaging.

REFERENCES

1. Acres, B., P. Beverley, and S. Scholl, *Tumor immunology and the Battle of Waterloo.* Mol Cancer Ther, 2002. **1**(8): p. 651-5.
2. Tacken, P.J., et al., *Dendritic-cell immunotherapy: from ex vivo loading to in vivo targeting.* Nat Rev Immunol, 2007. **7**(10): p. 790-802.
3. Elamanchili, P., et al., *Characterization of poly(D,L-lactic-co-glycolic acid) based nanoparticulate system for enhanced delivery of antigens to dendritic cells.* Vaccine, 2004. **22**(19): p. 2406-12.
4. Hamdy, S., et al., *Co-delivery of cancer-associated antigen and Toll-like receptor 4 ligand in PLGA nanoparticles induces potent CD8+ T cell-mediated anti-tumor immunity.* Vaccine, 2008. **26**(39): p. 5046-57.
5. Maes, W., et al., *In vivo bioluminescence imaging in an experimental mouse model for dendritic cell based immunotherapy against malignant glioma.* J Neurooncol, 2009. **91**(2): p. 127-39.
6. Gambhir, S.S., *Molecular imaging of cancer with positron emission tomography.* Nat Rev Cancer, 2002. **2**(9): p. 683-93.
7. Nahrendorf, M., et al., *Nanoparticle PET-CT imaging of macrophages in inflammatory atherosclerosis.* Circulation, 2008. **117**(3): p. 379-87.
8. Paans, A.M., et al., *Positron emission tomography: the conceptual idea using a multidisciplinary approach.* Methods, 2002. **27**(3): p. 195-207.
9. Swirski, F.K., et al., *A near-infrared cell tracker reagent for multiscopic in vivo imaging and quantification of leukocyte immune responses.* PLoS One, 2007. **2**(10): p. e1075.
10. Lutsiak, M.E., et al., *Analysis of poly(D,L-lactic-co-glycolic acid) nanosphere uptake by human dendritic cells and macrophages in vitro.* Pharm Res, 2002. **19**(10): p. 1480-7.
11. Khalili, P., et al., *Dose-dependent pharmacokinetics of 1-(2-deoxy-beta-D-ribofuranosyl)-2,4-difluoro-5-iodobenzene: a potential mimic of 5-iodo-2'-deoxyuridine.* Biopharm Drug Dispos, 2003. **24**(9): p. 385-95.
12. A.Stahlshmidt, Radiolabeling and bio-evaluation of 2, 4-difluoro-5-iodo -1-(2-Deoxy-b-Dribofuranosyl) benzene (5-IDFPdR), Faculty of pharmacy and Pharmaceutical Sciences. Edmonton: University of Alberta, 2004
13. Wang, Z.X., et al., *Synthesis of 1-(2-deoxy-beta-D-ribofuranosyl)-2,4-difluoro-5-substituted-benzene thymidine mimics, some related alpha-anomers, and their evaluation as antiviral and anticancer agents.* Nucleosides Nucleotides Nucleic Acids, 2001. **20**(1-2): p. 11-40.
14. Astete, C.E. and C.M. Sabliov, *Synthesis and characterization of PLGA nanoparticles.* J Biomater Sci Polym Ed, 2006. **17**(3): p. 247-89.
15. Freitas, S., H.P. Merkle, and B. Gander, *Microencapsulation by solvent extraction/evaporation: reviewing the state of the art of microsphere preparation process technology.* J Control Release, 2005. **102**(2): p. 313-32.
16. Sanders, L.M., et al., *Prolonged controlled-release of nafarelin, a luteinizing hormone-releasing hormone analogue, from biodegradable*

polymeric implants: influence of composition and molecular weight of polymer. J Pharm Sci, 1986. **75**(4): p. 356-60.
17. Mehta, R., C., et al., Biodegradable microspheres as depot system for parenteral delivery of peptide drugs. J contr rel, 1994.29 (3):p.375-384.
18. Yeo, Y. and K. Park, *Control of encapsulation efficiency and initial burst in polymeric microparticle systems.* Arch Pharm Res, 2004. **27**(1): p. 1-12.
19. Foged, C., et al., *Particle size and surface charge affect particle uptake by human dendritic cells in an in vitro model.* Int J Pharm, 2005. **298**(2): p. 315-22.
20. Huang, X. and C.S. Brazel, *On the importance and mechanisms of burst release in matrix-controlled drug delivery systems.* J Control Release, 2001. **73**(2-3): p. 121-36.
21. Holzer, M., et al., *Physico-chemical characterisation of PLGA-nanoparticles after freeze-drying and storage.* Eur J Pharm Biopharm, 2009.
22. Igartua, M., et al., *Influence of formulation variables on the in-vitro release of albumin from biodegradable microparticulate systems.* J Microencapsul, 1997. **14**(3): p. 349-56.
23. Yang, Y.Y., H.H. Chia, and T.S. Chung, *Effect of preparation temperature on the characteristics and release profiles of PLGA microspheres containing protein fabricated by double-emulsion solvent extraction/evaporation method.* J Control Release, 2000. **69**(1): p. 81-96.
24. Kim, T.H. and T.G. Park, *Critical effect of freezing/freeze-drying on sustained release of FITC-dextran encapsulated within PLGA microspheres.* Int J Pharm, 2004. **271**(1-2): p. 207-14.

Chapter Six:

General discussions and conclusions

6.1. General discussions

Current cancer vaccines have demonstrated only limited success in clinic (3-7%), despite the efficacy in pre-clinical stages. This can be attributed to aspects such as ***1***) insufficient immnuostimulation by cancer vaccines, ***2***) inadequate trafficking of immune cells, and ***3***) immunosuppressive tumour microenvironment or a combination of those [1]. The overall goal of this research is to enhance the effectiveness of current cancer vaccines to overcome these limitations. We address the first aspect by active targeting of DC surface receptors *in vivo* to improve the immunostimulatory responses. In this context, simultaneous delivery of antigens along with adjuvants actively to DCs through targeting of CLRs on DC surface (e.g. MR, which is predominantly expressed on macrophages and immature DCs) is suggested as an efficient strategy to improve the effectiveness of cancer vaccines. Several studies have demonstrated that targeting antigens to CLRs can result in strong anti-tumour responses [2, 3]. On the other hand, immunomonitoring of DCs *in vivo* in their actual environment with imaging modalities can be used to investigate the trafficking of immune cells [4] and shed light on the migration and function of DCs in a molecular level during DC vaccination.

The ***first*** objective of this research was to utilize decorated PLGA-NPs as vehicles for active targeting of DC-expressed MR to enhance DC uptake and immunological responses in DC vaccination [5]. Decorated PLGA-NPs can protect the antigen and adjuvants from degradation, and directly deliver them to phagocytic cells (mostly DCs) in a selectively targeted and prolonged manner while restricting the entrance of cargo to the systemic circulation [6, 7]. Besides, PLGA-NPs can incorporate immunomodulating molecules (such as MN; a branched polymannose ligand of MR) for active targeting of DCs through chemical or physical means. MR are particularly important for recognition and uptake of mannose moieties into intracellular compartments in DCs, inducing processing and presentation of antigens on MHC class I and II molecules. Uptake of soluble antigens through MR has been associated with a substantial increase in both antigen presentation and T cell stimulation (up to 100-fold).

To achieve our ***first*** goal, PLGA NPs were decorated with two MR ligands: MN that can also be recognizing as an adjuvant, as well as hydrophobized MN (OPM). The MN used in this study was derived from the cell wall of *S. cerevisiae* and was structurally identical to the MN from *C. Albicans* [8]. The immunomodulatory roles of MN is evidenced by its capability of inducing CTLs through MHC-I antigen presentation pathway, direct influence on the production and release of the IL-6 (a pro-inflammatory cytokine crucial for the activation and modulation of the adaptive immune responses) [9-12]. In addition, the recognition of MN jointly by MR and TLR4 is suggested to be essential for immune sensing of PAMPs. Therefore, we can take advantage of MN recognition by DC-expressed MR leading to enhanced uptake of decorated formulations on one hand and induction of cellular immune responses by MN on the other hand. A Pilot phase III immunotherapy study in early-stage cancer patients using oxidized MN-MUC1 strongly supported the effectiveness of this strategy [13].

The research study reported in **Chapter 2** was dedicated to the incorporation of MN into PLGA-NPs using two different types of polymers: ester and carboxyl terminated PLGA. In **Chapter 4**, due to difference in the physico-chemical properties of hydrophobic ester-terminated PLGA and hydrophilic MN; we shifted the MN characteristic to a more hydrophobic molecule by synthesis of OPM, to achieve a stronger incorporation in NPs. In **Chapter 3**, the MN incorporated formulations were tested for their effect on the induction of DC maturation and function.

The nanoparticulate formulations were prepared with two assorted sets of strategies. The first approach was physical incorporation of MN in PLGA-NPs, resulting to MN-W1-NPs, MN-W2-NPs and MN-Ads-NPs; whereas in the second strategy MN was chemically attached to the prepared COOH-terminated NPs (MN-Cov-NPs). OPM was also incorporated physically to both PLGA NPs using similar methods. Since OPM is soluble only in a narrow range of organic solvents, we used DMSO for dissolving OPM in the process of formulation. In

fact, the solubility of PLGA in DMSO hinders the success of OPM formulations to some extent.

Considering the limited solubility of MN in water (~20 mg/ml) and in order to keep the nanoparticulate size as small as possible by controlling the volume of W1 or W2, we had a restriction in the amount of MN added during the process of NP preparation (MN-W1- and MN-W2-NP formulations). At the end, all prepared PLGA-NPs were shown to be within the size range suitable for uptake by DCs [14] (average size ranging between 300-500 nm) (**Chapter 2**).

The level of MN incorporation was determined by a Phenol-sulphuric assay, a classical colorimetric technique for the quantification of carbohydrates [15]. The method was insensitive to the traces of organic solvents remaining after extraction of MN from NPs. A linear relationship between the MN concentration and the optical absorption was obtained which verified its usefulness in our studies (**Chapter 2**). However, this method did not work for the quantification of OPM. The restricted solubility of OPM in water and most of the organic solvents, including DCM, chloroform, DMF, THF, acetone, diethyl ether, acetonitrile and methanol (**Chapter 4**) rendered extraction of OPM from NPs prior to the colorimetric assay.

The MN incorporation was considerably higher than all other formulations in MN-Cov-COOH NPs. The second highest incorporation was observed when adsorption of MN to the NPs was used. This level was slightly higher for ester-terminated PLGA NPs (**Chapter 2**), which may be related to the presence of negative charge on the phosphate groups present in natural MN [8] disrupting the MN adsorption onto more negatively charged COOH-terminated NPs.

The net negative surface charge of NPs increased significantly after MN incorporation, which was higher for MN-Cov-COOH NPs and MN-Ads-NPs (regardless of the polymer type)**.** These findings in conjunction with the high MN content for the above formulations could be attributed to the presence of MN on the surface of NPs (rather than MN encapsulation by NPs).

Among the formulations the covalent binding of MN to PLGA (MN-Cov-COOH-NPs) showed the highest increase (2-folds) in the level of DC uptake of

NPs relative to non-decorated (plain) NPs. (**Chapter 2**). The formulations with adsorbed MN to the PLGA-NPs also demonstrated a significant increase in the level of uptake (with a slight difference among the different PLGAs). No significant effect on uptake was observed by MN-W1-NPs, which can be explained by the incorporation of MN in the inner layers of PLGA rather than the surface. Evidence for the uptake of MN-decorated NPs rather than their mere binding to cells was provided by confocal microscopy (**Chapter2**).

OPM incorporation led to a predominant increase in the association of OPM-Ads-NPs (both PLGAs) with DCs **(Chapter 4).** Shifting MN characteristics towards a more hydrophobic molecule appears not to improve the incorporation and consequent effect of OPM-decorated NPs on DC uptake. The highest fold-increase in uptake was observed for OPM-Ads-COOH NPs (1.67±0.12).

The influence of the MN incorporation in PLGA NPs on DC maturation was verified by assessing the upregulation of DC surface markers (CD40 and CD86) and the production of cytokines including IL-12, IL-6 and TNF-α. Moreover, T cell proliferation by DCs was evaluated by MLR in the presence of the formulations. In all these sets of experiments, non-decorated (plain) NPs and the soluble MN were used as controls.

Decoration of MN on COOH-terminated NPs showed a significant effect on DC maturation, predominantly induced by MN-Cov-COOH-NPs and MN-Ads-COOH NPs. Consistent with the potential of MN-Cov-COOH-NPs, the capability of this formulation to induce immunostimulatory activity of DCs relative to plain-NPs (**Chapter 3**) was shown to be the highest amongst the MN-decorated formulations.

Remarkably, the extent of the observed effects with MN decorated NPs was higher than the soluble MN at the same concentration (**Chapter 3**). In fact, the ability of MN-Cov-COOH-NPs is equivalent to the addition of 1.5-13 mg soluble MN, while the content of MN in this formulation is only 0.37 mg. Similarly, MN-Ads-COOH-NPs were shown to be able to induce the DC maturation as well as T cell proliferation by DCs significantly more than the plain

NPs, and MN in nanoparticulate system showed better activities in this regard when compared to soluble MN.

According to our findings, the MN-decorated-COOH NP formulations that showed higher DC uptake were also able to enhance DC maturation and function (**Chapter 2 and 3**). This was not the case for ester-terminated PLGA-NPs, which have failed to show consistent results in terms of activity to that of DC uptake studies (**Chapter 2**). This can be attributed to the different fates of PLGAs following the active internalization of NPs by DCs and their transport to intracellular compartments. The hydrophilic COOH-terminated PLGA and its hydrophobic ester-terminated counterpart may have different susceptibility and outcomes in acidic intracellular compartments (endosomes), which in turn could affect the subsequent intracellular signalling events. This needs further investigations. The ester-terminated NPs were studied and used more than their COOH-terminated counterparts. The behaviour of COOH-terminated NPs during the storage also remains to be investigated.

The ***second*** objective of this research was to utilise PLGA-NPs for development of a nanoprobe as a specific, accurate and non-invasive imaging technique to investigate efficacy of DC vaccination by tracking DCs in live animals in a molecular basis. Considering the ability of DCs to take up the PLGA-NPs, the encapsulation of the probe in PLGA-NPs can restrict delivery of the probe to DCs, protect the probe, decrease the dose of the tracer and provide low-background images.

Amongst the imaging modalities PET and MRI are particularly of interest. PET potentially offers a supreme sensitivity and specificity in detection with the ability to monitor even in the picomolar range [16, 17]. This allows lowering the dose substantially and accomplishing cellular-molecular investigation without any adverse effects from the labelled probe. Moreover, direct linear correlation between the count densities measured by PET with the concentration of an established labelled biomarker allows to readily quantifying the PET signal in a molecular scale [17].

Loading a PET probe into PLGA NPs can be used to produce a PET nanoprobe. The nanoscale probe can be readily internalized by DCs, carry the PET tracer to DCs and provide a detection tool for DC monitoring *in vivo* to provide information on phenotypic and activation status, dynamics of recruitment, differentiation and fate of DCs [18, 19] for development of successful vaccines. The PET-nanoprobe is expected to be internalized by DCs and remain in them for several hours (during DC activation and migration to lymph nodes). The PET-tracer ^{124}I with a fairly long physical half-life compared to other commonly used PET- tracers (4.15 days) can last sufficiently long until radiolabeling, NP preparation, DC uptake and DC migration are completed.

Although, radioiodinated 5-IDFPdR was a lipophilic molecule, it was not encapsulated efficiently in PLGA-NPs and released rapidly from NPs (23% in average within the first hour). It was assumed that such nanoprobes cannot provide high quality images because of the high level of background resulted from burst release of the PET tracer from NPs (**chapter 5**). The manipulations by increase cycles of washing the nanoprobe, freeze-drying the nanoprobe and changing the emulsification technique from double emulsion to single emulsion was not successful in controlling the extent of burst release (**chapter 5**).

6.2. Conclusions

Decoration of PLGA-NPs with MN can be used as a successful strategy to enhance the uptake of NPs by DCs. Among different MN incorporation strategies, covalent attachment of MN to COOH-terminated PLGA-NPs (MN-Cov-COOH-NPs) appears to provide a higher level of MN surface decoration on NPs leading to enhanced uptake of NPs by DCs. The nanoparticulate formulations of MN, particularly MN-Cov-COOH-NPs and MN-Ads-COOHNPs, showed success in the enhancement of the upregulation of co-stimulatory molecules, DC maturation and immunostimulatory activity of DCs compared to soluble MN at similar concentrations. OPM-decorated NPs showed capability to enhance DC uptake relative to non-decorated NPs. However, the effect of OPM incorporation in DC

uptake of NPs is less significant than what observed for the MN-incorporated PLGA-NPs. Overall; these findings suggest the capability of MN-PLGA- NPs as vehicles to enhance the efficacy of PLGA-based nanoparticulate vaccines in cancer immunotherapy.

On the other hand, we developed the PLGA-NPs loaded with a PET probe (the PET nanoprobe) as means for DC tracking by PET imaging. The lipophilic molecule of the radioiodinated PET probe ([^{125}I] 5-IDFPdR) was encapsulated poorly into PLGA-NPs and showed signs of burst release. Manipulation of the nanoparticulate system did not diminish the burst release of ^{125}I] 5-IDFPdR from NPs or lead to its improved encapsulation. Since a favourable micro-PET nanoprobe for DC monitoring is supposed to be internalized by DCs and remain in the cells for several hours, we conclude that the [^{125}I] 5-IDFPdR was not an appropriate PET tracer for the production of PLGA nanoprobes.

6.3. Future perspectives

Over the past two decades PLGA nano/micro particulate systems have been studied and utilized extensively for their applications in drug delivery and vaccine technology. The promising results of current study on the positive impact of MN decoration of PLGA-NPs on the uptake and immunostimulatory activity of DCs, opens up new avenues for the design and development of a multivalent single administration vaccine based on MN-decorated PLGA-NPs. In this context, MN-decorated NP formulations, particularly MN-Cov-COOH and MN-Ads-COOH NPs, co-encapsulated with a model antigen (such as Ovalbumin) along with adjuvants can be developed and evaluated for the induction of immunological responses against tumours transfected with the model antigen, both *in vitro* and *in vivo.* In addition, co-encapsulation of TLR ligands along with the model antigen in MN decorated PLGA-NPs can be explored for cancer vaccines. PLGA-NPs could provide simultaneous delivery of model antigen, TLR ligands and MR ligands to the same targeted DC. Synthetic LPS derivatives (such as MPLA and 7-acyl lipid A) have been utilized in our group as TLR4 ligands

with promising results [20, 21]. The facilitated uptake of NPs through MR as well as the cross-talk between MR and TLR4 could result to improved antigen processing and presentation. The co-delivery of MR and TLR4 ligands could result in generation of mature DCs capable of activating cellular immune responses and may lead to suppression of tolerogenic responses [2]. Since the Expression of MR by DCs in mice is strain-depended, the C3H/HeN inbred mice can be used which expresses higher levels of MR compared to C57BL/6 [22]. The involvement of MR in these set of studies can also be verified by using MR-knockout mice [11].

Although our results showed the positive impact of MN incorporation on the uptake of NPs by DCs and subsequent immunomodulation, we have not shown the involvement of MR in these events directly. In general, the precise involvement of a specific receptor in observed events can be verified by receptor competition assay. Today, MR is the only identified DC-expressed receptor for MN in C57BL/6 mice strains. The expression of DC-SIGN, which has a proved affinity towards MN, has not been detected on DCs in mice and DC-SIGN expression seems to be restricted to the human DCs [23]. Competition assays can be carried out in future to verify the involvement of MR on DC maturation as well as MR- mediated internalization in the uptake of MN decorated NPs.

It is known that the MR is expressed by macrophage population as well as DCs [24]. This may lead to undesired capture of MN-decorated NPs by macrophages as well as DC population, *in vivo*. Although the small size of NPs and i.d. administration [25] of the MN-decorated PLGA-NP vaccines, can favour better uptake by the DC population to some extent, a better approach will be to decorate PLGA-NPs with more specific ligands of DC population such as ligands for CD11c in future studies. It can be also advantageous for cancer vaccination, since it is demonstrated recently that targeting antigen towards CD11c facilitates efficient CD4+ and CD8+ T cell activation [26].

The study in **Chapter 5** clearly demonstrated inability of the PET-probe (5-IDFPdR) to be loaded in PLGA-NPs (PET-nanoprobe) strongly and stably, implying inadequate physico-chemical properties of this molecule for this

purpose. For a competent imaging by PLGA-NPs, an efficient encapsulation of the PET-probe along with its retention in NPs in the time frame of imaging is required. Furthermore, the NPs should be taken up by DCs successfully. These features suggest using a high MWt and highly lipophilic PET probe for incorporation into PLGA-NPs in future studies. As an alternative, β-CIT (a cocaine analog), which is a non-toxic PET-probe using routinely in platelet radio-labelling, is suggested. The other possible alternatives could have been the lipophilic and high MWt molecules of IBZM and I-SAP. Moreover, carbohydrate and polyol-coated NPs have emerged as powerful affinity labels for *in vivo* imaging of phagocytic cells based on their active uptake and intracellular trapping [27]. With this in mind, our results suggest decoration of the PET-nanoprobe with MN, in the covalent conjugation or adsorbed form can potentially provide a powerful tool for the PET imaging through facilitating the recognition of nanoprobe by DCs *in vivo* and enhanced active internalization into DCs.

References

1. Rosenberg, S.A., J.C. Yang, and N.P. Restifo, *Cancer immunotherapy: moving beyond current vaccines.* Nat Med, 2004. **10**(9): p. 909-15.
2. Geijtenbeek, T.B. and S.I. Gringhuis, *Signalling through C-type lectin receptors: shaping immune responses.* Nat Rev Immunol, 2009. **9**(7): p. 465-79.
3. van Kooyk, Y., *C-type lectins on dendritic cells: key modulators for the induction of immune responses.* Biochem Soc Trans, 2008. **36**(Pt 6): p. 1478-81.
4. Weissleder, R. and M.J. Pittet, *Imaging in the era of molecular oncology.* Nature, 2008. **452**(7187): p. 580-9.
5. He, L.Z., et al., *Antigenic targeting of the human mannose receptor induces tumor immunity.* J Immunol, 2007. **178**(10): p. 6259-67.
6. Xiang, S.D., et al., *Promising particle-based vaccines in cancer therapy.* Expert Rev Vaccines, 2008. **7**(7): p. 1103-19.
7. Audran, R., et al., *Encapsulation of peptides in biodegradable microspheres prolongs their MHC class-I presentation by dendritic cells and macrophages in vitro.* Vaccine, 2003. **21**(11-12): p. 1250-5.
8. Nelson, R.D., et al., *Candida mannan: chemistry, suppression of cell-mediated immunity, and possible mechanisms of action.* Clin Microbiol Rev, 1991. **4**(1): p. 1-19.
9. Apostolopoulos, V., et al., *Ex vivo targeting of the macrophage mannose receptor generates anti-tumor CTL responses.* Vaccine, 2000. **18**(27): p. 3174-84.
10. Tada, H., et al., *Saccharomyces cerevisiae- and Candida albicans-derived mannan induced production of tumor necrosis factor alpha by human monocytes in a CD14- and Toll-like receptor 4-dependent manner.* Microbiol Immunol, 2002. **46**(7): p. 503-12.
11. Cambi, A., et al., *Dendritic cell interaction with Candida albicans critically depends on N-linked mannan.* J Biol Chem, 2008. **283**(29): p. 20590-9.
12. Sheng, K.C., et al., *Mannan derivatives induce phenotypic and functional maturation of mouse dendritic cells.* Immunology, 2006. **118**(3): p. 372-83.
13. Apostolopoulos, V., et al., *Pilot phase III immunotherapy study in early-stage breast cancer patients using oxidized mannan-MUC1 [ISRCTN71711835].* Breast Cancer Res, 2006. **8**(3): p. R27.
14. Kalkanidis, M., et al., *Methods for nano-particle based vaccine formulation and evaluation of their immunogenicity.* Methods, 2006. **40**(1): p. 20-9.
15. Dubois, M., et al., *A colorimetric method for the determination of sugars.* Nature, 1951. **168**(4265): p. 167.
16. Gambhir, S.S., *Molecular imaging of cancer with positron emission tomography.* Nat Rev Cancer, 2002. **2**(9): p. 683-93.

17. Nahrendorf, M., et al., *Nanoparticle PET-CT imaging of macrophages in inflammatory atherosclerosis.* Circulation, 2008. **117**(3): p. 379-87.
18. Christian, N.A., et al., *In vivo dendritic cell tracking using fluorescence lifetime imaging and near-infrared-emissive polymersomes.* Mol Imaging Biol, 2009. **11**(3): p. 167-77.
19. Maes, W., et al., *In vivo bioluminescence imaging in an experimental mouse model for dendritic cell based immunotherapy against malignant glioma.* J Neurooncol, 2009. **91**(2): p. 127-39.
20. Elamanchili, P., et al., *"Pathogen-mimicking" nanoparticles for vaccine delivery to dendritic cells.* J Immunother, 2007. **30**(4): p. 378-95.
21. Hamdy, S., et al., *Co-delivery of cancer-associated antigen and Toll-like receptor 4 ligand in PLGA nanoparticles induces potent CD8+ T cell-mediated anti-tumor immunity.* Vaccine, 2008. **26**(39): p. 5046-57.
22. Autenrieth, S.E. and I.B. Autenrieth, *Variable antigen uptake due to different expression of the macrophage mannose receptor by dendritic cells in various inbred mouse strains.* Immunology, 2009. **127**(4): p. 523-9.
23. Hovius, J.W., et al., *Salp15 binding to DC-SIGN inhibits cytokine expression by impairing both nucleosome remodeling and mRNA stabilization.* PLoS Pathog, 2008. **4**(2): p. e31.
24. East, L. and C.M. Isacke, *The mannose receptor family.* Biochim Biophys Acta, 2002. **1572**(2-3): p. 364-86.
25. Newman, K.D., et al., *Uptake of poly(D,L-lactic-co-glycolic acid) microspheres by antigen-presenting cells in vivo.* J Biomed Mater Res, 2002. **60**(3): p. 480-6.
26. Kurts, C., *CD11c: not merely a murine DC marker, but also a useful vaccination target.* Eur J Immunol, 2008. **38**(8): p. 2072-5.
27. Jaffer, F.A., et al., *Cellular imaging of inflammation in atherosclerosis using magnetofluorescent nanomaterials.* Mol Imaging, 2006. **5**(2): p. 85-92.